National Aeronautics and
Space Administration

| | |
|---|---|
| **Document No.** | TR-757-001 |
| **Date** | July 12, 1993 |
| **Issue Date** | March 11, 1997 |

**Test Report**

# Feasibility Investigation for Performing Fireball Temperature Tests



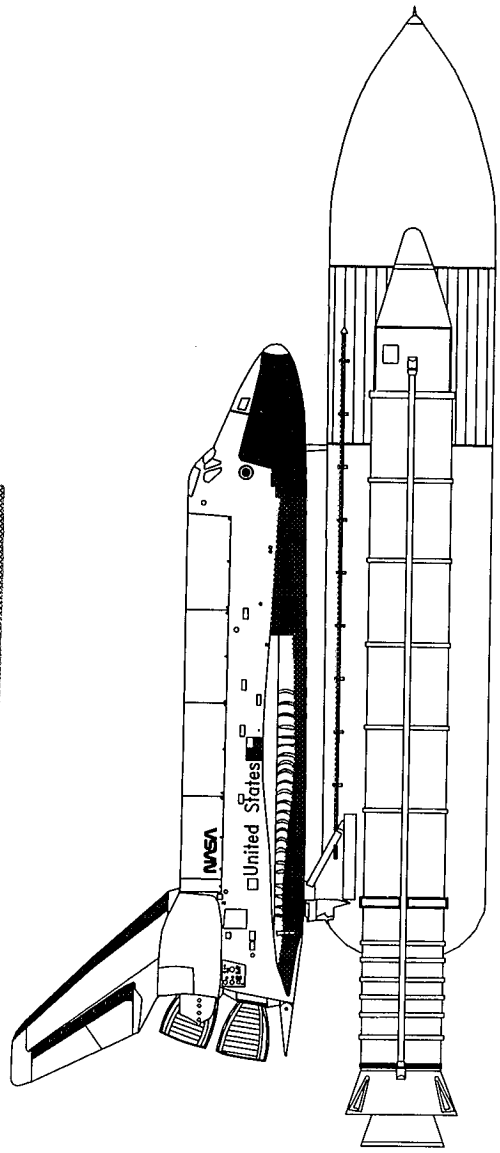


**Lyndon B. Johnson Space Center**
**White Sands Test Facility**
**P. O. Box 20**
**Las Cruces, NM 88004**
**(505) 524-5011**

TR-757-001

Test Report

# Feasibility Investigation for Performing Fireball Temperature Tests

Issued By
National Aeronautics and Space Administration
Johnson Space Center
White Sands Test Facility
Laboratories Office


Prepared By: _____
Ralph M. Tapphorn
AlliedSignal Technical Services Corp. Team

Prepared By: _____
Joe Kurtz
AlliedSignal Technical Services Corp. Team

Reviewed By: _____
Radel L. Bunker, Project Manager
NASA Laboratories Office

Approved By: _____
Harry T. Johnson, Chief
NASA Laboratories Office

# Abstract

NASA Johnson Space Center White Sands Test Facility (WSTF) was requested by the Launch Abort Subpanel and the Power Systems Subpanel of the Interagency Nuclear Safety Review Panel to investigate the feasibility of using spectroscopic techniques to measure propellant fireball gas temperatures. This report outlines the modeling and experimental approaches and results of this investigation. Descriptions of the theoretical particle temperature and mass effusion models are presented along with the results of the survivability of small plutonium dioxide ($\leq$ 1000-$\mu$m diameter) particles entrained in various propellant fireball scenarios. The experimental test systems used to measure the hydroxide radical, water, and particle graybody spectral emissions and absorptions are discussed. Spectral results along with temperatures extracted by analyzing the spectral features are presented for the flames investigated in the laboratory environment. Methods of implementing spectroscopic measurements for future testing using the WSTF Large-scale Hydrogen/Oxygen Explosion Facility are discussed, and the accuracy expected for these measurements is estimated from laboratory measurements.

# Contents

# Contents (continued)

# Figures

## 1.0 Introduction

The Launch Abort Subpanel (LASP) and the Power Systems Subpanel (PSSP) of the Interagency Nuclear Safety Review Panel (INSRP) requested the NASA Johnson Space Center White Sands Test Facility (WSTF) to investigate the feasibility of measuring propellant fireball gas temperatures using spectroscopic techniques. Measurement of temperature environments surrounding launch vehicle accident scenarios will aid in assessing the potential for vaporizing radioactive payload materials entrained in various propellant fireball mixtures including cryogenic liquid hydrogen/liquid oxygen ($LH_2/LO_2$) mixtures and hypergolic fuel/oxidizer mixtures. The potential launch vehicles for these payloads include the Atlas-Centaur, Titan IV, or Space Shuttle. These initial investigations will provide the scientific basis for assessing the fireball environments associated with intact impact accident scenarios involving the launch of nuclear reactors and radioactive thermal generators.

This investigation was conducted in two phases. For Phase I, the theoretical analysis of the mass effusion process for radioactive particles entrained in fireball gas streams was conducted. Mass effusion in this case is defined as the process of removing material from a localized diffusion cloud or surface shell surrounding a particle. Plutonium dioxide ($PuO_2$) was selected as a representative radioactive material for these analyses. For Phase II, experimental investigations of spectroscopic methods for measuring laboratory flame temperatures (using typical propellant gases) were conducted. Phase II focused on assessing the feasibility of performing spectroscopic temperature measurements of hydrogen ($H_2$) flames using the Large-scale Hydrogen/Oxygen Explosion (LSHOE) test facility located at WSTF.

Included in this document is a proposal for performing future fireball gas temperature and particle mass effusion measurements using the WSTF LSHOE test facility. An advanced project is also proposed with various implementation concepts following a preliminary field test investigation.

## 2.0 Objectives

The objectives of this project were as follows:

(1) For Phase I, investigate the theoretical mass effusion rates of selected radioactive materials ($PuO_2$ particles $\leq$ 1000-$\mu$m-diameter size) entrained in propellant fireballs as a function of fireball conditions including temperature, emissivity, and velocity of the fireball gas. Determine the critical parameters affecting the mass effusion rates.

(2) For Phase II, investigate the feasibility of measuring propellant fireball gas temperatures using spectroscopic techniques.

## 3.0 Approach

A two-phase approach was used to meet the objectives. In Phase I, a literature review was conducted, and a theoretical simulation model that calculates the temperature and mass effusion rates of $PuO_2$ particles entrained in propellant fireball gas streams as a function of fireball conditions was developed. The literature review was conducted to determine (1) what

models had been previously developed to characterize propellant fireball gas temperatures and mass effusion rates of entrained particles and (2) what methods had been previously employed to measure fireball gas temperatures. The theoretical simulation model for characterizing the gas temperature and mass effusion rates of small particles entrained in gas streams of a propellant fireball was developed, accounting for both heat transfer and convective evaporation processes. Lower and upper temperature bounds for the fireball gas temperature of various propellant mixtures were established with adiabatic flame limits calculated from the Gordon and McBride code (Gordon and McBride 1971).

Using a laboratory flame, the most prominent spectral features of $H_2/O_2$ and $H_2$/air flames were investigated for thermal equilibrium temperature information. In addition, a sooty flame was investigated since soot and other particulates were anticipated in the field-test environments which include container hardware and hypergolic propellants.

The spectroscopy measurements of Phase II involved the following. First, emission spectra of $H_2/O_2$ flames were taken in the laboratory and modeled as thermal equilibrium spectra. Second, an emission-to-absorption technique was used to identify spectral features that were able to yield thermal equilibrium temperatures as opposed to emission from species not in equilibrium with the gases. Third, seeded flames, which yielded thermal equilibrium spectral features, were used with various $H_2$/air mixtures to determine accuracies of measured spectroscopic flame temperatures as compared to Gordon and McBride code calculations of equilibrium gas temperatures. Fourth, temperatures of $H_2/O_2$ seeded flames were measured. Fifth, a hydrocarbon fuel was added to the $H_2$/air mixtures to create sooty flames to assess the applicability of the technique for hypergolic propellant fireball scenarios wherein soot particles were expected to be present.

Knowledge obtained from the modeling efforts and the spectroscopic measurements was then used to generate a preliminary proposal for performing fireball gas temperature and representative particle mass effusion measurements using the WSTF LSHOE test facility.

# 4.0 Phase I: Particle Temperature and Mass Effusion Modeling

## 4.1 Literature Review

### 4.1.1 Previous Modeling Efforts

Theoretical fireball gas temperatures have been estimated using the adiabatic flame temperature limits for various propellant mixtures. Temperature estimates associated with the project PYRO work (Mansfield 1969) and Aerojet General work (Pesante and Nishibayashi 1967) assumed a negligible contribution from convective heat transfer and used only the radiative component to convert heat flux to fireball temperatures. The basis for this assumption was that convective heat transfer was only important at supersonic flow velocities where the Reynolds number is largest. Fireball modeling associated with these and other projects has been performed by assuming adiabatic and blackbody flame emissions (Kite and Bader 1966; Bader, Donaldson, and Hardee 1970). The simplified models used in these projects tended to overestimate the fireball heat flux and temperature compared to the previously measured values for these parameters in the related experimental work and did not address the issue of heat transfer to small particles or mass effusion of particles entrained in propellant fireballs.

Hardee and Larson (1979) modeled the thermal heat flux resulting from $H_2$ fireballs burning in air using an adiabatic flame limit of 2045 K and concluded that significant thermal hazards (third-degree burns) potentially exist from large-scale $H_2$ fireballs ($10^7$ to $10^8$ kg) out to distances of several kilometers associated with transportation and storage accidents involving $H_2$ fuel. Again, the radiative coupling was the predominant heat transfer mechanism considered in this work.

Mass effusion modeling of $PuO_2$ particles injected into a propellant fireball was first performed for the Saturn V vehicle (Williams 1971) using a fireball gas temperature model (Van Nice and Carpenter 1965). More recently, the General Electric Astro Space Division calculated the vaporization of $PuO_2$ in a shuttle fireball based on the mass effusion model developed by Williams (1971) and two different heat flux models developed for the Shuttle (NSTS 08116, Rev. B, 1988). Particle temperatures for all these calculations were based solely on radiative heat transfer with a combustion gas emissivity of 1.0. Results of these calculations (diffusion coefficient and Sherwood number dependence) show appreciable mass effusion of $PuO_2$ particles (10- to 100-$\mu$m diameter) injected into the fireball within the first five seconds.

The thermochemical fireball gas temperature model, developed by Van Nice and Carpenter (1965), yields gas temperatures in the 2700 to 3000 K range for this duration. The particle velocity assumed in the Van Nice and Carpenter work (1965) was the gravitational terminal fall velocity of a particle in the fireball combustion gases.

As the physics of the fireball environment was considered in this work, the validity of using only radiative heat transfer to compute particle temperatures from heat flux models was questioned.[1] This work accounts explicitly for the convective and radiative heat transfer mechanisms in clean and sooty propellant fireballs, and numerically computes the surface temperature of the particles based on the solution to the heat conduction differential equation with a heat flux source term.

### 4.1.2 Previous Temperature Measurements

Thermocouples, heat flux slabs, "Gardon" radiometers, and photography have been used to measure fireball temperatures in previous propellant explosion testing (Pesante et al. 1964; Klein, Moeller, and Fago 1965; Kite, Webb, and Bader 1965; Pesante and Nishibayashi 1967; Mansfield 1969). Pyrometer measurements have also been used assuming an emissivity of 1.0 for blackbody fireball emissions (Mansfield 1969). Because the $LH_2/LO_2$ explosions may have emissivities less than 1.0 (at least for optically thin gaseous fireball streams), the pyrometer measurements are questionable and difficult to apply to other propellant fireball conditions. Also, emissions from chemiluminescent and thermal nonequilibrium species (e.g. hydroxyl radical (OH) production in the reactive zones) in the fireballs are sources of inaccuracies when using single- and two-color optical pyrometers (Gaydon 1974; Warren 1992).

Gas temperatures measured with thermocouples in the PYRO fireball tests ($LH_2/LO_2$) typically gave peak temperatures of 3000 K in the first second of fireball exposure, and frequently a second peak occurred two seconds after the initial blast having a peak value of 2650 K

[1] Private communication with J. Taylor, April 1992 - December 1992.

(Mansfield 1969). Discrepancies (150 to 200 percent) were noted in these data when the radiant heat flux was computed (emissivity of 1.0) from the thermocouple data and compared to the measured heat flux.

Fireball temperatures were measured in the Aerojet General fireball tests ($LH_2/LO_2$) by MidWest Research Institute (MRI) using thermocouples preheated in a balloon filled with an inert gas (Klein, Moeller, and Fago 1965). This technique was used to improve the response time of the thermocouple by initially heating the junction to temperatures slightly below the expected fireball temperature. The typical peak temperatures recorded in these tests ranged from 1000 to 2500 K depending on position in the fireball. The results of these tests for small-scale fireballs indicated that a preheated thermocouple gave a peak temperature that was 500 to 600 K higher than those recorded with unheated thermocouples. MRI speculated that the heat produced from surface oxidation of the thermocouples (tungsten-rhenium) may have driven the junction temperatures artificially high. This oxidation would have occurred after the shock wave broke the gas-filled balloon. Furthermore, MRI reported a potential design problem associated with unequal heating of the two wires with different composition on either side of the thermocouple junction after the balloon broke. All of these problems, plus failure of the preheating circuits for many of their tests, led MRI to conclude that the temperature data were questionable and that many improvements were required to make meaningful temperature measurements in fireballs.

Even in a more controlled environment such as a laboratory, flame temperature measurements made with "traditional" devices such as thermocouples or pyrometers may be inaccurate. For example, turbulent flame temperature measurements can be inaccurate if the devices are not properly compensated for fluctuations caused by the gaseous film properties surrounding the junction (Katsuki, Mizutani, and Matsumoto 1987). This is caused by the junction sampling different flame temperatures (turbulent gases) within times that are short compared to the response time of the thermocouple. In sooty pool fires, special transpiration radiometer designs (Moffat, Hunn, and Ayers 1971), which eliminate the convective heat flux contribution, are required to measure the radiative contribution to the measured temperature signals (Longenbaugh 1985). The historical problems associated with using traditional devices to measure flame and fireball temperatures suggest that new technology is required to accurately measure these temperatures on time scales consistent with the event turbulence.

Spectroscopic techniques have been used in the laboratory for measuring temperatures in flames (Gaydon and Wolfhard 1979) and in the aerospace industry for measuring temperatures of rocket plumes (Sappey and Funk 1991; Tejwani 1992). Therefore, the experimental approach for answering the Phase II objective was to investigate spectroscopic methods for these applications.

## 4.2 Developing the Model

To develop the theoretical simulation model for measuring fireball gas temperatures and mass effusion rates, four specific problems had to be addressed. First, the motion of the particle in a viscous fluid medium was needed to compute the Reynolds and Nusselt numbers which were needed for the convective heat transfer and convective evaporation calculations. Second, the total heat transfer to the particle was computed from the absorption of the convective and the radiative heat components. Third, the time dependent surface temperature of the particle was calculated from a numerical solution to the heat diffusion equation. Fourth, the convective

evaporation and mass effusion rate of the particle was determined for a two-second exposure in the fireball.

### 4.2.1 Particle Motion

The particle was modeled as a rotating sphere moving at a subsonic velocity in a viscous water vapor medium. This gaseous fluid medium was assumed to be representative of $LH_2/LO_2$ fireballs and adequate for the initial representation of hypergolic and $LH_2/LO_2$ mixtures. Furthermore, because there were no physical constraints on the system to prevent rotation, it was reasonable to assume that there would be some angular momentum imparted to the particle after a propellant explosion. The rotation rate here was assumed to be small enough so as not to induce turbulence, but sufficiently large enough to yield an isotropic temperature distribution on the surface of the sphere. The spherical particle geometry was chosen for convenience because the particles from an intact impact explosion had not been adequately characterized to dictate other shapes.

The motion of a smooth sphere in an infinite stationary nonrotating viscous fluid (water vapor) of uniform temperature distribution can be analytically derived from the Bernoulli dynamic pressure and Stoke's law for a sphere in a viscous medium (Equation 1):

$$m \frac{dv}{dt} = 6\pi\eta_f r_s v_r + \frac{1}{2}\rho_s v_r^2 4\pi r_s^2$$

where an analytical solution is given by,

$$v(t) = v_f - \frac{v_f\, e^{-t/\tau}}{1 + K\, v_f\, (1 - e^{-t/\tau})} \qquad (1)$$

$$v_r = v_f - v$$

$$\tau = \frac{m}{6\pi\eta_f r_s} = \textit{viscous time constant}$$

$$K = \frac{2 r_s \rho_f}{\eta_f}$$

and

| | | |
|---|---|---|
| $m$ | = | sphere mass |
| $\eta_f$ | = | empirical fluid viscosity evaluated at the fluid film temperature (Appendix A) |
| $r_s$ | = | sphere radius |
| $v_r$ | = | particle velocity relative to the fluid reference frame |
| $\rho_s$ | = | particle mass density |
| $v(t)$ | = | time dependent velocity |
| $v$ | = | particle velocity with respect to a fixed spatial laboratory coordinate |
| $v_f$ | = | fluid stream velocity |
| $\rho_f$ | = | film mass density defined as the fluid density adjusted by the film temperature (Appendix A) |

The analytical solution for the time dependent velocity, $v(t)$, in fixed spatial coordinates is solved by integration. The fluid stream velocity, $v_f$, is assumed to be constant in time. The value of 9.6 g/cm$^3$ for mass density of the particle was chosen corresponding to that of $PuO_2$. Since the fluid viscosity, $\eta_f$, is a function of the fluid film temperature surrounding the particle, an empirical polynomial function for water vapor viscosity as a function of temperature was implemented (Yaws 1977) (Appendix A). Note that the analytical solution of Equation 1 is valid only for laminar flow. This was a reasonable assumption for the model since the region of interest for the particle velocity was 1500 cm/s over a few seconds time duration. The boundary layer surrounding the particle was considered to be a film whose temperature is the average of the sphere surface temperature $T_s$ and the undisturbed fireball gas temperature $T_g$ at infinity. The gravitational buoyancy force was not included in this model because the magnitude of this force was not significantly compared to the other forces considered . Additionally, the gravitational buoyancy force requires a vector summation with the other forces to determine the acceleration vector of the particle. This simplified model did not specify the velocity vector of any particular fluid stream jet.

### 4.2.2 Convective and Radiative Heat Transfer

To determine the sphere convective energy gain, the Reynolds number, $R_e$, a function of the relative sphere/gas film velocity and sphere dimension, was computed along with the Prandtl number, $P_r$, which is an intrinsic function of the fluid evaluated at the fluid film temperature. From these two values, the Nusselt number, $N_u$, was computed. The fluid mass density, $\rho_f$, is based on the mole fractions of fireball combustion gases for stoichiometric conditions consistent with the fireball temperatures. These mole fractions and fireball gas temperatures were calculated using the Gordon and McBride Code (Gordon and McBride 1971). As shown in Appendix A, the film mass density was the fluid density adjusted by the film temperature (the temperature of the gaseous fluid in contact with the particle). A molecular weight of 18.0 (corresponding to water) was used to represent the average molecular weight of the fireball gases. The empirical thermal conductivity, $\kappa_f$, was computed as a function of fluid film temperature (Appendix A), $T_f$, using the formula given in Yaws (1977). The total convective heat flux, $Q_f$, is then given by the first term in Equation 2. The second term reduces the total heat flux by the heat of sublimation per unit area for an incremental mass loss as determined by the mass effusion rate (Equation 8 below).

$$Q_f = \frac{N_u \kappa_f (T_f - T_s)}{2r_s} + \frac{H_v \dot{m}}{4\pi r_s^2},$$

where

$$N_u = 2.0 + 0.6 R_e^{1/2} P_r^{1/3}; \qquad (2)$$

$$R_e = \frac{2 \rho_f v_r r_s}{\eta_f};$$

$$P_r = \frac{C_{pf} \eta_f}{\kappa_f}$$

and

| | | |
|---|---|---|
| $Q_f$ | = | total convective heat flux; |
| $\kappa_f$ | = | empirical thermal conductivity evaluated at the fluid film temperature (see Appendix A); |
| $T_f$ | = | fluid film temperature (gas in contact with the particle); |
| $T_s$ | = | sphere surface temperature; |
| $R_e$ | = | Reynolds number; |
| $P_r$ | = | Prandtl number; |
| $N_u$ | = | Nusselt number; |
| $C_{pf}$ | = | empirical isobaric specific heat of fireball gas (Appendix A); |
| $H_v$ | = | heat of sublimation of particle material (per unit mass); |
| $\dot{m}$ | = | mass loss rate as given by Equation 8 (below). |

Note: The heat of fusion (melting) was considered negligible.

For the particle speeds and sizes modeled, the Reynolds number is small, therefore the expression for the Nusselt number is valid. As the sphere accelerates and approaches the fireball speed, the Nusselt number approaches its theoretical value of 2. This nonzero value allows the sphere to continue receiving heat conductively, even after reaching terminal velocity, as long as the fluid film temperature exceeds the surface temperature of the sphere.

Radiative heat transfer is a function of the fireball gas and sphere surface temperatures and the intrinsic fireball gas and sphere emissivities, $\epsilon_g$ and $\epsilon_s$, respectively. The value of 0.8 was chosen for the sphere emissivity based on the properties of $PuO_2$ (General Electric Space Systems Division 1985). The fireball gas emissivity values were chosen over a range of 0.2 for a clean burning fireball and 0.8 for a soot-contaminated fireball. The net radiative heat flux of the sphere is given by Equation 3:

$$Q_r = \sigma \epsilon_s(\epsilon_g T_g^4 - T_s^4) \quad (3)$$

where

| | | |
|---|---|---|
| $Q_f$ | = | total radiative heat flux |
| $\sigma$ | = | Stefan-Boltzman constant |
| $\epsilon_s$ | = | sphere emissivity |
| $\epsilon_g$ | = | fireball gas emissivity |
| $T_g$ | = | fireball gas temperature at infinity |

and Kirchoff's law applies to the relationship between the absorptivity and emissivity of the sphere.

### 4.2.3 Conductive Heat Transfer in the Particle

The temperature at the surface of the sphere, $T_s$, can be determined from the time-dependent solution to the spherically symmetric case of the heat diffusion equation with a surface heat flux source term (Equation 4):

$$\nabla^2 T(r,t) + \frac{1}{\kappa_s r^2}\frac{\partial}{\partial r}\left(r^2(Q_f + Q_r)\right) = \frac{1}{D_s}\frac{\partial T(r,t)}{\partial t}, \quad (4)$$

where

$$D_s = \frac{\kappa_s}{\rho_s C_{ps}}$$

and

$T(r,t)$ = temperature of sphere as a function of radius $r$ and time $t$;
$D_s$ = thermal diffusivity constant of sphere.

Here, the implied radial dependence of the source terms $Q_f$ and $Q_r$ is simply $1/r^2$ except across the particle surface ($r=r_s$) where these fluxes are completely absorbed. Thus, the entire source term is non-zero only at $r=r_s$.

Solving this differential equation for the temperature was done numerically for each time iteration step in the simulation modeling using a radial increment given by 4 times the square root of the product of the diffusivity constant and time-step increment. The temperature was then evaluated at the particle surface as $T_s=T(r_s,t)$.

### 4.2.4 Mass Effusion of Particle

The model for particle mass effusion was developed based on a relationship for convective evaporation of particles in gas streams. This relationship was also applicable for diffusional mass effusion because of the limiting value for the convective Sherwood number used in the relationship.

To address the diffusion of the evaporated material into the fireball gas stream, an estimate of the diffusion coefficient, $D_{fs}$, was made using a binary gas diffusion theory (Reid, Prausnitz, and Sherwood 1977). This binary diffusion coefficient is calculated from a dimensionless collision integral. The collision integral is based on the Lennard-Jones 12/6 potential which gives the intermolecular potential energy, $V(r)$, as a function of distance, r, between two molecules (Equation 5):

$$V(r) = 4\,\chi_{fs}\left[\left(\frac{\sigma_{fs}}{r}\right)^{12} - \left(\frac{\sigma_{fs}}{r}\right)^{6}\right] \quad (5)$$

where $\sigma_{fs} = \frac{\sigma_f + \sigma_s}{2}$

$$\chi_{fs} = (\chi_f\,\chi_s)^{1/2}$$

and

| | | |
|---|---|---|
| $V(r)$ | = | intermolecular potential energy |
| $\sigma_f$ | = | characteristic Lennard-Jones length for fireball gas molecules |
| $\sigma_s$ | = | characteristic Lennard-Jones length for sphere molecules |
| $r$ | = | distance between two molecules |
| $x_f$ | = | characteristic Lennard-Jones energy for fireball gas molecules |
| $x_s$ | = | characteristic Lennard-Jones energy for sphere molecules |

For binary gas systems, the expressions for $\chi_{fs}$ and $\sigma_{fs}$ (i.e. the fireball-sphere gas system) are valid for low pressures. The collision integral, $\Omega_D$, for the Lennard-Jones potential is given by Equation 6:

$$\Omega_D = \frac{A}{T^{*B}} + \frac{C}{e^{DT^*}} + \frac{E}{e^{FT^*}} + \frac{G}{e^{HT^*}}$$

$$A = 1.06036 \qquad B = 0.15610$$

$$C = 0.19300 \qquad D = 0.47635$$

$$E = 1.03587 \qquad F = 1.52996 \qquad \textbf{(6)}$$

$$G = 1.76474 \qquad H = 3.89411$$

$$T^* = \frac{k_B\, T_f}{\chi_{fs}}$$

where

| | | |
|---|---|---|
| $\Omega_D$ | = | collision integral |
| $k_B$ | = | Boltzman constant |

The parameters A through H in Equation 6 have been determined empirically. From the collision integral, $\Omega_D$, the diffusion coefficient for the binary system is calculated by Equation 7:

$$D_{fs} = 1.858 \times 10^{-3}\, T_f^{3/2}\, \frac{[(M_f + M_s) / (M_f M_s)]^{1/2}}{P_{atm}\, \sigma_{fs}^2\, \Omega_D} \qquad \textbf{(7)}$$

where

| | | |
|---|---|---|
| $D_{fs}$ | = | diffusion coefficient for the binary system |
| $M_f$ | = | molecular weight of the fireball gas |
| $M_s$ | = | molecular weight of the sphere |
| $P_{atm}$ | = | atmospheric pressure |

The convective mass effusion rate (Orr 1966) is given then by Equation 8:

$$-\frac{dm}{dt} = \frac{2\,\pi\,M_s\,D_{fs}\,r_s\,(P - P_p)}{R\,T_s}\,[(2 + a\,R_e^{1/2}\,S_c^{1/3})]$$

where $P = 10^n\,e^{-\frac{64700}{T_s}}$

$a \simeq 0.55 - 0.60$

$S_c = \frac{\eta_f}{\rho_f\,D_{fs}}$ **(8)**

and

| | | |
|---|---|---|
| $-dm/dt$ | = | convective mass effusion rate |
| $P$ | = | equilibrium vapor pressure of the particle material |
| $P_p$ | = | partial pressure of the particle material in the ambient gas |
| $R$ | = | molar gas constant |
| $S_c$ | = | Schmidt number |

The vapor pressure as function of temperature is obtained from Williams (1971), where "n" in the exponent is 13.5 to 14.5 in cgs units. A value of 14 was used in this simulation.[1]

The expression in brackets is the Sherwood number which is computed from the Reynolds and Schmidt numbers, $R_e$ and $S_c$ respectively. For this investigation, the partial pressure of $PuO_2$ in the fireball gas stream was assumed to be negligible based on limited amounts of the material initially injected into the fireball. Note, a mass effusion relationship[2] derived from the steady state solution to the diffusion equation with a finite boundary cutoff for zero vapor density can be shown to be nearly equivalent to Equation 8 for the small Sherwood numbers considered in this work. A more rigorous treatment[2] explicitly using momentum exchange between the flowing fireball gas and the evaporating particle vapor density is required to refine the mass effusion rates at low velocities ($< 10$ cm/s).

### 4.3 Model Execution

The model is a time dependent simulation of a sphere moving through a viscous fluid. A time increment of 1 $\mu$s was chosen because it is much smaller than the viscous time constant and the heat/mass diffusion time constants. For each time step, both the radiative heat transfer (from the gas temperature at infinity) and the convective heat transfer (from both film temperature and relative gas/sphere motion) were computed. Both heat transfer gains were summed after subtracting an incremental heat of sublimation from the previous iteration. The surface temperature of the sphere was determined by numerically solving the heat conduction differential equation with the heat flux source term.

---

[1] Private communication with J. Taylor, April 1992 - December 1992.

[2] Private communication with J. Taylor, May 1993.

The simulation was terminated when a maximum exposure duration of 2 s was exceeded or the particle was diminished to less than 5 percent of the initial mass.

## 4.4 Results

The model of the mass effusion of $PuO_2$ particles entrained in propellant fireball environments was evaluated to assess the sensitivity of the particle mass effusion to parameters such as flame temperature, combustion gas emissivity, particle size, particle emissivity, and relative particle velocity. Previous calculations assumed the radiative process to be the predominant heat transfer mechanism for these fireballs, but by modeling all the heat transfer processes, it was shown that the convective heat transfer is equally important for particles having diameters less than 1000 $\mu$m entrained in subsonic flows. By modeling the time dependent heat flow within the sphere, a more accurate characterization of the surface temperature for large particles (100- to 1000-$\mu$m diameter) was achieved.

An intact impact of a launch vehicle within a few seconds after liftoff could cause an accident scenario in which sensitive radioactive payload materials ($PuO_2$ or uranium dioxide ($UO_2$)) are injected into the propellant fireball. The initial particles' sizes of interest are those having diameters less than 1000 $\mu$m, because it is demonstrated that these particles have the potential for becoming entrained and dispersed in the fireball gases. It is particularly important to track particles in the 3- to 10-$\mu$m-diameter range as these particles are respirable and have the potential for being carried in the wind. Therefore, this modeling work focused on the mass effusion properties of $PuO_2$ particles having diameters in the 3- to 10-$\mu$m-diameter range after being exposed to fireball events.

A typical propellant fireball for the model was constructed based on the observations of previous vehicle accidents and measurements of propellant fireball conditions. The fireballs associated with previous PYRO's testing (Mansfield 1969) yielded gas velocities ranging from 3000 to 12 000 cm/s. Analysis of the Titan 32D accident[1] provided other information as to the magnitude of a typical fireball gas stream velocity (1500 cm/s). Therefore, 1500 cm/s was selected as a representative subsonic velocity for this modeling work. Gas stream velocities below 1500 cm/s were considered most important for this work since the mass effusion mechanisms are critically dependent on the magnitude of the convective parameters at the lower velocities and the transition to diffusional evaporation.

The temperatures of the typical propellant fireballs were bounded by the adiabatic flame temperatures computed, and the gas stream emissivities were estimated based on clean (emissivity = 0.2) and sooty (emissivity = 0.8) fireball conditions. This allowed the model to simulate propellant fireballs ranging from cryogenic $LH_2/LO_2$ mixtures to hypergolic fuel/oxidizer mixtures.

The model was run with fireball gas temperatures of 1700 to 3000 K, gas stream velocity of 1500 cm/s, sphere emissivity of 0.8, and fireball emissivities of 0.2 and 0.8. Appendix A lists the values of various other physical properties and empirical relationships used in the model calculations.

---

[1] Private communication with J. Taylor, April 1992 - December 1992.

### 4.4.1 Adiabatic Flame Temperature Calculations

Adiabatic flame temperatures for various stoichiometric mixtures of the fireball constituents were calculated and used as lower and upper temperature bounds for the particle mass effusion process. The expected flame temperatures for various propellant mixtures were calculated using the Gordon and McBride Code (Gordon and McBride 1971). These calculations were performed for both the fuel rich mixtures and the stoichiometric mixtures. These calculations also provided a benchmark for assessing the validity of the experimental temperature measurements as a function of propellant mixtures.

The results obtained from the Gordon and McBride code calculations for the various propellant mixtures are given in Table 1. The mixtures are expressed as fuel weight percent and as equivalence ratio. An equivalence ratio is the ratio of fuel to oxidizer divided by the ratio of fuel to oxidizer necessary for the complete conversion of reactants to products. A stoichiometric mixture has an equivalence ratio of 1.0 by definition. These data indicate adiabatic flame temperatures as high as 3080 K for stoichiometric $LH_2/LO_2$ fireballs to as low as 1400 K for a fuel rich mixture of $H_2$ and air. The selected range for the particle temperature and mass effusion modeling extended from 1700 to 3000 K for the particles entrained in the fireball gas streams.

**Table 1**
Gordon and McBride (1971) Adiabatic Flame Temperatures

| Fuel and Oxidizer Combinations | Equivalence Ratio | Fuel Percent | Flame Temperature (K) |
|---|---|---|---|
| $H_2[O_2]$[a] | 1 | 11.2 | 3080 |
| | 2 | 20.1 | 2830 |
| | 5 | 38.6 | 1770 |
| $H_2$[Air][a] | 1 | 2.9 | 2380 |
| | 2 | 5.5 | 2060 |
| | 5 | 12.8 | 1400 |
| $H_2/MMH[O_2]$[a] | 1 | 33.3 | 3080 |
| | 5 | 71.4 | 1640 |
| $H_2/MMH[O_2/N_2O_4]$[a] | 1 | 28.0 | 3010 |
| | 5 | 66.0 | 1610 |
| $H_2/MMH[Air/N_2O_4]$[a] | 1 | 17.3 | 2780 |
| | 5 | 51.2 | 1480 |

[a]Oxidizers used are listed in brackets

### 4.4.2 Mass Effusion Calculations

Typical results of the mass effusion modeling for the three sizes of $PuO_2$ particles injected into a fireball at gas temperatures of 2500 K (gas emissivity = 0.8) are plotted in Figures 1 through 3. The plots show the magnitude ($W/cm^2$) of the convective and radiative heat components as a function of time after injection of a particle at rest into the fireball gas stream. Note that an initial temperature of 1200 K was selected based on the operational temperature of the material (General Electric Space Systems Division 1985). In all cases the

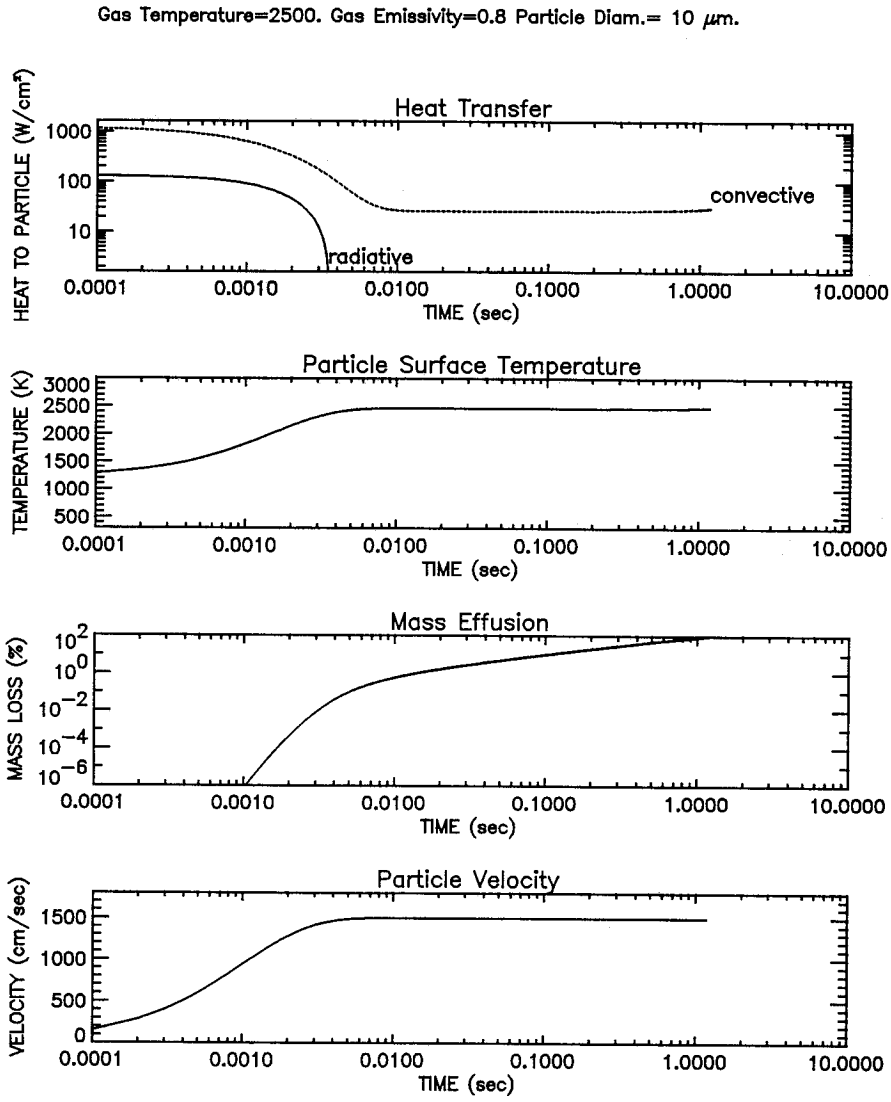


**Figure 1**
Mass Effusion Modeling of a 10-μm-diameter Particle in a Propellant Fireball (Fireball Gas: Velocity = 1500 cm/s, Emissivity = 0.8, Temperature = 2500 K)

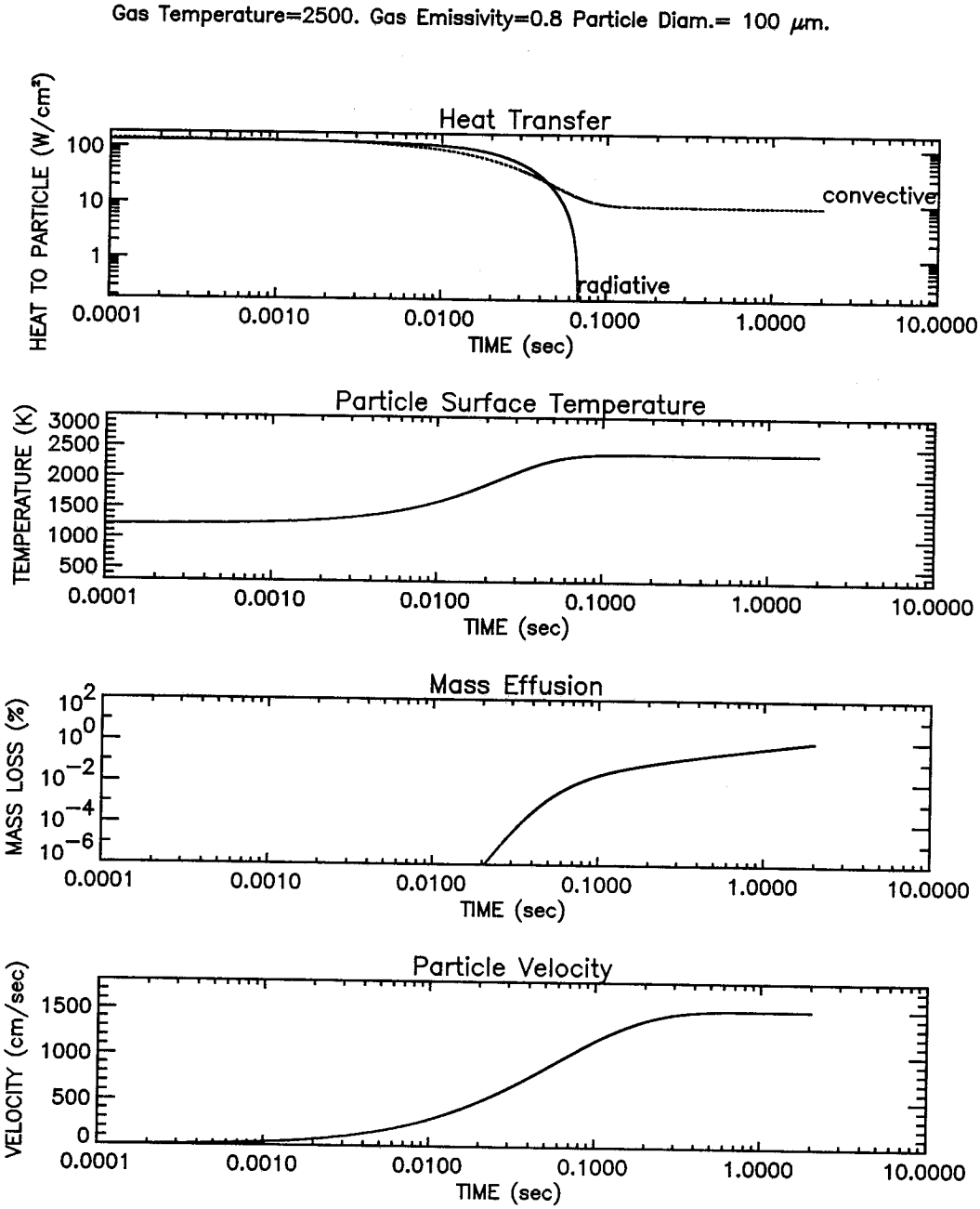


**Figure 2**
Mass Effusion Modeling of a 100-$\mu$m-diameter Particle in a Propellant Fireball (Fireball Gas: Velocity = 1500 cm/s, Emissivity = 0.8, Temperature 2500 K)

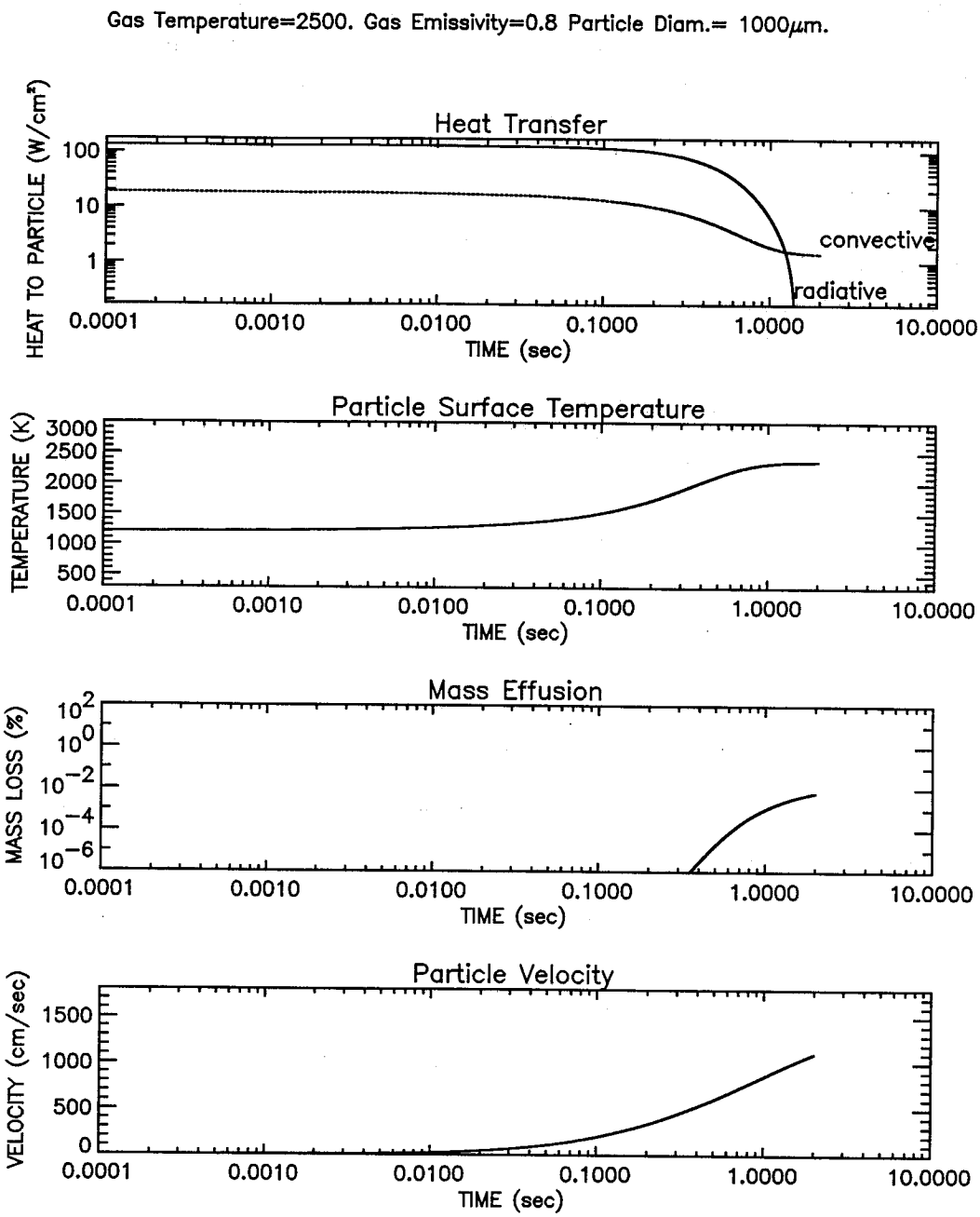


**Figure 3**
Mass Effusion Modeling of a 1000-$\mu$m-diameter Particle in a Propellant Fireball (Fireball Gas: Velocity = 1500 cm/s, Emissivity = 0.8, Temperature = 2500 K)

convective heat transfer is at least comparable (or an order of magnitude larger for the 10-$\mu$m-diameter particles) to the radiative component during the initial acceleration of the particle. As the particle velocity (also shown in Figures 1 through 3) approaches gas stream velocity and the surface temperature rises, the convective heat transfer diminishes. By this time, the particle surface temperature has achieved a temperature determined by the heat balance between the convective and radiative components. Note, the corresponding values of the heat transfer components which are lower than the three-cycle logarithmic range or negative are not plotted on the logarithmic scales of Figures 1 through 3.

The mass effusion process, plotted as the percentage mass loss of the original particle mass, is shown also in Figures 1 through 3. For the 1000-$\mu$m-diameter particle, the percentages are low, but it should be remembered that a 0.01-percent mass loss of a 1000-$\mu$m-diameter $PuO_2$ particle is equivalent to completely vaporizing and effusing one-hundred 10-$\mu$m-diameter particles in the fireball.

Table 2 summarizes the results of the mass effusion for the $PuO_2$ particles as a function of particle size, fireball flame temperatures, and gas emissivities. This table gives the particle percent mass loss for a two-second exposure in a fireball with gas stream velocities of 1500 cm/s. For the small particles, the mass effusion simulation was terminated when the particle percent mass loss reached 95 percent of the initial particle mass.

**Table 2**
Mass Effusion (Percent Mass Loss) of $PuO_2$ Particles in Propellant Fireballs Terminated by Two-Second Simulation or Complete Evaporation

| Size ($\mu$m) | Mass ($\mu$g) | $\epsilon_g$[a] | Flame Temperatures (K) 1700 | 2000 | 2200 | 2500 | 3000 |
|---|---|---|---|---|---|---|---|
| | | | Mass Effusion (Percent Mass Loss) of $PuO_2$ Particles | | | | |
| 10 | 0.00503 | 0.2 | 3.3E-04 | 0.11 | 2.2 | 75 | 100 |
| 100 | 5.03 | 0.2 | 6.5E-08 | 1.3E-05 | 2.1E-04 | 6.4E-03 | 0.51 |
| 1000 | 5030 | 0.2 | 0.0 | 0.0 | 0.0 | 1.5E-07 | 9.8E-05 |
| 10 | 0.00503 | 0.8 | 5.7E-04 | 0.23 | 5.2 | 100 | 100 |
| 100 | 5.03 | 0.8 | 2.4E-06 | 9.7E-04 | 0.022 | 0.97 | 72 |
| 1000 | 5030 | 0.8 | 0.0 | 2.6E-06 | 9.5E-05 | 6.6E-03 | 1.0 |

[a] $\epsilon_g$ = emissivity of fireball gas

The results of all the modeling work are plotted in Appendix B as a function of gas temperature, gas emissivity, and particle size.

### 4.5 Discussion

The results of the particle temperature modeling for the entrainment of small $PuO_2$ particles (10- to 1000-$\mu$m diameter) in propellant fireballs indicate the particle surface achieves a temperature determined by the detailed heat balance. This temperature is achieved within the two-second exposure for all cases and conditions considered in this work. For a gas emissivity of 0.8, this temperature is very nearly equal to the gas flame temperature. The rapid heating of the particles is driven by both the convective and radiative heat transfer components during the initial acceleration of the particles in the hot gas streams.

The results of the mass effusion modeling (Table 2) indicate that for fireball temperatures below 2000 K, the mass losses are limited to less than 0.1 ng per particle for particles up to 1000 $\mu$m in diameter. At 2500 K ($\epsilon_g = 0.8$), the mass losses increase to the 0.3 $\mu$g per particle for the 1000-$\mu$m-diameter particles, and at 3000 K the mass losses achieve a level of approximately 50 $\mu$g per particle (1000-$\mu$m diameter) within a fireball exposure duration of 2 s.

The results of this simulation clearly demonstrate the strong dependence of the mass effusion (mass loss per particle) process on the flame temperature, gas emissivity, convective parameters and particle size. With the exception of the detailed accounting for the convective, radiative, and conductive heat transfer mechanisms, this simulation is similar to that reported in the Ulysses FSAR (General Electric Astro Space Division 1990; Williams 1971). No attempt was made to make a detailed quantitative comparison with the Ulysses FSAR results, but qualitatively the current calculations indicate comparable mass effusion (within an order of magnitude) as a function of fireball gas temperature for the similar size particles. The difference in the detailed accounting of the heat transfer mechanisms primarily affects the exposure time required to achieve the same level of mass effusion.

## 5.0 Phase II: Temperature Measurements Using Spectroscopy

Two spectroscopic techniques were used to investigate temperature measurements of $H_2$ flames: emission (with modeling) and simultaneous emission and absorption. The emission technique was used on the prominent UV feature of a $H_2/O_2$ flame. The emission and absorption technique was used on this feature of a $H_2/O_2$ flame and also on near-infrared (IR) features of this type of flame. This technique also was used on the visible-wavelength atomic metal features of flames ($H_2/O_2$ and $H_2$/air) doped with metal salts and on a propane-enriched $H_2$ flame which provided heavy sooty flame conditions.

### 5.1 Theory of Spectroscopic Techniques

Atoms and molecules can absorb light and be excited (energized) by various means to emit light at many different and discrete wavelengths. For atoms, these emissions correspond to transitions from excited states of their electrons to states of lower electron energy. Similar electronic transitions are observed for molecules, but because of the additional vibrational and rotational degrees of freedom, the energy of each electronic level is further subdivided by quantization of vibrational and rotational energy as illustrated in Figure 4. This subdivision

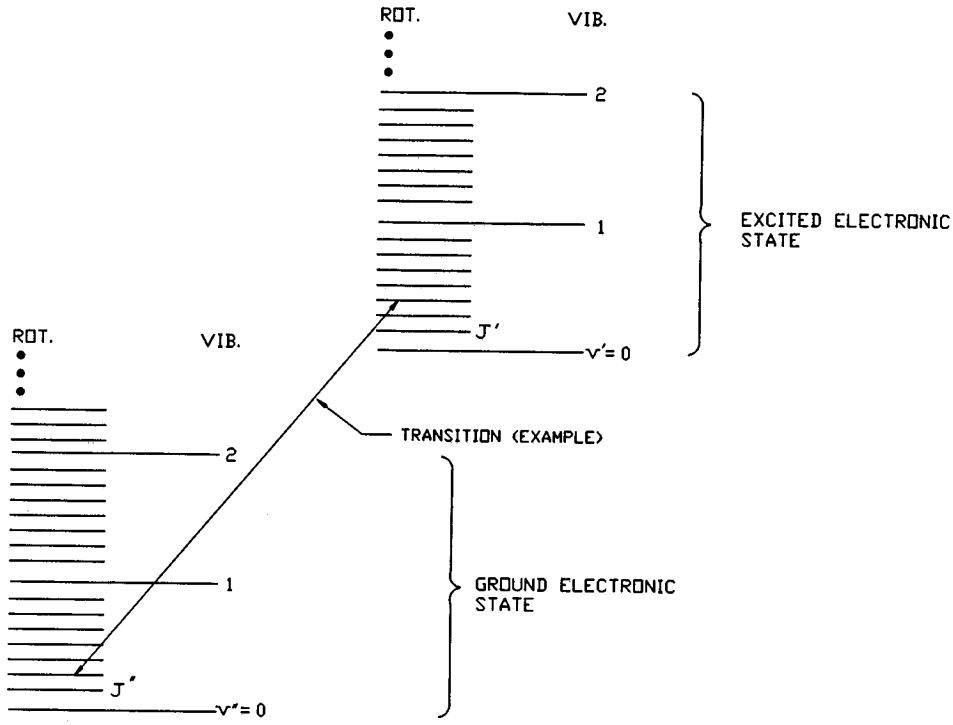


**Figure 4**
Typical Electronic, Vibrational, and Rotational Molecular Energy Levels

means that many discrete transition wavelengths are possible both between and within each electronic energy level. Note that the energy of a molecule is partitioned not just into electronic and kinetic energy as is the case with atoms, but also into rotational and vibrational energy.

Any group of molecules and atoms in thermal equilibrium with each other and with a thermal reservoir characterized by a temperature will have the available energy distributed equally among the available degrees of freedom. The distribution of energy over the ensemble of atoms and molecules within each degree of freedom is then characterized by a Boltzman distribution, i.e. for a state of energy E. The relative number of particles in that state is proportional to $e^{-E/k_BT}$ where $k_B$ is the Boltzman constant, and T is the temperature that characterizes the distribution. For thermal equilibrium, this temperature is the same for all degrees of freedom with the result that overall energy distribution can be characterized by a single temperature. Conversely, nonequilibrium ensembles cannot be in general characterized by a single temperature for all degrees of freedom, nor can the energy distribution for any particular degree of freedom be expected to be Boltzman.

### 5.1.1 Temperature Dependence of Emission Spectra

The intensity of light emission from a gas in equilibrium has contributions from spontaneous emission and stimulated emission. The intensity that reaches a detector is decreased by stimulated absorption that occurs within the sample gas and by other absorptions from materials between the emitter and the detector. For flames, spontaneous emission dominates the process, and for optically thin flames, absorption within the flame may be neglected.

The rate of spontaneous emission from a molecule or an atom corresponding to a transition from an upper state of energy, $E_u$, to a lower state of energy $E_l$ $\{\nu_{ul}=(E_u-E_l)/h$ (h = Planck constant)$\}$ is given by the Einstein constant, $A_{ul}$, (transitions per unit time) associated with the particular transition. The rate of stimulated emission is given by the product of the light energy density, $\rho(\nu)$, (energy per unit volume per unit frequency interval) and the Einstein constant, $B_{ul}$. Similarly defined is the Einstein constant, $B_{lu}$, for the stimulated absorption rate. The total rate of transitions from one state to another per unit time per unit volume is given by Equation 9:

$$\text{Total transition rate} = N_u A_{ul} + \rho(\nu)(N_u B_{ul} - N_l B_{lu}) \tag{9}$$

where

| | | |
|---|---|---|
| $N_u$ | = | number density of upper state |
| $A_{ul}$ | = | Einstein constant for spontaneous emission |
| $\rho(\nu)$ | = | light energy density |
| $B_{ul}$ | = | Einstein constant for stimulated emission |
| $N_l$ | = | number density of lower state |
| $B_{lu}$ | = | Einstein constant for stimulated absorption |

The number density in the upper state can be related to the overall number density of the emitting species ($N_{total}$) by the Boltzman factor (Equation 10):

$$N_u = \frac{N_{total}}{Q(T)} g_u \exp\left[-\frac{E_u}{k_B T}\right] \tag{10}$$

where

| | | |
|---|---|---|
| $N_{(total)}$ | = | total number density of the emitting species |
| $g_u$ | = | degeneracy of the upper energy state |
| $Q(T)$ | = | partition function (i.e. the sum of Boltzman factors over all the states which depends only on the temperature) |

A similar formula holds for relating $N_l$ to $N_{total}$.

Absorption and stimulated emission contributions must be integrated over the line of sight through the flame to the detection instrument. This requires a detailed knowledge of the species density and light energy density. If these densities are sufficiently low and path lengths through the flame are sufficiently small, absorption of the flame can be negligible compared to spontaneous emission. Additionally, stimulated emission is proportional to absorption by a factor of $\exp(-h\nu_{ul}/k_B T)$ since $g_l B_{lu} = g_u B_{ul}$. For transitions at the visible and higher frequencies, $h\nu/k_B T$ is greater than 5 for temperatures less than 4000 K indicating that stimulated emission also can be neglected whenever absorption is neglected.

The formula for spontaneous emission is given by multiplying the first term in Equation 9 by the energy per transition and using Equation 10, which results in Equation 11:

$$E(\nu,T) = \frac{N_{total}(T)}{Q(T)} g_u \exp\left(-E_u/k_B T\right) A_{ul} h\nu_{ul} \tag{11}$$

where

| | | |
|---|---|---|
| E | = | radiant power per unit volume |
| $h\nu_{ul}$ | = | energy per transition |

The OH molecule emits prominently at approximately 306 nm wavelength. Initial attempts to measure a laboratory flame temperature focused on measuring and modeling these emissions as spontaneous emission. To obviate the need for supplementary measurements of OH number density, the ratio of the intensities of the transitions were modeled. Since the emissions were from the same sample flame, the number density and partition function cancel out the ratio, and temperature can be calculated or determined when accurate knowledge of $E_u$, $g_u$, $A_{ul}$, and $\nu_{ul}$ is known.

The spectrometer measures a finite wavelength interval in which intensities from various parts of that interval are weighted differently. This weighting is called the slit function of the spectrometer, and it can span the wavelengths of many OH transitions. For the measurements reported herein, the slit function taken to be triangular and its spectral width were estimated by fitting the calculated line profiles of the OH emissions to the bands of the experimental spectrum. Groups of transitions were ratioed as the ratio of sums over the calculated intensities of transitions in a wavelength interval weighted with the instrument slit function. The formula for the calculated emission, which was compared to the measured emission, is given by Equation 12:

$$E_{rel}(\nu,T) = \frac{1}{N}\sum_{\nu'} s(\nu-\nu')E(\nu',T) \qquad \textbf{(12)}$$

where

| | | |
|---|---|---|
| $E_{rel}$ | = | relative emission (calculated) |
| $N$ | = | arbitrary normalization |
| $s(\nu-\nu')$ | = | slit function (centered at a frequency $\nu$ and the summation is over its width) |
| $E(\nu',T)$ | = | given by Equation 11 |

### 5.1.2 Temperature Dependence of the Emission-to-Absorption Ratio

The equilibrium emission-to-absorption relation has a known temperature dependence. For a homogeneous gas sample in thermal equilibrium, the emission intensity, $E(\lambda)$, at a given wavelength, $\lambda$, is proportional to the absorptivity, $1-\tau$, of the gas and the Planck blackbody function, $B(T,\lambda)$. The relative emission intensity compared to its intensity at, $\lambda_0$, is given by Equation 13:

$$\frac{E(\lambda)}{E(\lambda_0)} = \frac{[1-\tau(\lambda)]B(T,\lambda)}{[1-\tau(\lambda_0)]B(T,\lambda_0)} \qquad \textbf{(13)}$$

This equation is based on Kirchoff's law that for a gas in thermal (and radiative) equilibrium, the emissivity, $\epsilon$, of the gas is equal to its absorptivity, $1-\tau$. If this is a valid assumption, then the simultaneous measurement of the relative emission and the transmissivity, $(\tau)$, from the same sample can lead to a measurement of the temperature from the best fit of the blackbody function to the above equation. Additionally, if the same instrument is used for both emission and absorption measurements, the influence of the instrument resolution (i.e. slit function) is negligible in the ratio to a close approximation. Taking both the emission and absorption

spectra at the same time was closely approximated by rapidly taking several sequentially interlaced spectra and then averaging every other one over the time period of interest.

For particle-laden flames, scattering, absorption, and emission of the particles must be taken into account. The emission and absorption of the gaseous constituents must be measured in a way that excludes contributions from the particles in order to apply Kirchoff's law to the gas. If the particulate contribution to the total measured absorptivity is a broad continuum and the gaseous contribution is dominated by distinct, sharp atomic and molecular absorptions above the continuum, then the particulate contribution can be easily subtracted to a close approximation by subtraction of the broad, featureless underlying extinction as a background baseline leaving only the distinct atomic and molecular spectral features. A similar subtraction for the emission spectrum also can be done if necessary. The applicability of this approach for temperature measurement depends on the particle size regime and composition. For soot particles, overall optical extinction (absorption plus scattering) seen in transmission measurements is such a featureless continuum which gradually increases toward the visible-UV and usually has a broad peak in the UV. Hot soot particles emit light also as a featureless continuum (nearly graybody) in the visible spectral region.

Experimental investigation was required to verify that these assumptions hold for a given flame condition. This investigation used a propane-enriched $H_2/O_2$ flame seeded with sodium (Na), lithium (Li), and potassium (K) salts. The broad soot emission-to-absorption features were subtracted as a baseline from the atomic features of the metal salts. The emission and absorption of the metal atoms were then used with Equation 13 to calculate a gas temperature. The broad-soot emission was fitted to a blackbody emission temperature, i.e. the soot emissivity was assumed to be unity. Comparison of the two experimental temperatures to each other and to calculated temperatures gave a good indication of the accuracy of the technique (Section 5.3.6).

This is a line-of-sight technique. As such, it has the disadvantage of yielding a spatial average temperature. Since flames are generally cooler at the outer edges, the resulting temperatures are expected to be lower than the maximum temperatures of the flames (Gaydon and Wolfhard 1979). The difference in temperatures depends on the actual flame conditions. This disadvantage can be overcome by making several lines-of-sight measurements and using well-established tomographic inversion techniques to calculate the spatial dependence of the flame temperature. The simplest of these techniques assumes an axial symmetry of the gas or flame spatial distribution.

Inaccuracies in the technique may occur from possibly measuring a temperature that is too low which is due to the cooler gases at the edge of the flame. Inaccuracies may also occur from measuring emission dominated by the hotter parts of the flame nearest the detection system (Gaydon and Wolfhard 1979). This near-side radiation will not be absorbed by the flame as much as the background light source which measures absorption throughout the flame. This could increase the emission-to-absorption ratio which would have the effect of indicating a temperature that is too high. Thus, if absorption is dominated by the cool outer portions of the flame, and emission is dominated by the hot inner portions, the two effects tend to cancel. The final accuracy of the technique must be corroborated independently for any given flame conditions. Comparison to calculated flame temperatures has been the traditional method of this corroboration in the past, and it is used here as well (Section 5.3.4).

## 5.2 Laboratory Measurements

The experimental setup for the simultaneous measurement of emission and absorption is depicted in Figure 5. A tungsten-halogen lamp (quartz envelope) was used as the light source for the absorption (transmissivity) measurement in the UV. Visible and near-IR measurements were conducted using a blackbody furnace as a light source (Mikron Instrument Co., model M330). The emission measurement was made with the light source blocked by a light chopper. The chopper consisted of a rotating wheel which permitted light to pass through only during part of its rotation. The light was chopped at a rate of 5 to 15 hertz for these experiments. During the chopping cycle, the light reaching the spectrometer was from both the lamp and the flame during part of the cycle and from the flame only during another part of the cycle. Care was taken to reject spectra taken during the transition from light-on to light-off (Figure 5). Several (10 to 50) light-on spectra and light-off spectra were co-added to create a time-averaged spectrum for each part of the cycle over the same time interval. The time-averaged results were assumed to be "simultaneous" light-on and light-off spectra. Similar light-on and light-off spectra were taken when the flame was not present.

The results of the measurements were four time-averaged spectra (intensity versus wavelength) which will be denoted $I_{l+f+b}$, $I_{f+b}$, $I_{l+b}$, and $I_b$, where the subscripts $l$, $f$, and $b$ denote lamp, flame, and background respectively. A flame emission spectrum was calculated using Equation 14:

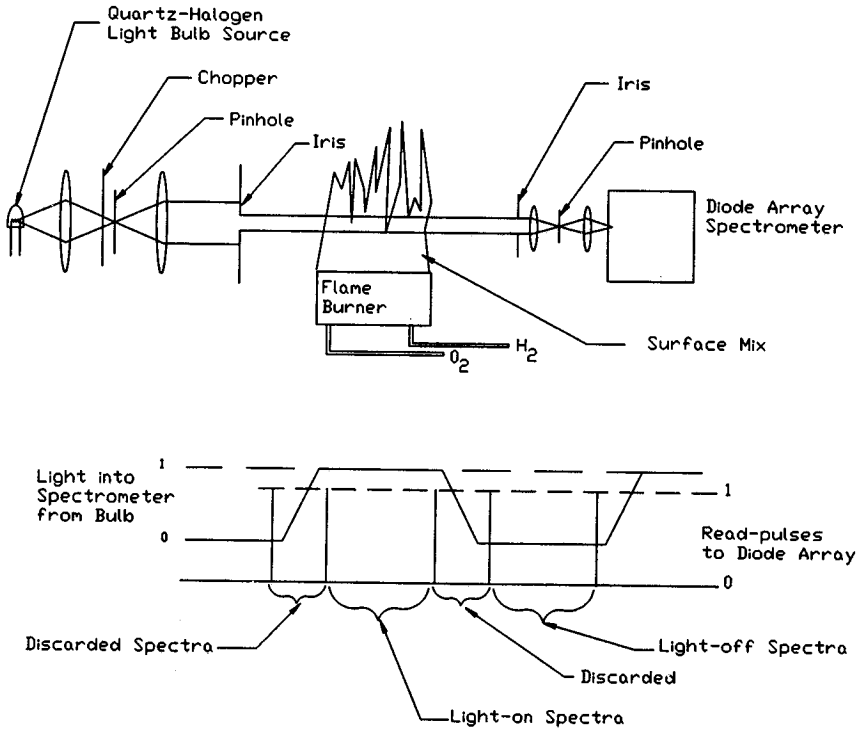


**Figure 5**
Experimental Setup Used for Emission-to-Absorption Measurements of Laboratory Flames

$$E(\lambda)=(I_{f+b}-I_b)/R(\lambda) \quad (14)$$

where

$I_{f+b}$ = intensity of flame and background
$I_b$ = intensity of background
$R(\lambda)$ = relative response function of the optical system and detector

An example result of using this equation is shown in Figure 6 where the atomic emission lines of Na, Li, and K from a doped $H_2/O_2$ flame burning in air are shown.

The transmissivity of the flame was calculated using Equation 15:

$$\tau(\lambda) = \frac{(I_{l+f+b}-I_{f+b})}{(I_{l+b}-I_b)} \quad (15)$$

where

$I_{l+f+b}$ = intensity of lamp, flame, and background
$I_{l+b}$ = intensity of lamp and background

This equation is the lamp intensity when the flame was present divided by its intensity when the flame was not present. Scattering of the lamp light from the flame also contributes to the measured transmissivity spectrum. In the situation where few or no particles were in the flame, scattering was detected as a broad curvature in the apparent baseline of the absorption features. For these measurements, an overall baseline was subtracted from 1-$\tau$ to correct for

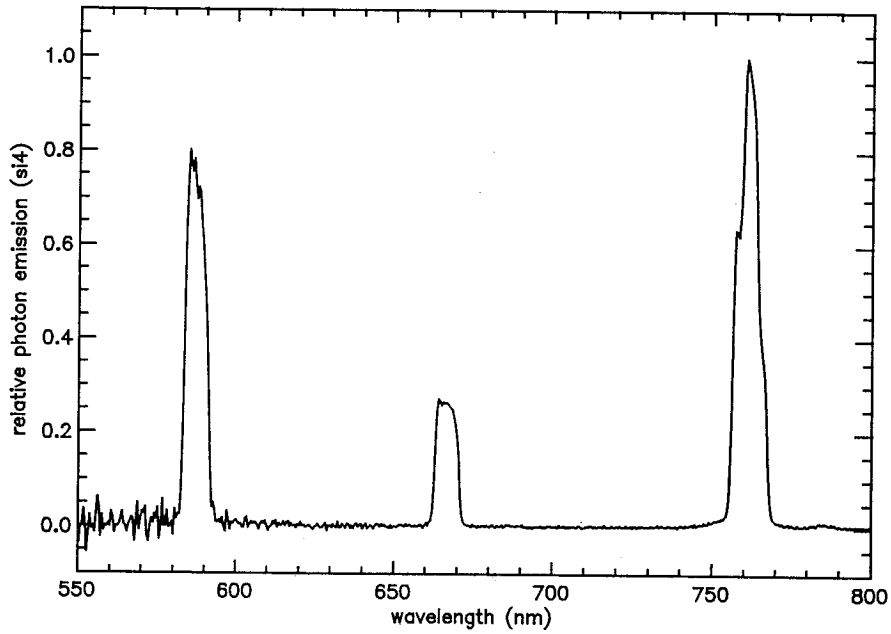


**Figure 6**
Emission Spectrum from a Flame Doped with Metal Salts
(Na, Li, and K Emissions are Shown)

this type of scattering. An example of the measured absorptivity and the assumed baseline is shown in Figure 7. The relative emission divided by the relative absorptivity for each of the three atomic features shown in these figures yields temperature information (Section 5.3.5).

Two burners were used; both were the surface-mix type wherein the fuel and the oxidizer are brought to the surface of the burner through separate tubes. The alternative type of burners are pre-mix. These could not be used with $H_2/O_2$ because of the explosion hazard (although some are rated for use with $H_2$/air).

The first burner (Carlisle Machine Works model 11B019) used was a brass burner designed for quartz glass working. This burner mixed the fuel and the oxidizer gases at its surface but had no provision for doping the flame or isolating it from the ambient atmosphere.

A more sophisticated research-grade burner (Research Technologies model RD1X1) was also used. This burner had a separate feed tube in the center for doping the flame and a co-flow provision for isolating the flame from ambient air by surrounding it with a flow of inert gas. It is important to note that without the co-flow, the $H_2/O_2$ ratio could not be controlled.

For detection in the spectral range of 200 to 1000 nm, a silicon 1024-diode array detector (Princeton Instruments, Inc.) placed at the exit plane of a grating spectrometer was used to measure the flame and light source emissions. The spectrometer/detector system was optically coupled to the sources by the lens/pinhole system shown in Figure 5. For the

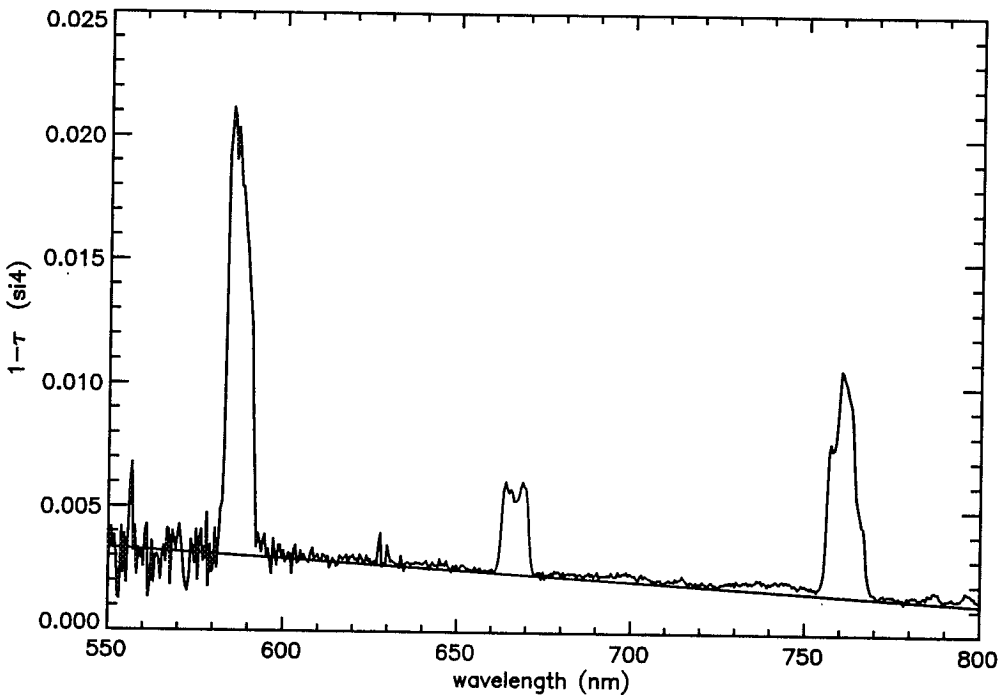


**Figure 7**
Absorptivity Spectrum of a Flame Doped with Metal Salts
(The assumed baseline is also drawn.)

spectral region of 900 to 1400 nm, the same spectrometers were used with a germanium (Ge)-diode array (Princeton Instruments, Inc.) of 256 elements. This diode array did not perform flawlessly because it had a number of bad diodes (pixels) and rather severe nonlinearity at low light levels. Corrections were made to the data to eliminate the bad pixels. A small incandescent bulb placed near an opening in the spectrometer cover provided a high background light level in the spectrometer in order to get the response curve of the diodes in a linear region (i.e. response proportional to light intensity).

One of two spectrometers was used, depending on the spectral region of interest. An f#3.2 spectrometer (Instruments, S.A., Inc., model HR320) was used with various gratings. This instrument was used exclusively for measurements involving the UV emissions of OH. A smaller f#2.0 spectrometer (Instruments, S.A., Inc., model UFS200) was also used for some of the visible-to-near IR measurements.

For experiments involving metal salts added to the flame, the research-grade burner had a central feed tube (in place of a fuel tube) that extended through the bottom of the burner. A dilute lithium hydroxide aqueous solution containing sodium chloride, potassium bromide and lithium dioxide was forced through the feed tube to the top of the burner. The liquid quickly evaporated leaving a residue of salts that slowly eroded into the flame gases. The resulting distribution of atomic species in the flame was not uniform spatially or temporally, but some time was allowed for the emissions to stabilize before measurements proceeded.

Doping of the flames from the brass burner was accomplished by injecting the salt solution onto the burner face with the flame present. The high temperature of the burner evaporated the water and left a salt residue which seeded the flame gases. As with the research-grade burner, the spatial and temporal distribution of atomic species was not uniform.

For the experiments with soot-containing flames, propane was pre-mixed with the $H_2$ just before flowing into the fuel port of the burner. The research-grade burner was used with air as the oxidant and without the inert gas co-flow.

### 5.3 Results

An early laboratory observation was that a $H_2$ flame burning in air was almost transparent in the visible wavelength regions with only the outer flame envelope showing some yellow and blue tinge. Also, very little UV (306 to 325 nm) emission could be collected from this diffusion flame. This quickly changed however, as pure $O_2$ was added to the surface-mix burner. The flame went from blue to white as $O_2$ was added, and the tips of the flames became yellow. The UV emission at first increased as $O_2$ was added, then decreased as the flame became fuel-lean.

The prominent UV bands of OH from a $H_2/O_2$ flame were first analyzed for the feasibility of extracting overall gas temperature. It became clear that a definitive temperature could not be attained from these bands because the energy pumped into them from the chemical reaction does not thermalize on a time scale that is comparable to the radiation-quenching collisions of OH with water molecules (Garland and Crosley 1986; Jeffries et al. 1988). These OH bands were not measured from a $H_2$/air flame.

The near-IR wavelength region was then analyzed, but success was impeded by instrumental difficulties.

The visible wavelength region (400 to 900 nm) of the flame spectra only showed features too weak to be of practical use with the emission-to-absorption technique.

The temperature information of the flames finally came from atomic metal species that were added in salt form to the flame gases. The prominent features of Na, Li, and K in emission and absorption usually provided two independent emission-to-absorption ratios, each of which indicated a temperature of the flame. The two ratios usually agreed with estimated experimental uncertainties and also agreed with calculated temperatures when estimates of fuel and oxidizer were feasible. This gave confidence in the accuracy of the results.

### 5.3.1 Hydroxyl Radical (OH) Ultraviolet $A^2\Pi$-$X^2\Sigma$ System

Emission and emission-to-absorption measurements were made for the OH lines at 306- to 325-nm wavelengths. The emission measurements were modeled using the Equations 11 and 12 (Section 5.1.1), a temperature of 3000 K, and the molecular parameters of the $A^2\Pi$-$X^2\Sigma(0,0)$ ro-vibronic band as given in Goldman and Gillis (1981). The measured emission spectrum is compared to the calculated emission spectrum in Figure 8. The two are only comparable between 306 and approximately 311 nm since contributions from the (1,1) and (2,2) transitions were not included in the calculation but are known to contribute significantly to the observed $A^2\Pi$-$X^2\Sigma$ system. The measurement was performed as a part of an emission-to-absorption measurement (described in Section 5.2).

The absorptivity ($1-\tau$) of the OH lines is presented in Figure 9 along with the emission-to-absorption ratio of the spectrum from 304 to 316 nm. This measured emission-to-absorption (dotted line) was compared to the predicted curve (solid lines) for equilibrium emissions for

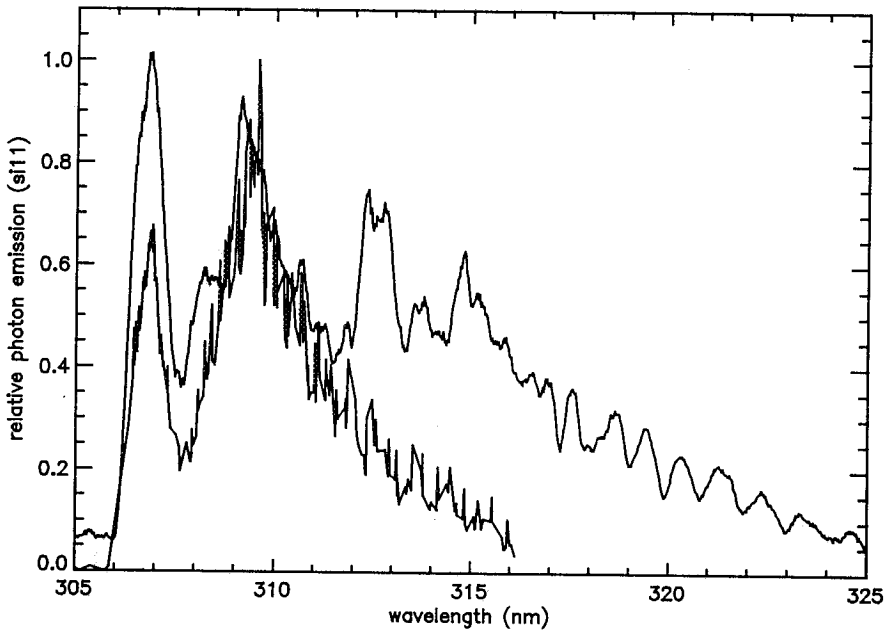


**Figure 8**
Measured and Calculated UV Emission Spectrum of OH from a $H_2/O_2$ Flame Burning in Air

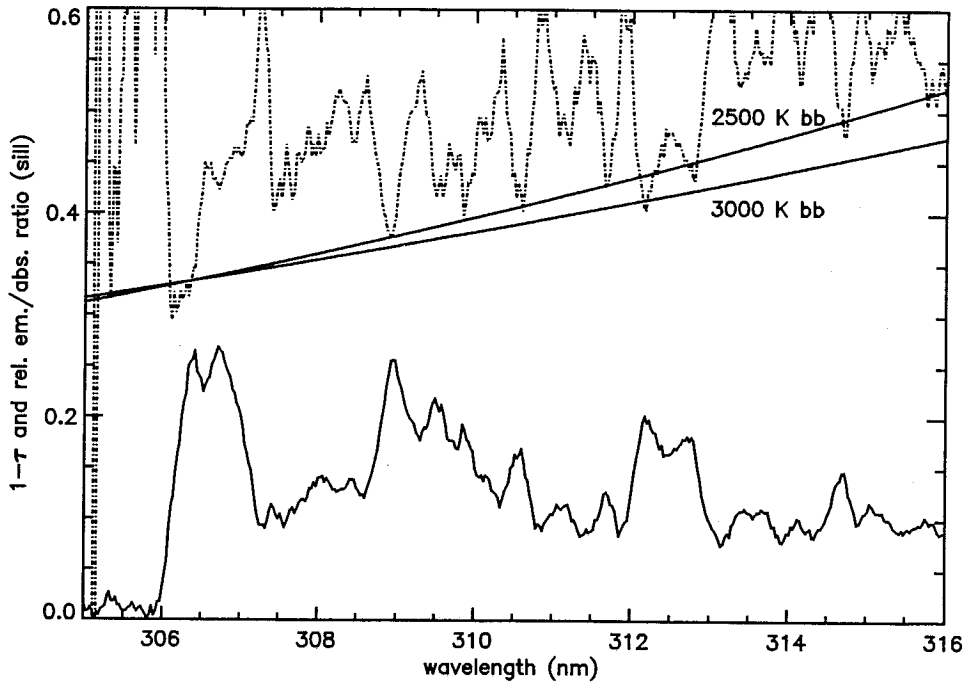


**Figure 9**
Absorptivity of OH from a $H_2/O_2$ Flame and the Corresponding Emission-to-Absorption Ratio

temperatures of 2500 and 3000 K. It can be seen that the ratio for many of the peaks in the spectrum fall in the vicinity of the equilibrium ratios expected for these temperatures. Many other peaks fall far from the predicted curves which is inconsistent with the equilibrium assumptions. The most significant result of the measurement is that these features do not in general yield equilibrium temperatures. Any agreement between the temperature predicted by the relative emission-to-absorption ratio of any two features and the equilibrium temperature of the flame (as measured, for example, with emission-to-absorption of spectator species) must be considered fortuitus until consistency is established under a variety of flame conditions. An additional issue in using these OH emissions is that the small wavelength range limits the precision with which any two features can be used to measure temperature.

### 5.3.2 Bands in the Near Infrared

The emission-to-absorption technique was used with the Ge-diode array detector in order to measure the overtone spectra of the vibrational fundamentals of water and possibly OH in the near-IR wavelength region. As shown in Figure 10, there were prominent emission features at approximately 1350 and 1400 nm (which extends beyond the region shown here) and a broad feature between approximately 1080 and 1300 nm. The emitting molecule is probably water though no effort was undertaken to rigorously identify the species responsible. Also seen Figure 10 is a high background continuum emission of uncertain origin. The transmission curve collected with this spectrum also has baseline uncertainty. Because of this uncertainty and the problems experienced using the Ge-diode array, a large uncertainty exists as to whether these bands exhibit local thermodynamic equilibrium behavior. For these data, the emission-to-absorption ratio is shown in Figure 11. Of the emission-to-absorption ratio in

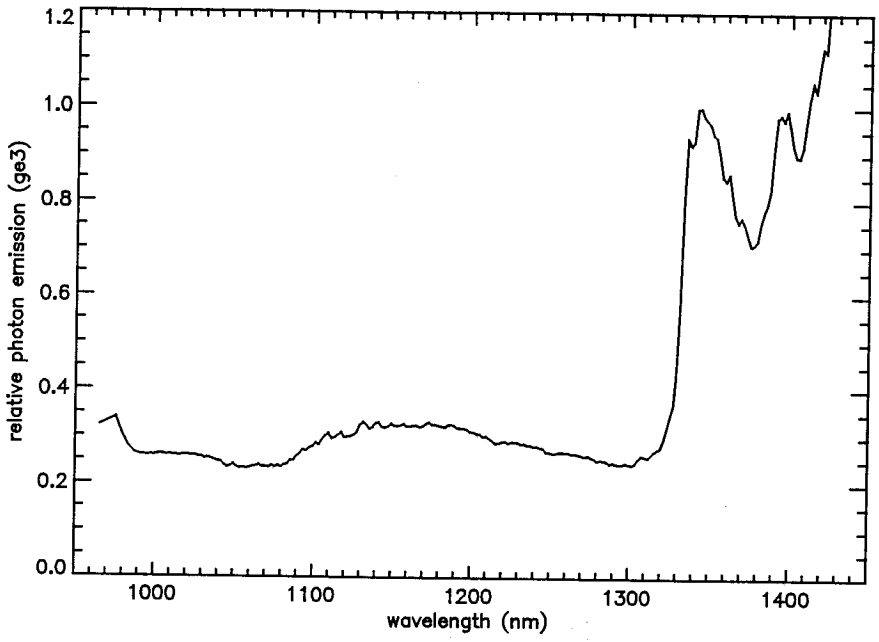


**Figure 10**
Relative Emission in the Near IR from a $H_2/O_2$ Flame Burning in Air

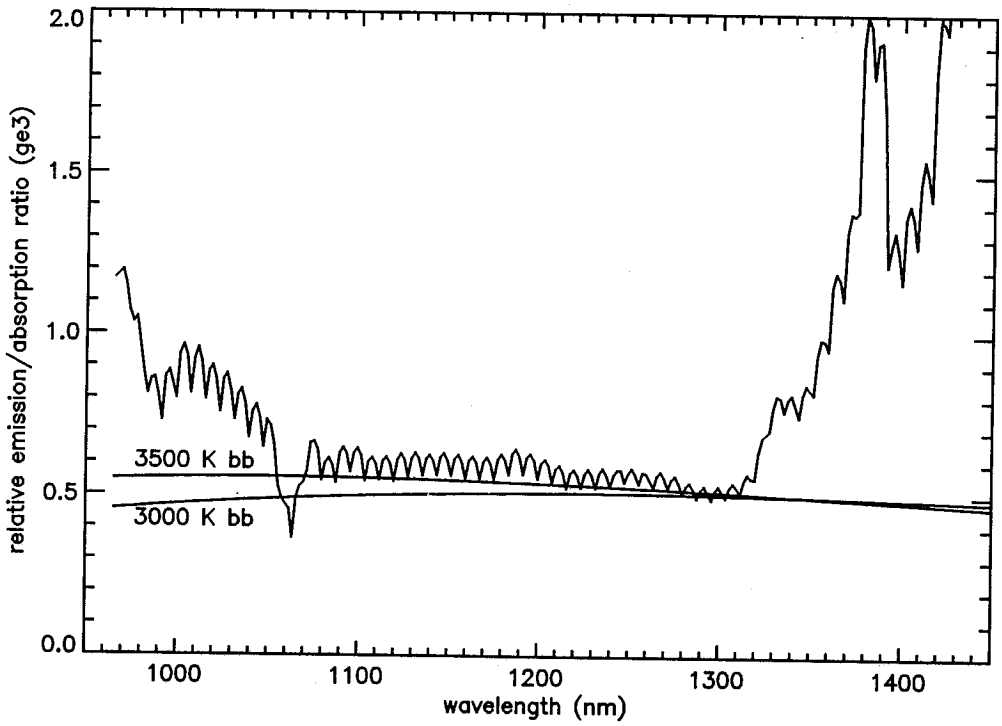


**Figure 11**
Relative Emission-to-Absorption Ratio in the Near IR from a
$H_2/O_2$ Flame Burning in Air

this spectrum, the broad feature seems to follow the expected curve for a temperature of approximately 3500 K. The wave-like structure is an experimental artifact.

### 5.3.3 Atomic Lines from Metal Dopants

In order to get emission and absorption features that better indicated the overall gas temperature of the flames, metal salts were added to the flame gases. These salts dissociated and the metal atoms then emitted and absorbed at a characteristic temperature which depended on the manner in which these species interacted with the flame constituents. The hypothesis is that the atomic metal species do not participate in the flame combustion reactions and therefore have electronic energy distributions produced by collision processes that constitute local thermodynamic equilibrium with the flame gases. This assumption for Na is known to be inaccurate in some regions of the flame where both the Na and atomic H are present in high concentrations. In that case, the reaction $Na + 2H \rightarrow Na^* + H_2$ can produce a significant amount of Na chemiluminescence from the activated $Na^*$ (Gaydon 1974). A similar reaction may occur for K. If true, these lines may produce emission-to-absorption ratios that lead to inaccurate temperatures. A similar reaction is not known to be significant for Li. Li atom concentrations, however, may be increased in these regions by the reaction $H + LiOH \rightleftarrows Li + H_2O$, since metal hydroxides are known to form in metal-doped $H_2$ flames (Gaydon 1974).

The derivation of temperature from the atomic lines was done by calculating the average emission-to-absorption ratio over a spectral range in the vicinity of each line. For each line, this spectral range was chosen to correspond to where the emission data were higher than 50 to 80 percent of its peak value. The uncertainty of each average emission-to-absorption ratio was calculated as the standard deviation of the ratios calculated over the so-chosen spectral range. The emission-to-absorption ratios were ratioed to that of the Na line, and the uncertainties were propagated quadratically. These ratios were then compared to that of the blackbody function normalized to unity at the Na wavelength. For example, if the emission-to-absorption ratio of the K line ($\sim$768 nm) was 9.6 times that of the Na line ($\sim$589 nm), the Planck blackbody ratio (photons per unit wavelength interval) $B(\lambda=768\ nm,T)/B(\lambda=589\ nm,T)$ must equal 9.6. The temperature at which this is true is approximately 1710 K. The temperature uncertainties were calculated from the minimum and maximum temperatures arrived at by adding and subtracting the uncertainties to the average of the relative ratios.

### 5.3.4 Hydrogen/Air Flames — Temperature versus Stoichiometry

The validity of the flame temperature measurement technique was tested by comparison of measured flame temperatures to those predicted by the Gordon and McBride code for the same fuel-to-oxidizer equivalence ratios. For these measurements, the flame had to be produced using the research-grade burner with a gaseous nitrogen co-flow to isolate it from ambient air. Even this did not produce a flame that was completely unaffected by room $O_2$, though that part of the flame nearest the burner head was the most isolated.

Unfortunately, this study could not be done using $H_2/O_2$ with this burner because when using the co-flow with the fuel-to-oxidizer ratios near a stoichiometric equivalence of 1, the burner surface was much too hot and started vaporizing. Conversely, with fuel-to-oxidizer far from an equivalence of 1, the flame was too cool to give adequate atomic emissions for a narrow line-of-sight near the burner head. Using air as the oxidizer (instead of pure $O_2$), it was

found that a wide range of mixture ratios produced adequate signal-to-noise in the experimental data. Therefore, a study of measured flame temperature versus Gordon and McBride code calculations for various $H_2$/air flames was performed. The results are summarized in Table 3. In addition to these results, a number of experiments were conducted with the brass burner using various $H_2$/air relative flowrates. Temperatures measured using the atomic metal lines were always around 2200 K. The Gordon and McBride code for a fuel-to-oxidizer equivalence ratio of 1 (fuel at 2.9 percent w/w) yields a temperature of 2380 K. It would appear that a small, well-mixed $H_2$/air flame burning in an air atmosphere results in a near-stoichiometric temperature away from the reaction zone regardless of relative $H_2$/air flowrates to the burner.

### 5.3.5 Temperatures from Hydrogen/Oxygen Flames in Air

Temperatures of several $H_2/O_2$ flames were determined using the emission-to-absorption method with the atomic lines produced from the metal salt dopants. Results of these measurements on flames of varying flowrates of $H_2$ and $O_2$ and various regions of the flame are given in Table 4 as derived from the relative emission-to-absorption ratios of the sodium and potassium lines. These flames were in ambient air and the actual ratios of fuel to oxygen are not accurately represented by the measured flowrates. The measurements made above the burner were sufficiently high enough to ensure good mixing and combustion, thus the high flame temperatures seem reasonable compared to the calculated stoichiometric temperature of 3080 K.

By contrast, much lower temperatures were measured in a region of the flame where the UV OH emissions were strongest (close to the burner surface). For these measurements, a flame was produced under nearly identical conditions as the flame whose OH emission is presented in Section 5.3.1 but was doped with sodium, potassium, and lithium salts. Figure 12 depicts the relative atomic emissions of these species along with relative emission-to-absorption ratios (diamond-shaped points). Predicted equilibrium curves for two temperatures are also depicted. The measurements yielded a temperature of 1750 K from the sodium-potassium ratio and a temperature of 1930 K from the sodium-lithium ratio. The disagreement between the two ratios may have several causes which will be discussed in Section 5.4. The lower temperatures seem reasonable if one considers that the mixing and the combustion are not as extensive or as complete near the burner surface. Note also that the relative emission-to-absorption ratios of the UV features in Figure 9 indicate nonequilibrium conditions.

**Table 3**
Measured Temperatures of $H_2$/Air Flames Burning in Air

| Data Set Name | Fuel-to-Air (% w/w) | Temperature | | Gordon and McBride Calc. Temp (K) |
|---|---|---|---|---|
| | | Li/Na Ratio (K) | K/Na Ratio (K) | |
| RD7 | 15.0 | 1290 ± 50 | 1710 ± 40 | 1270 |
| RD8 | 4.7 | 2040 ± 230 | 2120 ± 60 | 2150 |
| RD9 | 3.5 | No Data | 2500 ± 150 | 2300 |

**Table 4**
Typical Measured Temperatures of $H_2/O_2$ Flames Burning in Air

| Data Set Name | Measured Temperature and Uncertainty (K) | $H_2/O_2$ Flow Ratio (v/v) |
|---|---|---|
| si4 | 3000 ± 100 | 3.6 |
| si5 | 2950 + 750, -400 | 3.6 |
| si6 | 2800 ± 400 | 1.8 |

### 5.3.6 Temperatures of Soot-forming Flames

In launch accident scenarios, flammable materials including some hypergolic propellants can produce soot-laden flames. Two temperatures are of interest for these conditions, that of the flame gases and that of the soot particles. The emission-to-absorption technique was used to collect separate emission and transmissivity spectra. For flames containing significant particulate, gaseous absorption does not dominate the transmissivity measurement. Particle scattering and absorption contribute significantly, and therefore, the overall measurement is absorption plus scattering which is defined as *extinction*. The experimental distinction between extinction and absorptivity measurements lies primarily in the care that must be taken to exclude detection of light scattered off-axis by the particles in the flame. The lens-pinhole

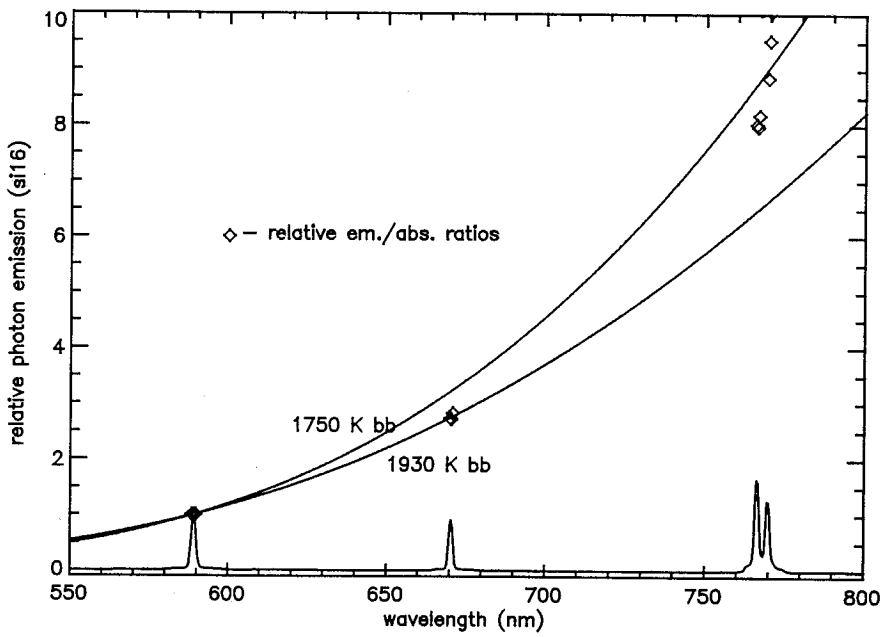


**Figure 12**
Relative Emission from a $H_2/O_2$
Flame Doped with Metal Salts

arrangement (spatial filtering) in the experimental set-up limits the detected emissions to an axial direction parallel with the optical axis of the transmission source.

Using the broad-band subtraction techniques for emission and absorption described in Section 5.1.2, a gas temperature was derived from the atomic metal features detected in a doped propane-$H_2/O_2$ flame burning in air. The spectrum was taken from a region of the flame that was bright orange. A glass slide placed into the flame at that point collected a noticeable amount of soot after only a few seconds. Figure 13 depicts the overall detected emission spectrum from the flame. Distinct features caused by the K and Na emissions (at 770 and 590 nm, respectively) as well as molecular $C_2$-emission bands between about 500 and 590 nm are readily apparent above the continuum. The continuum emission fits well to a blackbody emission curve with a temperature of 2100 $\pm$ 100 K (dotted line).

Figure 14 presents the relative emission after subtraction of the assumed blackbody baseline as well as the relative emission-to-absorption ratios (open diamonds) of the Na and K atomic lines. The data fit a temperature of 1880 K with uncertainties estimated at +120 and -90 K. The $C_2$-emission bands can be seen at wavelengths shorter than that of the Na lines. The relative emission-to-absorption ratio for these $C_2$-emission bands are not included in the figure but vary widely. Although this could be due to poor signal-to-noise in this region of the spectrum, it probably indicates that, as with the OH, this combustion reactant is not emitting and absorbing at equilibrium with the flame gases.

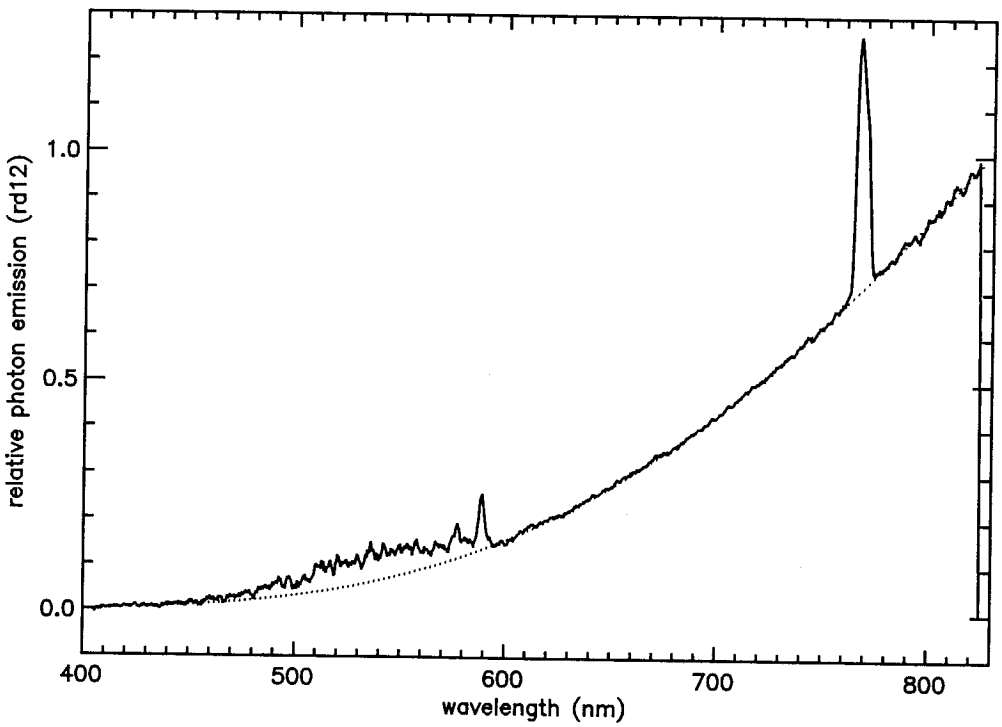


**Figure 13**
Relative Emission Measured from a Propane-Rich, $H_2$-Propane-Air Flame

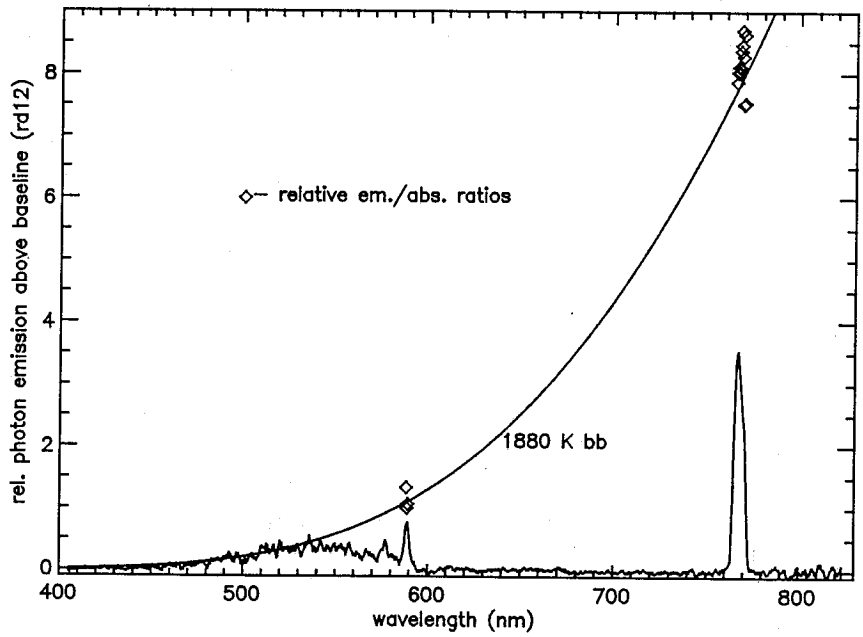


**Figure 14**
Relative Emission Above the Baseline Continuum for the Flame (See Figure 13)

The temperature extracted from the soot particles (2100 K) is higher than that of the gas temperature as determined by this Na/K line ratio when a wavelength-independent emissivity is assumed for the soot. The accuracy of this assumption, however, is no better than 10 or 20 percent. The fact that the two temperatures have overlapping uncertainties is encouraging.

The Gordon and McBride code calculation for $H_2$, propane, and air with a $H_2$-to-propane ratio, set equal to that of the experimental flame and with enough air to give a fuel-to-oxidizer equivalence of 1.0 (i.e. a stoichiometric flame), yields an equilibrium temperature of 1850 K. The same calculation with a 10-percent excess of air yields a temperature of 1945 K. As was seen for both $H_2$/air and $H_2/O_2$ flames, the stoichiometric temperature seems difficult to avoid with small, well-mixed flames burning in air.

## 5.4 Discussion

### 5.4.1 Analysis of Laboratory Results

The first result of the laboratory measurements was that the OH UV emission system did not contain much equilibrium gas temperature information. As a combustion intermediate, it is produced in a high energy state and must undergo many collisions to come to equilibrium with the surrounding gases. As noted earlier, however, the first few collisions endured by an OH molecule, especially with water molecules (Garland and Crosley 1986; Jeffries et al. 1988), tend to de-energize the molecule to the ground electronic state from which no UV radiation can emit. This implies that most of the UV radiation detected from a flame at atmospheric pressure (from parts of the flame where the product $H_2O$ is abundant) is not thermal equilibrium radiation. (A similar conclusion may be reached regarding the $H_2O$ emissions in the near-IR, although the data obtained in our laboratory are not as conclusive on this point.)

Other emissions known to occur from $H_2$/air and $H_2/O_2$ flames are relatively weak in the UV-visible-near IR regions. These include an OH emission continuum in the 400 to 500 nm wavelength region, $O_2$ Schumann-Runge emissions in the 300 to 400 nm region, and nitric oxide yellow-green continuum for $H_2$/air flames. Water and OH vibrational overtone spectra are also known to extend into the visible spectral region (Gaydon 1974). Although further laboratory and literature research would be required in order for any of these emissions to be shown useful as temperature indicators, experience with the OH, $H_2O$, and $C_2$ bands indicates that combustion intermediates and products may be poor thermometers.

The dopant species were found to be rather good thermometers for the flame gases in certain regions of the flame. The Na/K line pair provided credible temperatures for the hotter flames of $H_2$/air and $H_2/O_2$. This pair did not indicate a credible temperature for a $H_2$-rich air flame (Table 4). A possible reason is that the Na and K lines may be luminescing from different parts of the flame along the line-of-sight because of spatial variation in the flame structure and/or different spatial distribution in the species concentrations. Another possible explanation is the chemiluminescence reaction (Section 5.3.3) in these flames since the reaction produces the excited $Na^*$ in regions of the flame that have high atomic H concentrations. This would increase the emission-to-absorption ratio of the Na relative to the K and increase the temperature estimate.

The Na/Li line pair usually worked well as a thermometer. The main problem associated with using this pair was getting good signal-to-noise for the Li emission-to-absorption ratio. This may have been because of low atomic Li concentrations in the flames, which in turn may have been because of a low concentration in the dopant solution, low efficiency of entrainment of Li into the flame gases, or a large fraction of the Li in the flame being in the form of LiOH rather than atomic Li (Section 5.3.3). For the fuel-rich case of the $H_2$/air flame in Table 3, these lines gave a temperature much closer to the calculated temperature than the Na/K line pair. If the Na is chemiluminescing as postulated to explain the high temperature given by the Na/K ratio, then the Li must also be chemiluminescing. This has apparently not been previously observed. Thus, there is an overall uncertainty in the temperature measurement of a $H_2$-rich flame. Further experimental investigation is needed, especially if field explosions are $H_2$-rich.

It is interesting to note that for the part of the flame where OH emissions were strongest, some of the relative UV emission-to-absorption ratios yielded near-stoichiometric temperature (2500 to 3000 K in Figure 9), whereas the atomic metal lines gave low temperatures (1710 to 1930 K in Figure 14) for the reaction zone of the flame. This could be because of nonequilibrium discrepancy between the OH and atomic metal species since the combustion is pumping the OH. Higher in the flame, where OH is not emitting as strongly and the combustion is more complete, the atomic lines give temperatures that are much higher - close to the stoichiometric temperatures. In this case, it appears that some of the nonequilibrium temperatures given by the OH UV emissions from the reaction zone can predict equilibrium gas temperatures away from the reaction zone. If this can be shown for expected fireball scenarios, the OH UV emissions may be useful after all.

### 5.4.2 Implications for Feasible Field Measurements

Spectroscopic temperature measurements of fireballs from LSHOE may be feasible if flame conditions are similar to laboratory flames. The chief handicap in making a feasibility estimate is that more detailed information about field explosions of $LH_2/LO_2$ mixtures is not

available. As is demonstrated by considering several field measurement scenarios, a few preliminary measurements of typical fireballs would greatly increase the knowledge-base that is required to predict successful measurements. Simple measurements such as the optical density of the fireball and relative emissions strengths of OH and other species would serve to illuminate the applicability of the field measurements considered below.

If there are prominent OH emission in the UV spectral region, then this strongly suggests similar $H_2/O_2$ reaction conditions as was seen in the laboratory. If these emissions are relatively weak, then the reaction in the fireball may be dominated by $H_2$ burning in air. The criteria here (weak and strong), however, is indefinite. It may be possible that the OH emissions from the reaction zone could be "calibrated" in the laboratory to correspond to expected equilibrium conditions away from the reaction zone. That is, at pressures near atmospheric, the OH emissions may be reproducible as a function of fuel-to-$O_2$ ratio which is directly related to the eventual flame temperature. As such, OH emissions could provide specific information with regard to reaction conditions as well as temperature. Here, the structure of the fireball becomes important in that the OH emissions are predominantly from the reaction zone where the gases are not in equilibrium. The combustion products away from the reaction zone may be the hottest part of the fireball, but just where this occurs requires assumptions regarding the sources of $O_2$ (cryogen or air) and the combustion geometry. Such questions could be answered by imaging the fireball with a CCD camera filtered and intensified to be sensitive to the OH UV wavelengths (approximately 300 to 325 nm). This camera could also be calibrated to give quantitative intensity measurements that could be compared to laboratory flames.

It was noted earlier that small, well-mixed flames burning in air seem to come to a temperature that approaches the calculated stoichiometric temperature in the adiabatic limit. If this is true, one might postulate that fireballs will be hottest where the fuel is combusting in an excess of air where it is well-mixed with either vaporized $O_2$ or air. Speculation such as this points out the need for knowing the relative vaporization rates of the cryogenic $H_2$ and $O_2$ in an explosion scenario. The heat of vaporization of $LO_2$ is approximately 7.6 times that of $LH_2$ (on a per mole basis). This indicates that $LO_2$ would vaporize more slowly (1/7.6) than $LH_2$ given the same absorbed heat flux (not taking the dispersing of the liquids into account). If $O_2$ volatizes much more slowly than $H_2$, the typical explosion will be mostly $H_2$ burning in air. The temperatures in that case will be a maximum of 2380 K and probably lower depending on the efficiency of the mixing with air. The situation would obviously be quite different if there is plenty of $O_2$ vapor mixing with the $H_2$ since the adiabatic flame limit is much higher (3080 K). Preliminary investigations in field explosions should try to estimate the amount of liquid $O_2$ that vaporizes on the time scales (1 to 2 s) of interest.

Seeding the cryogenic fluids with metal salts may produce very useful emissions for temperature measurements. These emissions would require spatial and temporal resolvent measurements at two or more wavelengths. Additionally, absorption or fluorescence measurements would have to be made simultaneously in at least some parts of the flame in order to gain knowledge of the spatial variation of the seed-species density distributions. Emission-to-absorption measurements may be feasible along several lines-of-sight if the amount of particulate matter and optical density permit absorption measurements. Many line-of-sight measurements can produce the spatial dependence of the temperature. The number of lines-of-sight required depends on the geometry of the flame. If axial or spherical symmetry can be assumed, the number of measurements could be on the order of ten or less.

Fluorescent measurements would require suitable lasers which have the disadvantage of being expensive and the advantage of being spatially specific. This enables imaging over many points in the fireball and overcomes some line-of-sight disadvantages. Na is known to fluoresce very efficiently, but a possible complication is that the Na in the glass dewars containing the cryogens may interfere with Na vapor emissions. Calibration would be required in the field situation.

The possibility of making emission-to-absorption measurements from a distributed network of fiber optics also exists. A fiber pair would transmit light to and from a point in the fireball where simultaneous emission-to-absorption measurements would be taken. Specially designed end-optics would pass a beam over a small path through part of the fireball. A simpler arrangement using only a receiving fiber and end-optics flushes to the ground at each location to take simple emission measurements at various points in the flame. Some of these could be pointed in a direction of a distant modulated light source to take absorption measurements. The chief disadvantages would be the probable destruction or damage of the end-optics and the cost of fibers.

Temperature measurements from particles in the flame also seem feasible as was demonstrated with soot (Section 5.3.6). Particles may produce enough emissions to be fitted to an emission curve over the visible and near-IR wavelengths. An accurate temperature requires knowledge of particle emissivity as a function of wavelength. Seeding the propellants with particles of known emissivity may produce a preponderance of their emissions. Also, the LSHOE program already uses a large amount of glass, metal, and organic insulation in the cryogenic containers. These emissions must be characterized in the laboratory in order to extract temperature information.

Mid-IR emissions from these flames present another possible avenue for temperature determinations. The emission characteristics of $H_2$ flames in the IR may be amenable to radiometric measurement and calibration to temperatures as could be demonstrated in the laboratory. The extrapolation to the field measurements would require measurement of ambient air absorptions and measurements of IR absorptions of the fireball cloud, at least in the outer layers. IR absorption measurements may be more feasible than higher wavelength absorption measurements since extinction by particulate is usually less severe.

## 6.0 Discussion of Phase I and Phase II Combined Results

The critical fireball conditions effecting mass effusion of the $PuO_2$ particles are easily visualized if the minimum temperature required to lose (mass effuse) 0.01 percent of the particle mass is plotted as a function of particle size for various fireball gas emissivities. An example of this is shown in Figure 15 for gas emissivities of 0.2 and 0.8.

These results, which have been obtained from interpolation of the data given in Table 2 for the Phase I modeling work, show the strong dependence of the mass effusion process on the fireball gas temperature, gas emissivity, and particle size. For the larger particles (100- to 1000-$\mu$m diameter), fireball gas temperatures above 2500 K are required to achieve mass loss in excess of 0.01 percent per particle in clean burning flames (gas emissivity = 0.2), while for sooty flames temperatures in the 2000 to 2500 K will achieve the same percent mass loss per particle. For the smaller particles (10- to 100-$\mu$m diameter), this same percentage mass

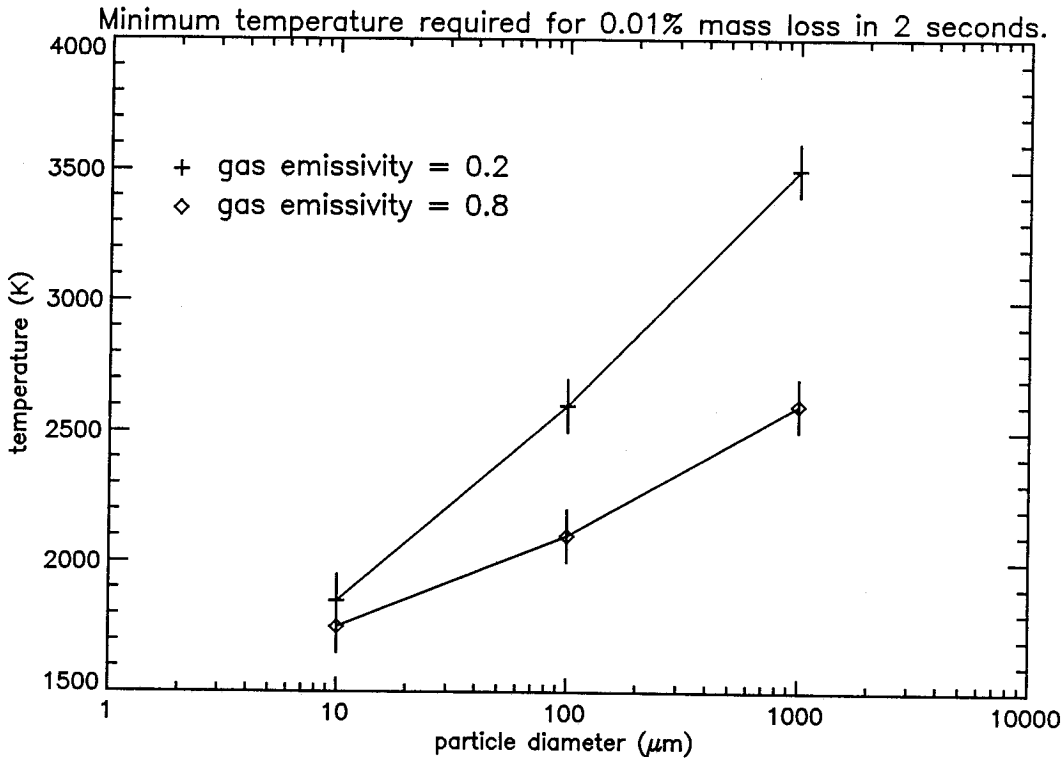


**Figure 15**

Minimum Gas Temperature Required to Lose 0.01% of the Particle Mass as a Function of Particle Size During a Two-Second Fireball Exposure

loss per particle is achieved within the range of 1800 to 2500 K with the larger size requiring a higher gas temperature or higher gas emissivity.

The results of the Phase II laboratory investigations indicate a propensity for the small, well-mixed $H_2$ flames burning in air to approach the calculated stoichiometric temperature in the adiabatic limit. If this is the case, one might expect fireball temperatures typically in the 2400 K range (Section 5.3.4) which according to the data presented in Figure 15 demonstrates the need for additional field testing of fireball environments to determine gas temperatures and gas emissivities.

# 7.0 Conclusions

## 7.1 Phase I

The Phase I theoretical modeling results show that the mass effusion rates of the $PuO_2$ particles (< 1000-$\mu$m diameter) entrained in fireballs are strongly dependent on the gas flame temperatures, gas emissivities, and particle size. The results of the simulation modeling have identified the need to accurately measure gas temperatures, gas emissivities, and mass effusion rates of representative particles in typical propellant fireball environments.

## 7.2 Phase II

The Phase II investigation results show that it is feasible to use spectroscopic techniques for measuring propellant fireball gas temperatures with the following list of implications for field-measurement scenarios.

- OH UV emissions do not provide temperature information directly, but must be calibrated to stoichiometry and temperature in laboratory experiments.

- OH UV emissions may provide reaction-condition information from a fireball via a stoichiometry-versus-laboratory calibration measurement.

- Near-IR emissions may be useful; however, more research is required. Care must be taken to account for atmospheric absorptions.

- Atomic lines from dopant materials should be useful temperature indicators for some parts of the fireball. Further investigations of their accuracy are needed for $H_2$-rich flames.

- Complimentary absorption or fluorescence measurements, along with emission measurements, are required for accurate temperature information. The feasibility of these measurements depends on the optical density of typical fireballs at the wavelengths of interest. This will have a spatial dependence.

- Broad emissions in the visible-near-IR wavelengths from particles can be used to measure particle temperatures. The precision of the measurements can be expected to be $\pm 100$ K or less. The accuracy of the measurements depends on knowledge of the optical properties of the particles.

These Phase II conclusions are supported by the following observations regarding the laboratory flames at atmospheric pressure.

- The OH $A^2\Pi$-$X^2\Sigma$ UV emissions between 306 and 315 nm are not characteristic of equilibrium emissions. Some bands of these emission may yield temperature information for the combusted gases if properly correlated to temperatures measured by another technique.

- The OH UV system is most prominent in emission from the reaction zones for $H_2/O_2$ flames. The emissions grow as the fuel-to-$O_2$ equivalence ratio approaches 1.

- Most other emissions in the UV-visible are probably too weak to yield much information during a one- to two-second simulation.

- Atomic metal dopant species give emissions and absorptions of equilibrium character in most parts of $H_2/O_2$, $H_2$/air, and $H_2$/air/propane flames. A very $H_2$-rich flame and the reaction zone of a $H_2/O_2$ flame may be the exceptions.

- Soot particulate emission and extinction in a $H_2$/air/propane flame can be distinguished from atomic metal vapor emission and absorption. Separate temperatures were measured for the gas and the particles.

## 8.0 Proposed Fireball Field Testing

The Phase I conclusions of this study identified the need to accurately measure gas temperatures, gas emissivities and mass effusion rates of representative particles in typical propellant fireballs, while the Phase II conclusions support the feasibility of performing the gas temperature tests using spectroscopic techniques. This section outlines the proposal for conducting fireball temperature and particle mass effusion testing using the WSTF LSHOE test facility.

WSTF proposes preliminary fireball measurements to investigate some of the basic optical properties of the fireball events. The information obtained from the preliminary investigations is a prerequisite to designing and building a reliable measurement system for investigating specific fireball properties such as gas temperature, gas turbulence, gas velocities and mass effusion of simulated radioactive particles.

### 8.1 Proposed Preliminary Fireball Measurements

Preliminary spectroscopic measurements of the fireballs are recommended parallel with the planned LSHOE propellant testing. These measurements will be performed from the existing camera bunkers. The only new equipment required to perform these measurements is a spectrometer telescope and optical windows for the camera bunkers.

- Perform remote UV-visible-near-IR emission spectroscopy measurements of fireballs.
- Perform remote UV-visible-near-IR absorption spectroscopy measurements of portions of fireballs.
- Analyze field spectra and perform laboratory investigations of analogous laboratory flames where applicable in order to
  - Identify emitting and absorbing atomic or molecular species;
  - Identify emission and extinction from fireball particulates.
- Analyze fireball photography data (high frame rates) for turbulent velocities.
- Use UV (OH band filters) cameras at high frame rates to investigate reactive zones in the fireballs.
- Develop methods of seeding the fuel with representative particles for post-event analysis of recovered particle materials for one or two special tests.

In the best case, the work proposed for the preliminary fireball measurements may yield sufficient information to verify the fireball gas temperatures and some information on the mass effusion of fireball particles.

## 8.2 Advanced Fireball Measurements

These measurements will focus on getting temporal and spatial detailed temperature and particle mass effusion (size and velocity) information from fireball events. Because of the lack of knowledge of the fireball environment, the following may be considered as merely a list of possibilities rather than direct recommendations. After preliminary measurements are completed, the choice of measurement approach can be made with more confidence.

- Assuming the OH chemi-luminescent emission structure can be calibrated as a function of thermal temperature, use arrays of UV-filtered cameras (high frame rates) and UV-visible spectrometers to perform tomographic measurements of the fireballs along multiple lines-of-sight.

- Assuming the fireball emissions have significant particulate emission that can be used to identify fireball temperatures, use arrays of UV-visible-near-IR spectrometers to map temperature of the fireballs along multiple lines-of-sight.

- Develop distributed fiber-optic probes to perform emission-to-absorption measurements within Na, Li, and K seeded fireballs.

- Develop planar laser-induced fluorescent imaging techniques for measuring temperatures and particulate mass effusion in seeded fireballs parallel with emissions measurements along multiple lines-of-sight.

- Develop fiber-optic phase doppler particle anemometry techniques for tracking small particles and the mass effusion process in the fireballs.

# Acknowledgements

WSTF would like to thank Lou Ullian for funding this work.

The authors wish to thank Mark Murray, LESC-WSTF, for his competent assistance in performing the laboratory spectroscopic measurements. The authors also wish to thank Brian Davis, New Mexico State University, Physical Science Laboratory, for his initial work in developing the simulation model.

# References


Bader, B. E., A. B. Donaldson, and H. C. Hardee. *Liquid-Propellant Rocket Abort Fire Model*. SC-RR-70-454, Sandia National Laboratories, Albuquerque, NM, October 1970.

Garland, N. L., and D. R. Crosley. "On the Collisional Quenching of Electronically Excited OH, NH, and CH in Flames." *Twenty-first Symposium (International) on Combustion/The Combustion Institute*. Pittsburgh, PA: The Combustion Institute, 1986, pp. 1693-1702.

Gaydon, A. G. *Spectroscopy of Flames*. Second Edition, London, England: Chapman & Hall, Ltd., 1974.

Gaydon, A. G., and H. G. Wolfhard. *Flames: Their Structure, Radiation and Temperature*. Second Edition, London, England: Chapman & Hall, Ltd., 1979.

General Electric Astro Space Division. *Final Safety Analysis Report (FSAR) for the Ulysses Mission*. Vol. II (Book 2), ULS-FSAR-004, Philadelphia, PA, March 1990.

General Electric Space Systems Division. *Final Safety Analysis Report (FSAR) for the Galileo Mission and the Ulysses Mission*. Vol. I, GESP 7200, Philadelphia, PA, October 1985.

Goldman, A., and J. R. Gillis. "Spectral Line Parameters for the $A^2\Pi$-$X^2\Sigma(0,0)$ Band of OH for Atmospheric and High Temperatures." *Journal of Quantitative Spectroscopy and Radiative Transfer.*, Vol. 25, (1981): pp. 111.

Gordon, S., and B. J. McBride. *Computer Program for Calculation of Complex Chemical Equilibrium Compositions, Rocket Performance, Incident and Reflected Shocks, and Chapman-Jouguet Detonations*. NASA SP-273, National Aeronautics and Space Administrations, Washington, DC, 1971.

Hardee, H. C., and D. W. Larson. *Thermal Hazard from Hydrogen Fireballs*. SAND78-1589, Sandia National Laboratories, Albuquerque, NM, March 1979.

Jefferies, J. B., K. Kohse-Höinghaus, G. P. Smith, R. A. Copeland, and D. R. Crosley. "Rotational Level-dependent Quenching of $OH(A^2\Sigma^+)$ at Flame Temperatures." *Chemical Physics Letters*, Vol 152 (1988): pp. 160.

Katsuki M., Y. Mizutani, and Y. Matsumoto. "An Improved Thermocouple Technique for Measurement of Fluctuating Temperatures in Flames." *Combustion and Flame*, Vol. 67 (1987): pp. 27-36.

Kite, F. D. and B. E. Bader. *Pad-Abort Thermal Flux Model for Liquid Rocket Propellants*. SC-RR-66-577, Sandia National Laboratories, Albuquerque, NM, November 1966.

# References (continued)


Kite, F. D., D. M. Webb, and B. E. Bader. *Launch Hazards Assessment Program Report on Atlas/Centaur Abort*. SC-RR-65-333, Sandia National Laboratories, Albuquerque, NM, October 1965.

Klein, V. W., C. E. Moeller, and E. T. Fago. *Determination of Transient Temperatures During The Expansion of Fireballs*. M.R.I. Project No. 2885-E, Contract No. NAS 9-4448, NASA Manned Spacecraft Center, Houston, TX, September 1965.

Longenbaugh, R. S. *Experimental and Theoretical Analysis of the Radiative Transfer Inside of a Sooty Pool Fire*. Master of Science Thesis, New Mexico State University, Las Cruces, NM, May 1985.

Mansfield J. A. *Heat Transfer Hazards of Liquid Rocket Propellant Explosions*. AFRPL TR-69-89, URS Research Company, Burlingame, CA, February 1969.

Moffat, R. J., B. D. Hunn, and J. F. Ayers. "Development of a Transpiration Radiometer." *Instrument Society of America, Conference Proceedings, Paper No. 613*. Chicago, IL: Instrument Society of America Research Triangle Park, October 1971.

NASA. *Space Shuttle Data for Planetary Mission Radioisotope Thermoelectric Generator (RTG) Safety Analysis*. NSTS 08116, Rev. B, 1988.

Orr Jr., C. *Particulate Technology*. New York, NY: MacMillan Co., 1966.

Pesante, R. E., and M. Nishibayashi. *Evaluation of the Blast Parameters and Fireball Characteristics of $LO_2/LH_2$ Propellant*. 0954-01(01)FP, Contract No. NAS 9-4355, NASA Manned Spacecraft Center, Houston, TX, April 1967.

Pesante, R. E., M. Nishibayashi, D. G. Frutchey, R. D. Erickson, and W. J. Helm. *Blast and Fireball Comparison of Cryogenic and Hypergolic Propellants*. Final Report, 0822-01(01)FP, Contract No. NAS 9-2055, NASA Manned Spacecraft Center, Houston, TX, June 1964.

Reid, R. C., J. M. Prausnitz, and T. K. Sherwood. *The Properties of Gases and Liquids*. New York, NY: McGraw-Hill Co., 1977.

Sappey, A. D., and D. J. Funk. "Laser-Based Diagnostics for Density, Temperature, Velocity, and Dissociation Fraction in High Temperature Hydrogen Flow." *AIAA/NASA/OAI Conference on Advanced SEI Technologies*. Cleveland, OH: American Institute of Aeronautics and Astronautics, September 1991.

Tejwani, G. D. "SSME (TTB) and DTFT Spectal Data Quantitative Analysis." *Advanced Earth-to-Orbit Propulsion Technology 1992 Conference Proceedings*. Huntsville, AL, May 1992.

# References (continued)

Van Nice, L. J., and H. J. Carpenter. *Thermal Radiation from Saturn Fireballs*. TRW Systems, Inc. Task ASPO-24, Contract No. NAS9-4810, NASA Manned Spacecraft Center, Houston, TX, December 1965.

Warren, C. "Spectral Response and IR Temperature Measurement." *Sensors*, Vol. 9, No. 1 (1992): pp. 16-21.

Williams, D. C. *Vaporization of Radioisotope Fuels in Launch Vehicle Abort Fires*. SC-RR-71 0118, Sandia National Laboratories, Albuquerque, NM, December 1971.

Yaws, C. L. *Physical Properties - A Guide to the Physical, Thermodynamic and Transport Property Data of Industrially Important Chemical Compounds*. New York, NY: McGraw-Hill, 1977.

# Appendix A

## Values and Functional Relationships of Various Physical Properties Used in Mass Effusion Modeling Simulation

# Appendix B
## Mass Effusion Modeling Results

This appendix gives the values and functional relationships (Yaws 1977) of various physical properties used in the mass effusion modeling simulation. All units in the simulation model are computed in cgs units.

Particle Properties:

| | | | |
|---|---|---|---|
| Material: | $PuO_2$ | | |
| Density: | $\rho_s$ | = | 9.6 g/cm$^3$ |
| Molecular Weight: | $M_s$ | = | 270 g/mole |
| Thermal Conductivity: | $\kappa_s$ | = | $1.923 \times 10^5$ erg/(gcmK) |
| Isobaric Specific Heat: | $C_{ps}$ | = | $3.43 \times 10^6$ erg/(gK) |
| Thermal Diffusivity: | $D_s$ | = | $5.8 \times 10^{-3}$ cm$^2$/s |
| Emissivity: | $\epsilon_s$ | = | 0.8 |
| Heat of Sublimation | $H_v$ | = | $2.045 \times 10^{10}$ erg/g |

Fireball Gas Properties:

| | | | |
|---|---|---|---|
| Material: | $H_2O$ | | |
| Density: | $\rho_s$ | = | $(4.1 \times 10^{-5}) \times (T_g/T_f)$ g/cm$^3$ |
| Molecular Weight: | $M_f$ | = | 18 g/mole |
| Viscosity: | $\eta_f$ | = | $-31.89 + 0.4145 \times T_f - 8.272 \times 10^{-6} \times T_f^2$ $\mu$poise for $T_f < 1273$ K and $\eta_f$ (1273) for $T_f > 1273$ K |
| Thermal Conductivity: | $\kappa_f$ | = | $733.8 - 1.013 \times T_f + 1.8 \times 10^{-2} \times T_f^2 - 9.096 \times 10^{-6} \times T_f^3$ erg/(scmK) for $T_f < 1073$ K and $\kappa_f$ (1073) for $T_f > 1073$ K |
| Isobaric Specific Heat: | $C_{pf}$ | = | $3.39 \times 10^8 - 3.01 \times 10^4 \times T_f + 1.52 \times 10^2 \times T_f^2 - 4.86 \times 10^{-2} \times T_f^3$ erg/(moleK) for $T_f < 1500$ K and $C_f$ (1500) for $T_f > 1500$ K |

# Appendix A Reference

Yaws, C. L. *Physical Properties - A Guide to the Physical, Thermodynamic and Transport Property Data of Industrially Important Chemical Compounds.* New York, New York: McGraw-Hill, 1977.

Appendix B gives the mass effusion modeling results as a function of gas temperature, gas emissivity, and particle size. The plots terminate when the two-second simulation time is completed or when 95 percent of the particle initial mass has evaporated. The first group of plots is for a gas emissivity equal to 0.2, while the second group is for a gas emissivity equal to 0.8. The convective heat transfer component is plotted by the dashed line, while the radiative heat transfer component is shown as the solid line. Note, as the particle velocity approaches the gas stream velocity and the surface temperature rises, the convective heat transfer diminishes. By this time, the particle surface temperature has achieved a temperature determined by the heat balance between the convective and radiative components. The corresponding values of the heat transfer components which are lower than the three-cycle range or negative are not plotted on the logarithmic scales of these plots.

Stream Temp=1700. Particle Diameter= 10. Time for run= 2.00 Emissivity= 0.2

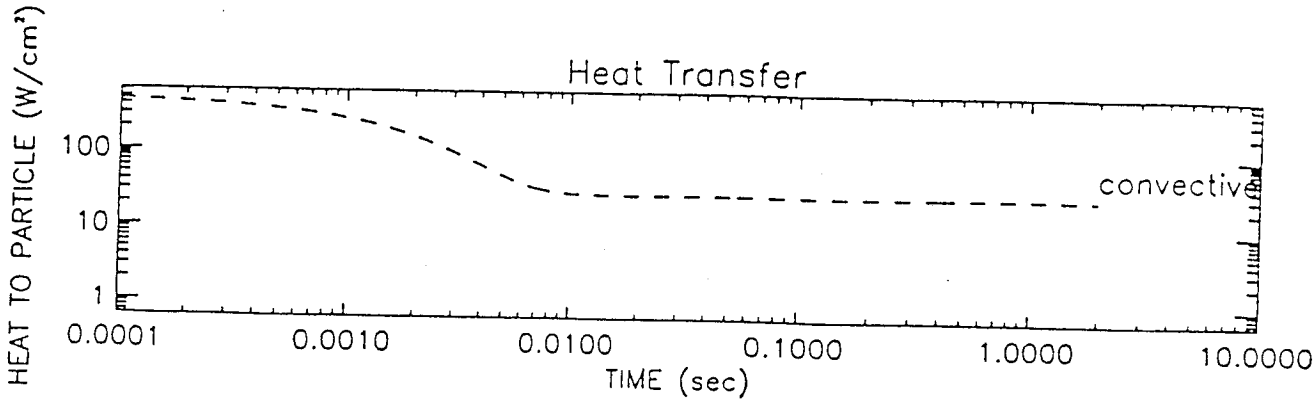


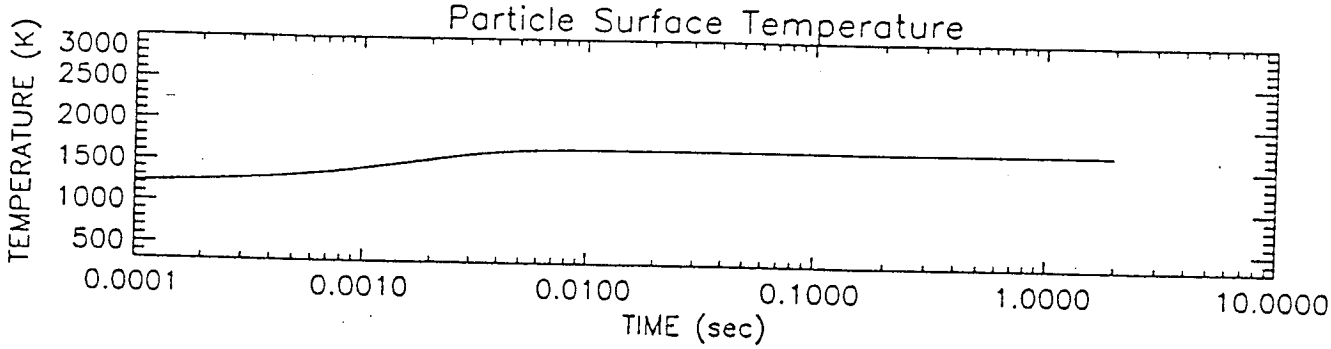


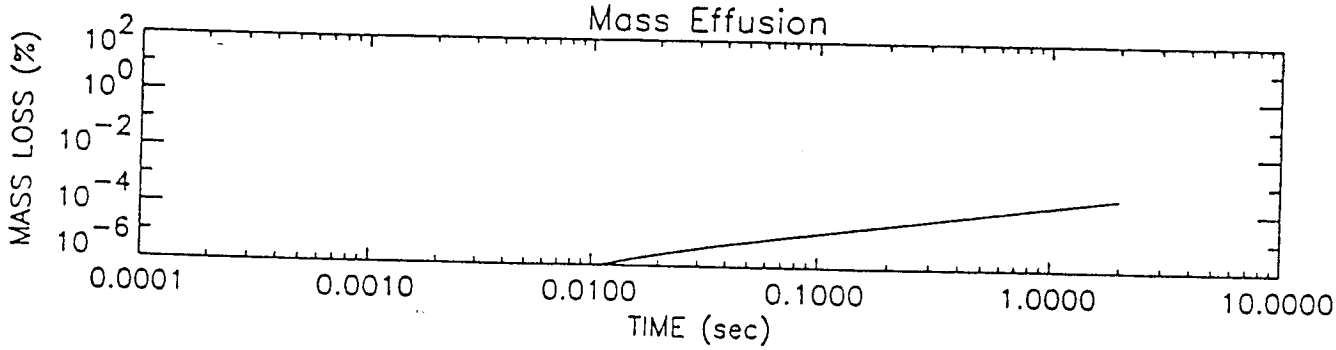


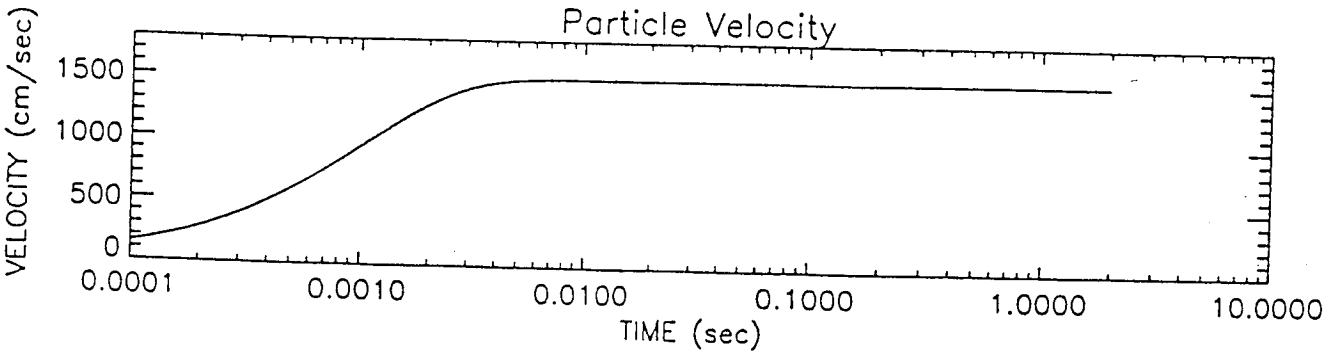

Stream Temp=1700. Particle Diameter= 100. Time for run= 2.00 Emissivity= 0.2

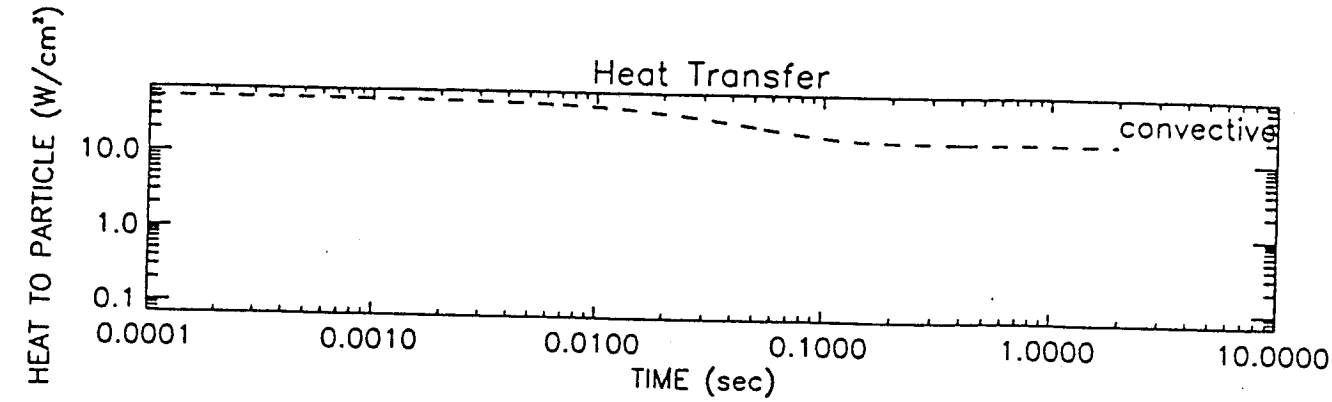


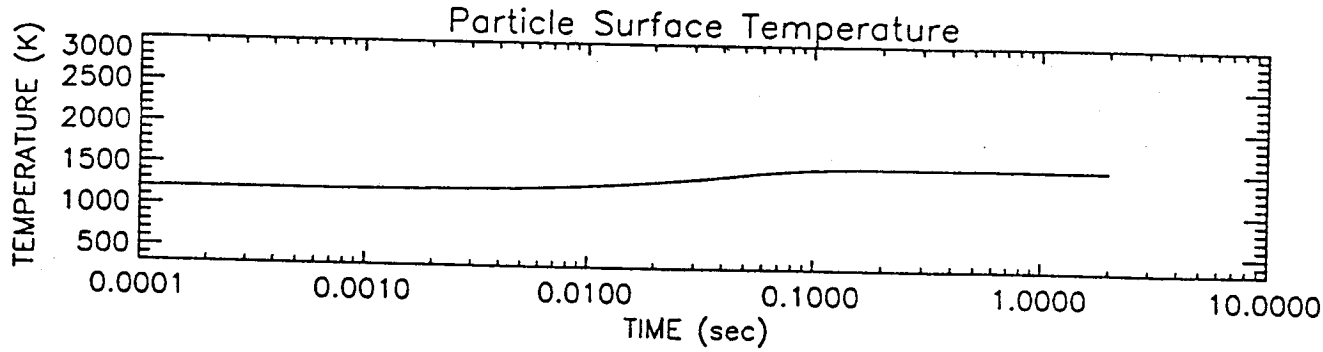


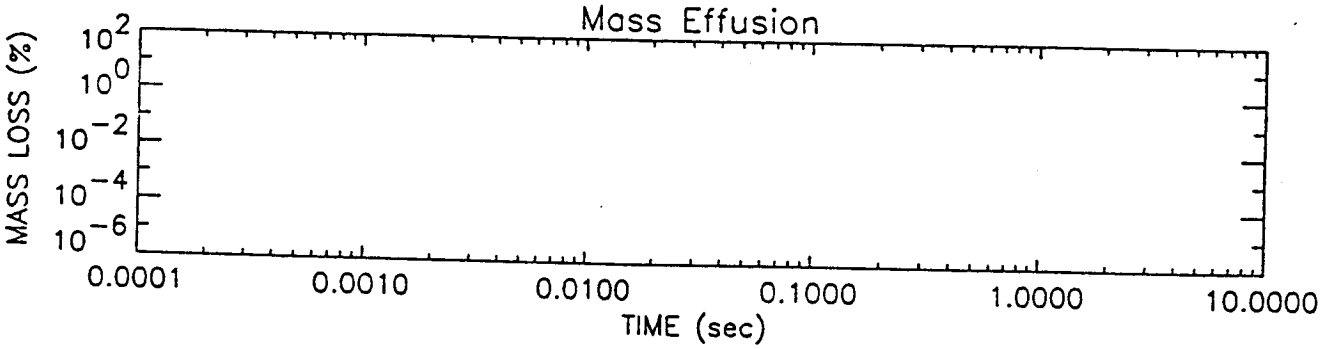


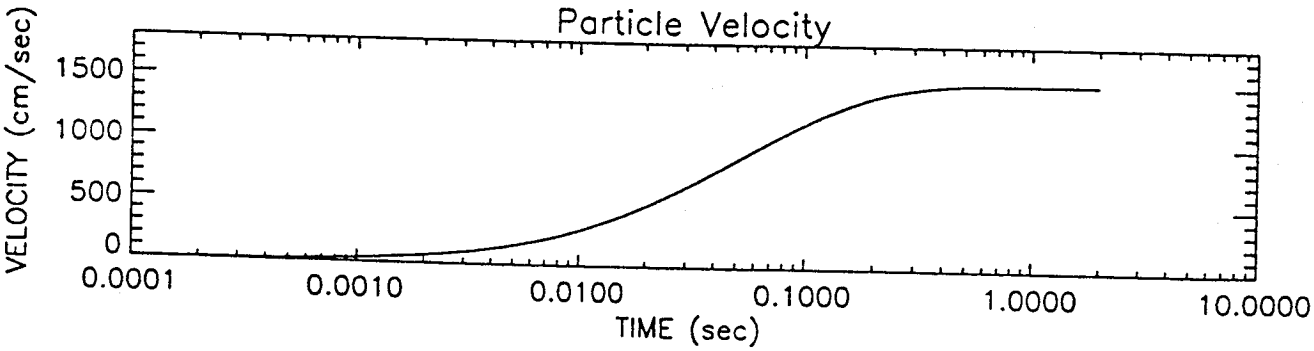

Stream Temp=1700. Particle Diameter=1000. Time for run= 2.00 Emissivity= 0.2

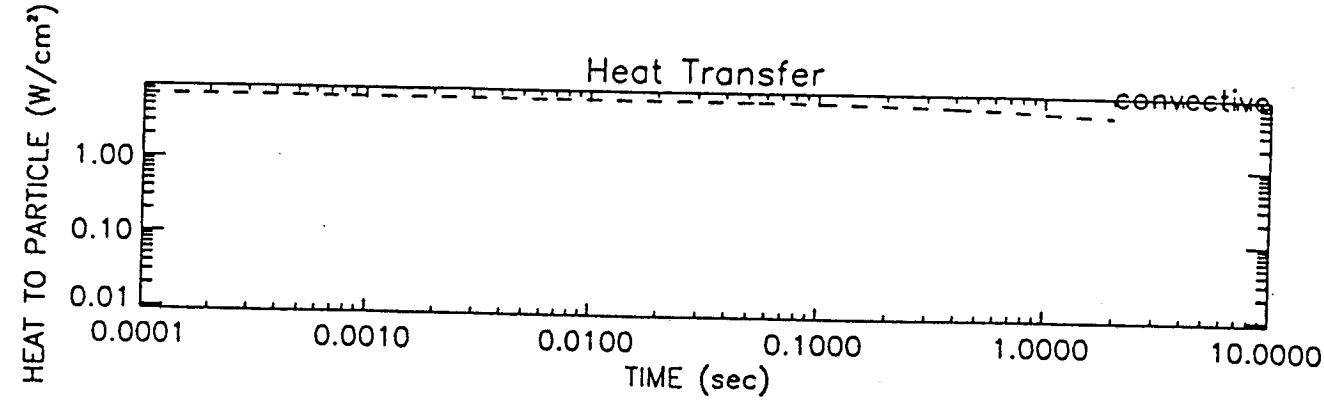


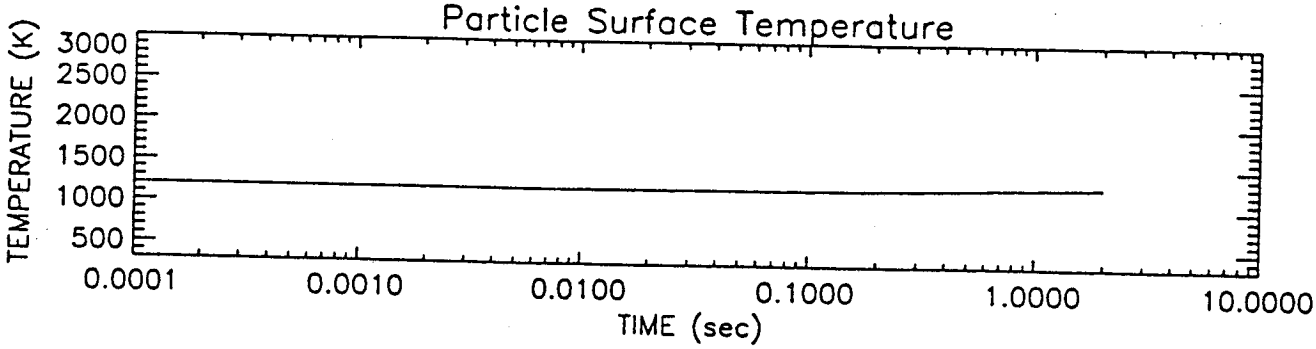


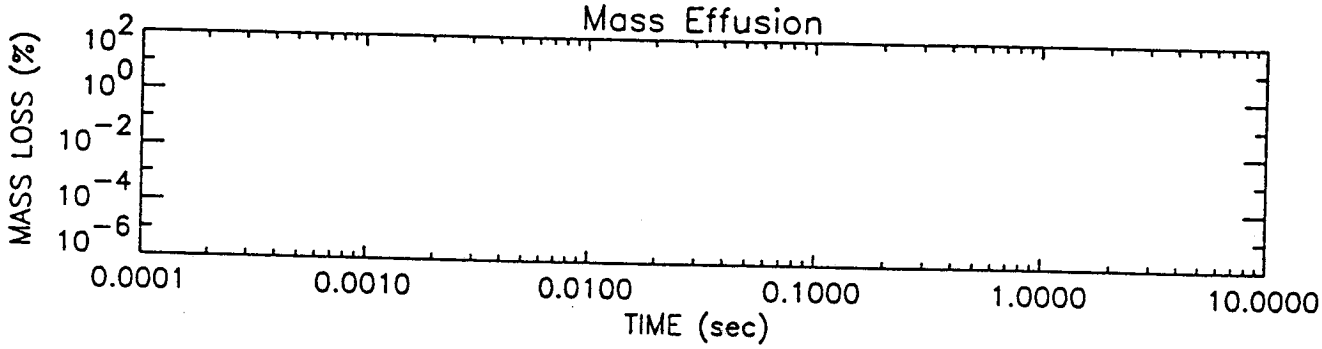


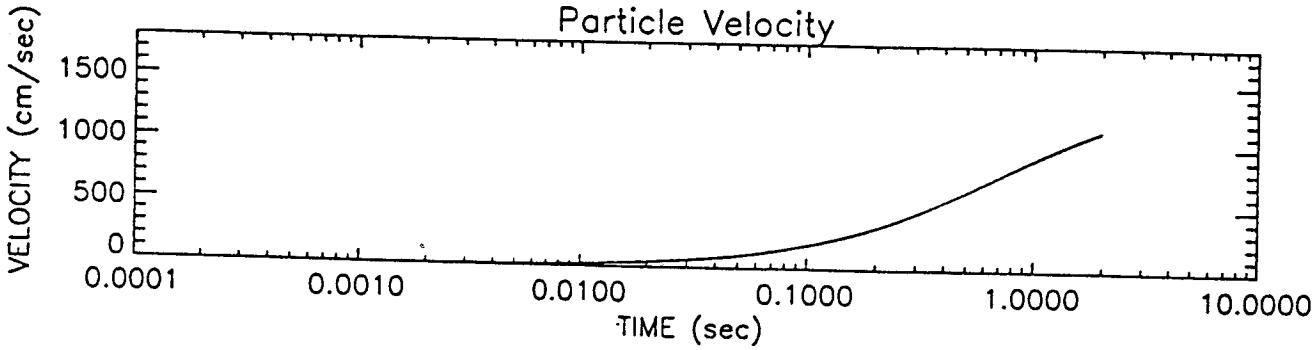

Stream Temp=2000. Particle Diameter= 10. Time for run= 2.00 Emissivity= 0.2

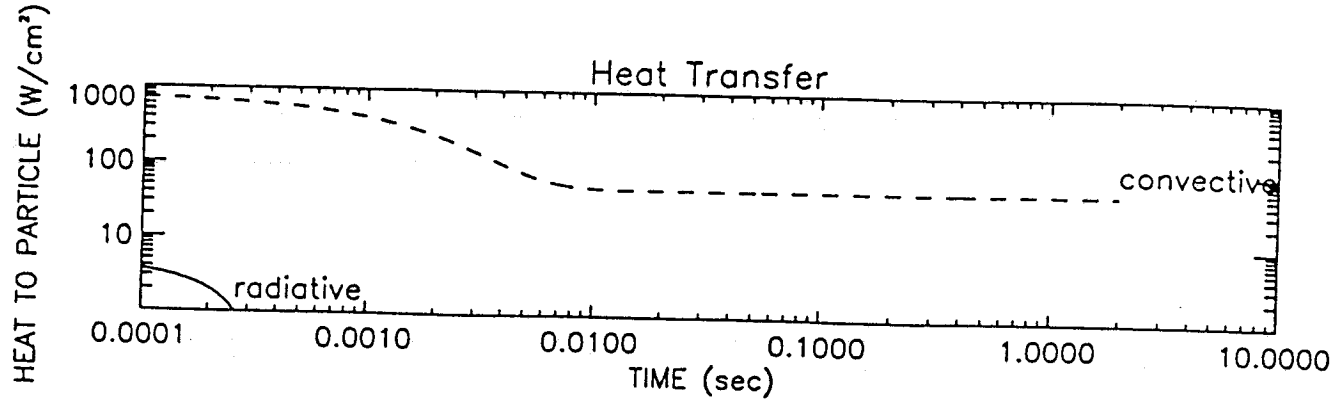


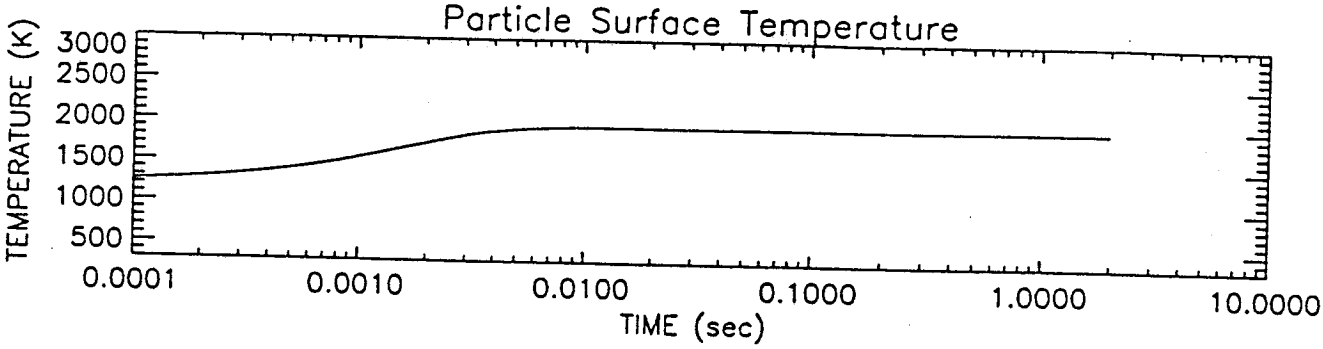


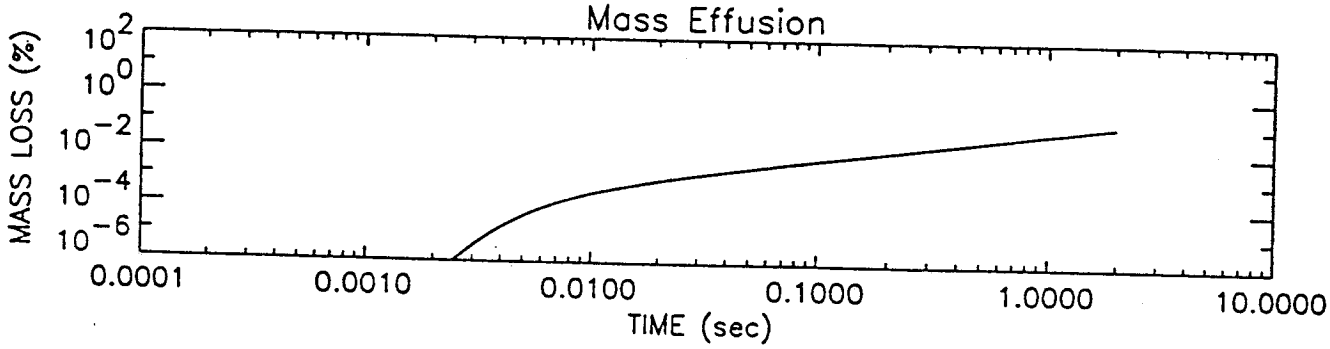


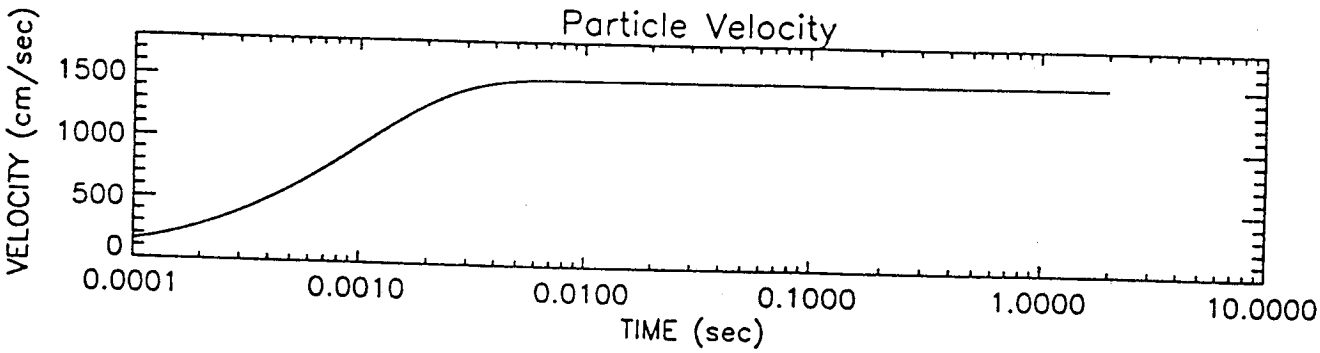

Stream Temp=2000. Particle Diameter= 100. Time for run= 2.00 Emissivity= 0.2

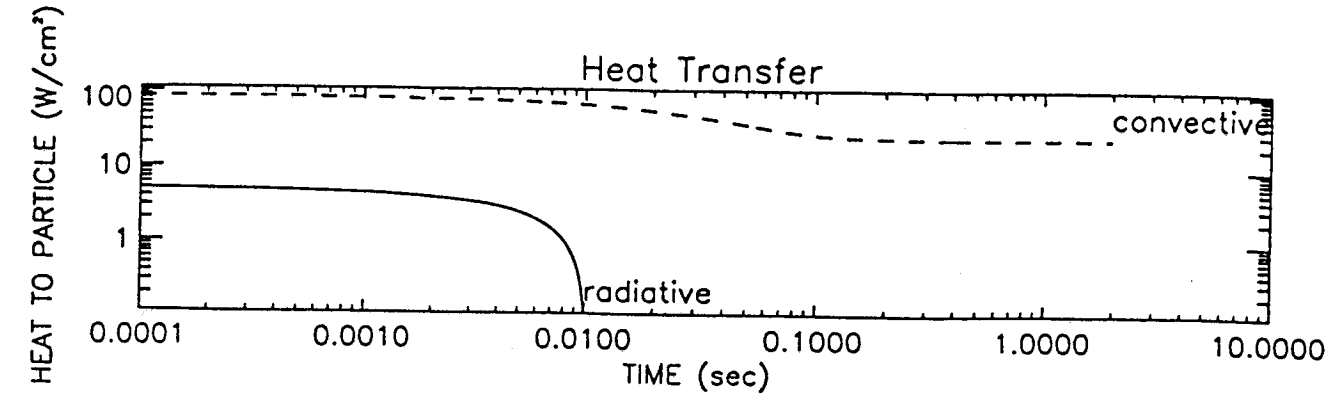


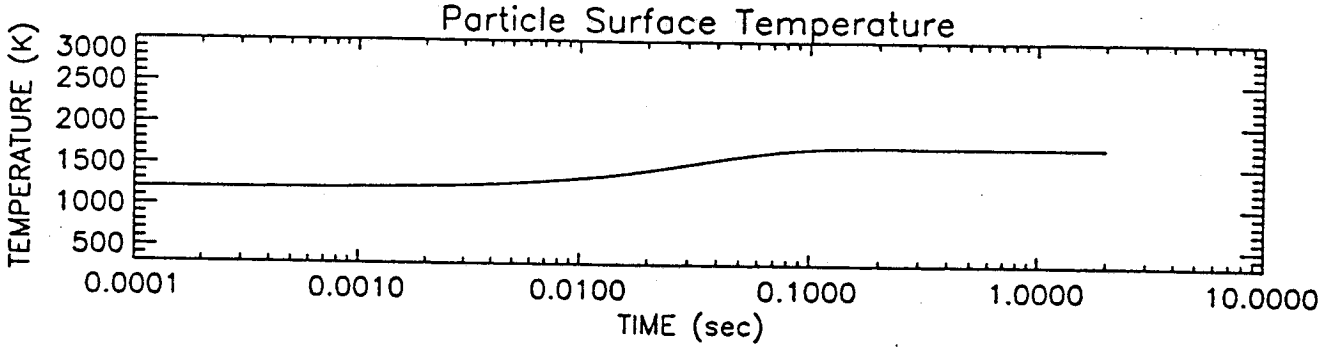


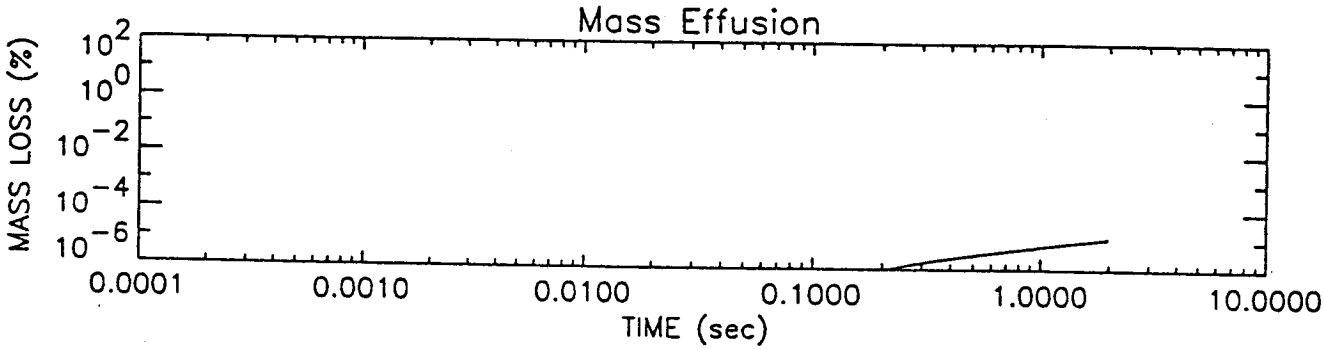


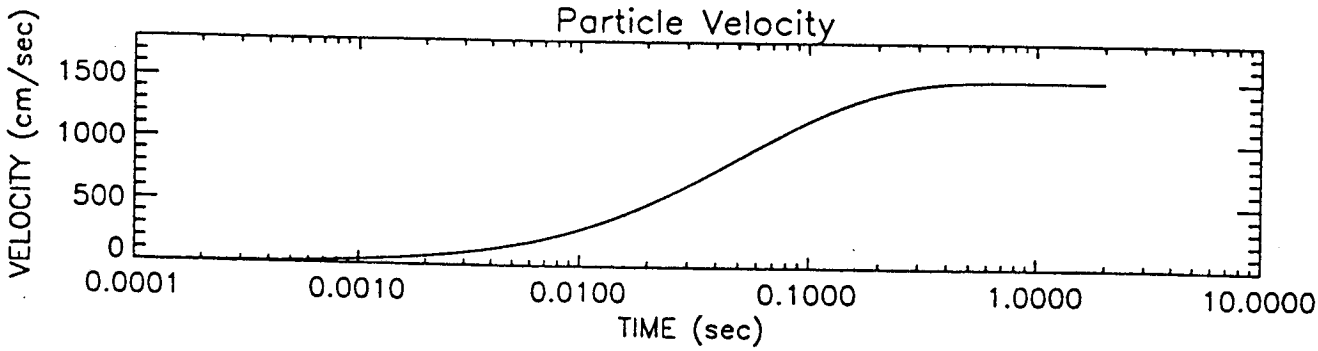

Stream Temp=2000. Particle Diameter=1000. Time for run= 2.00 Emissivity= 0.2

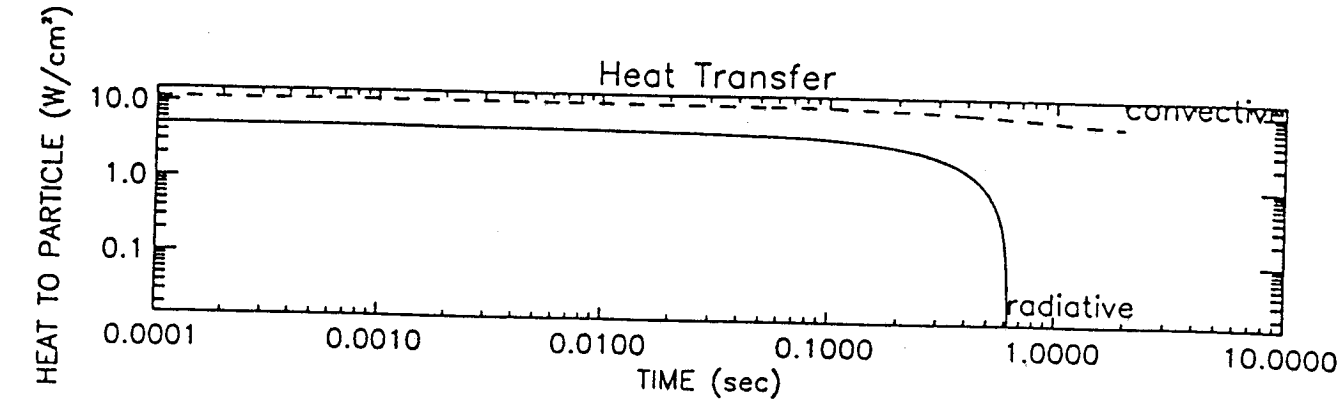


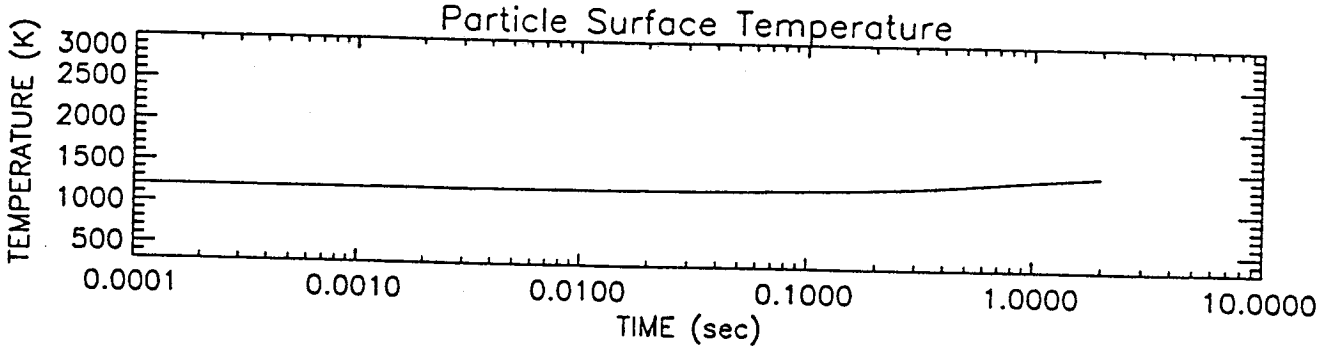


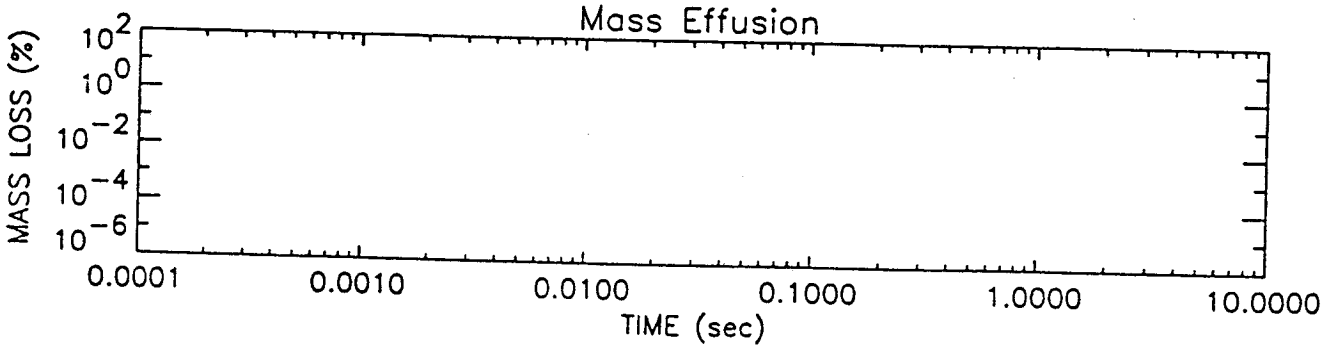


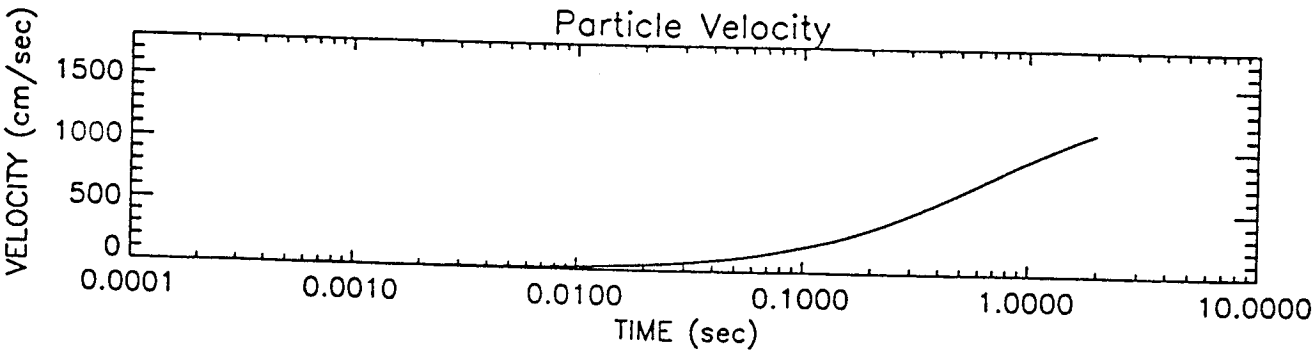

Stream Temp=2200. Particle Diameter= 10. Time for run= 2.00 Emissivity= 0.2

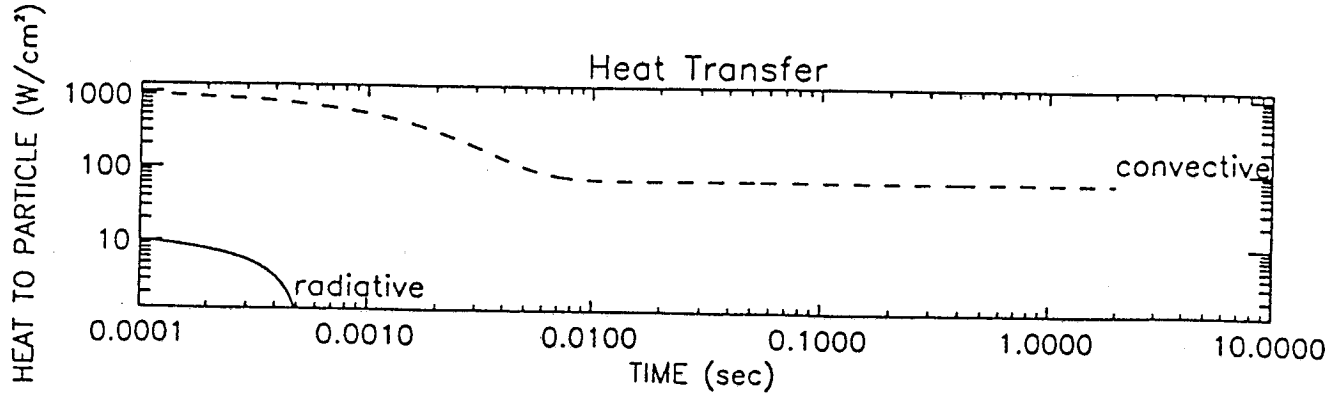


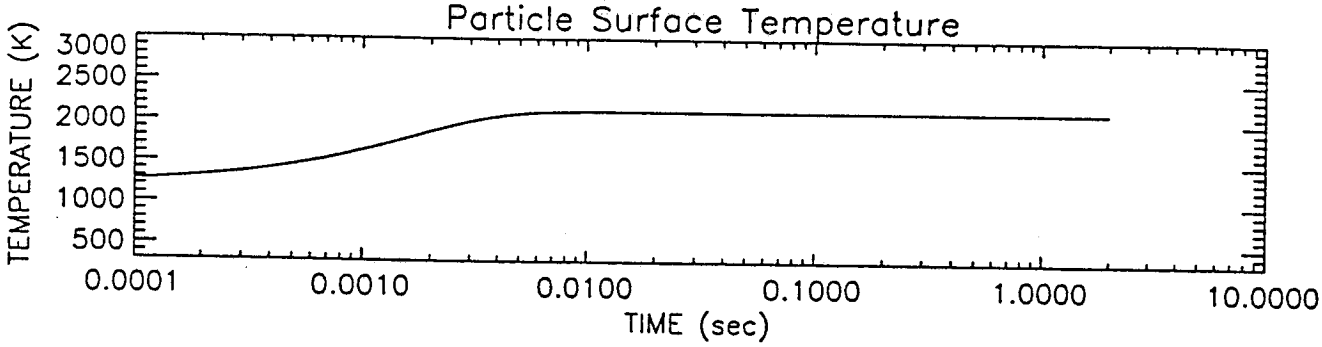


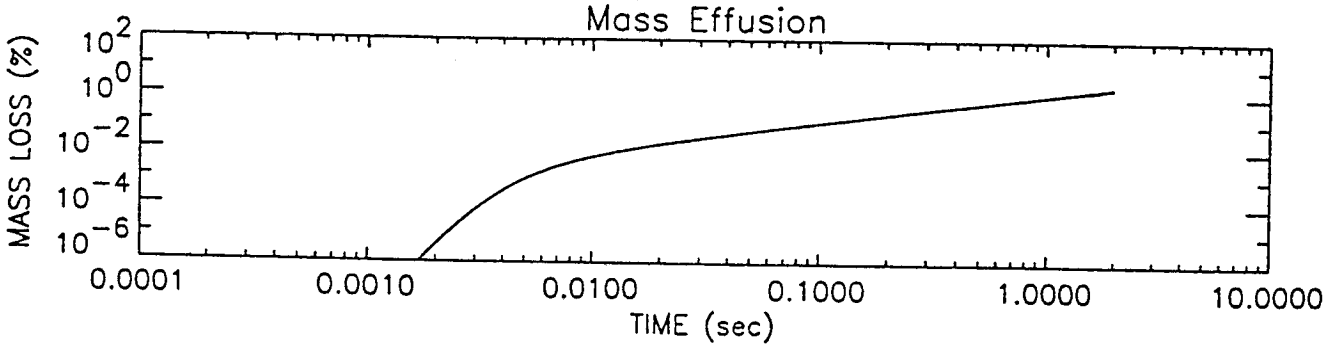


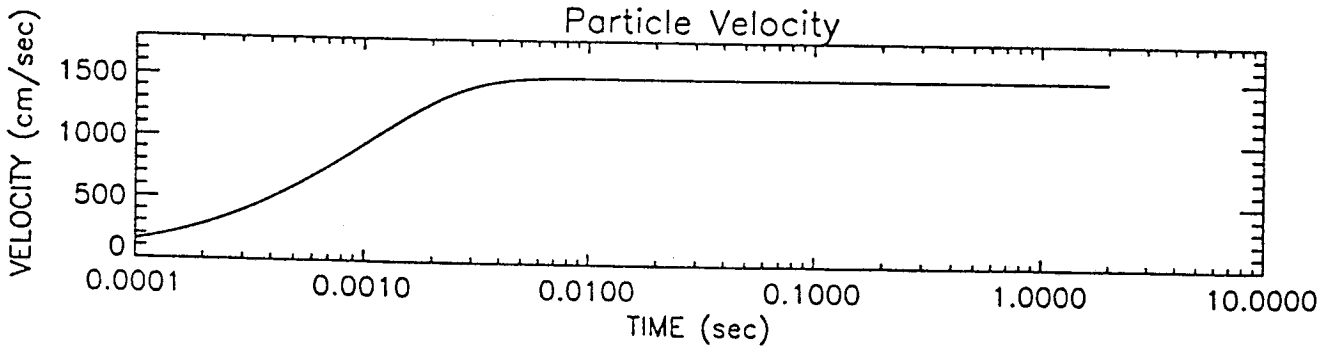

Stream Temp=2200. Particle Diameter= 100. Time for run= 2.00 Emissivity= 0.2

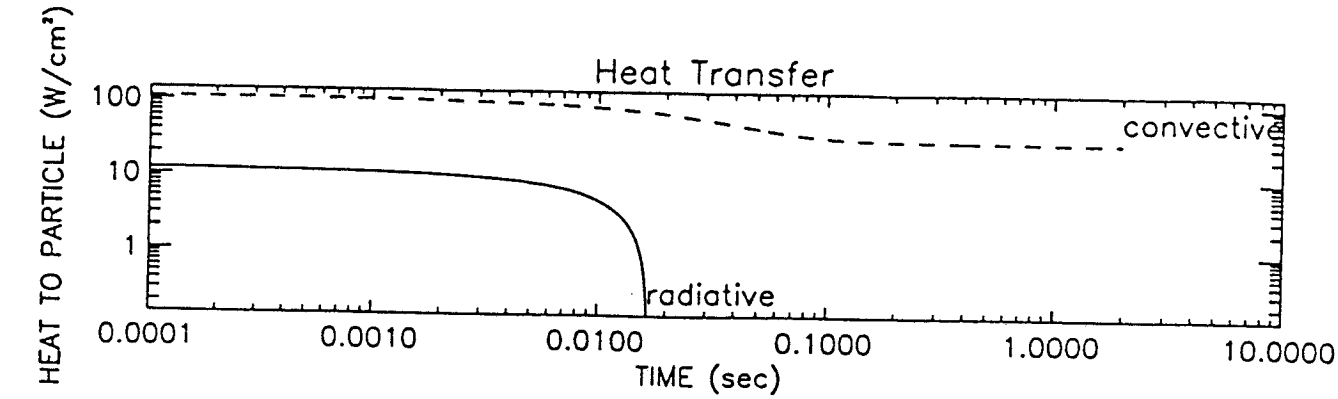


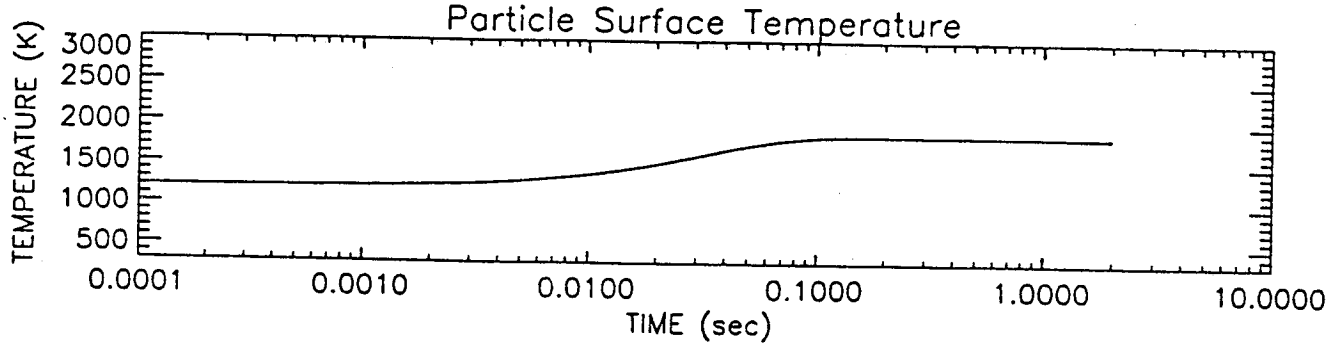


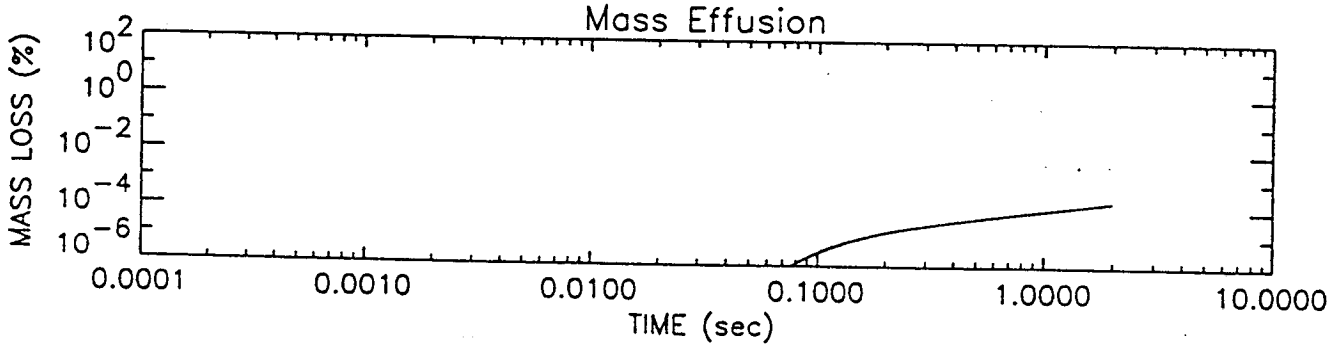


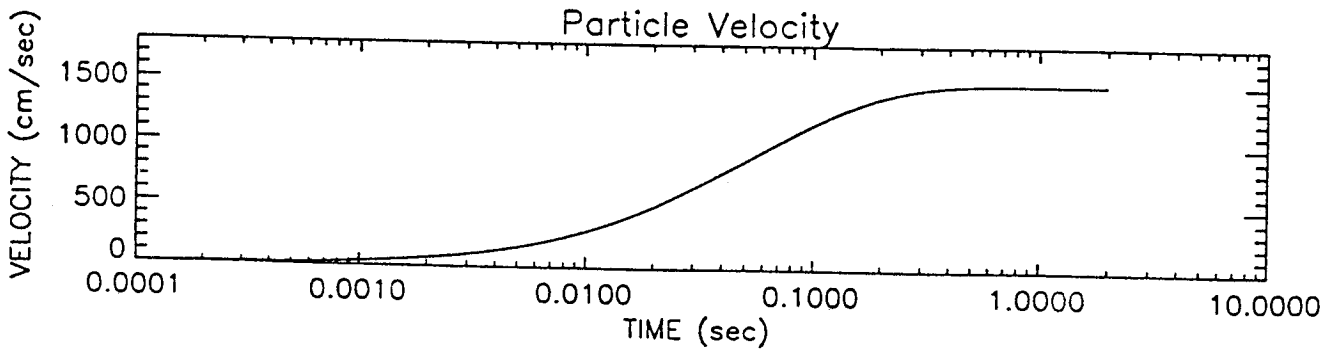

Stream Temp=3000. Particle Diameter= 10. Time for run= 2.00 Emissivity= 0.2

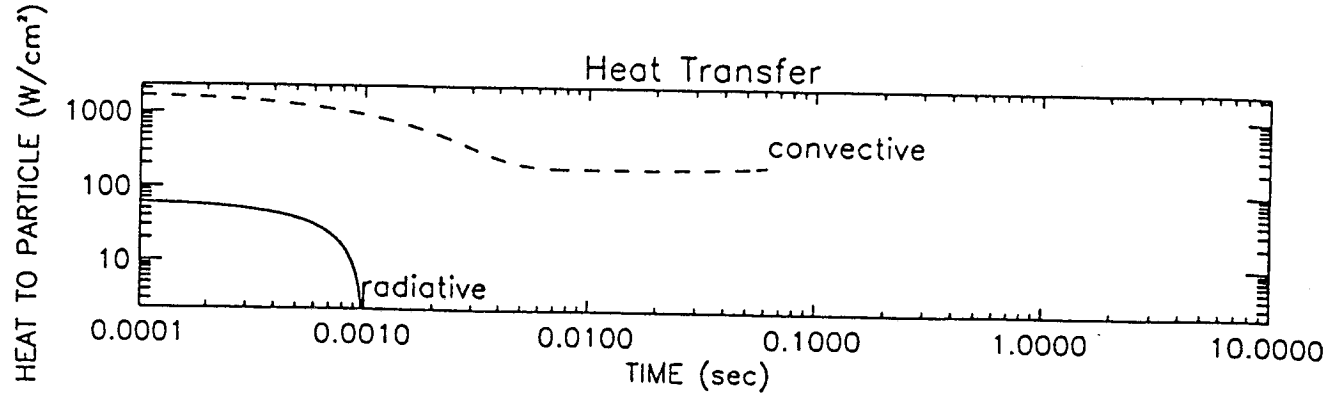


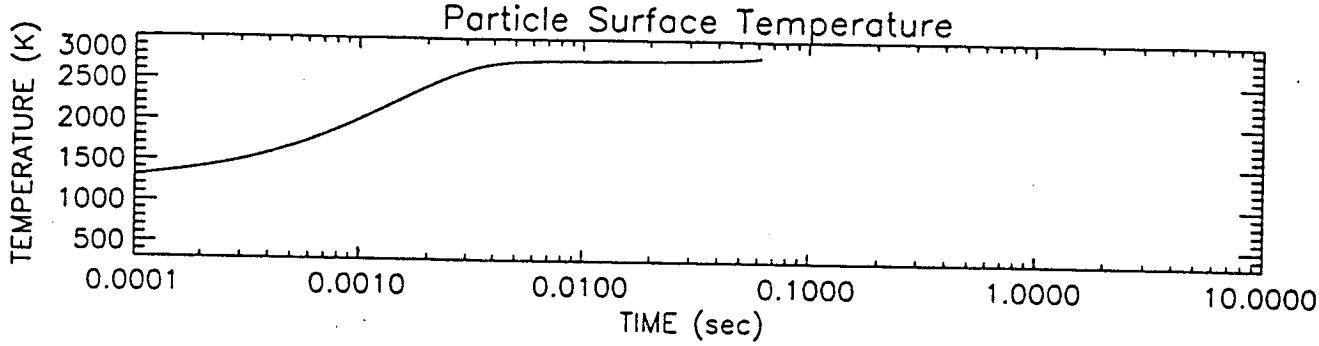


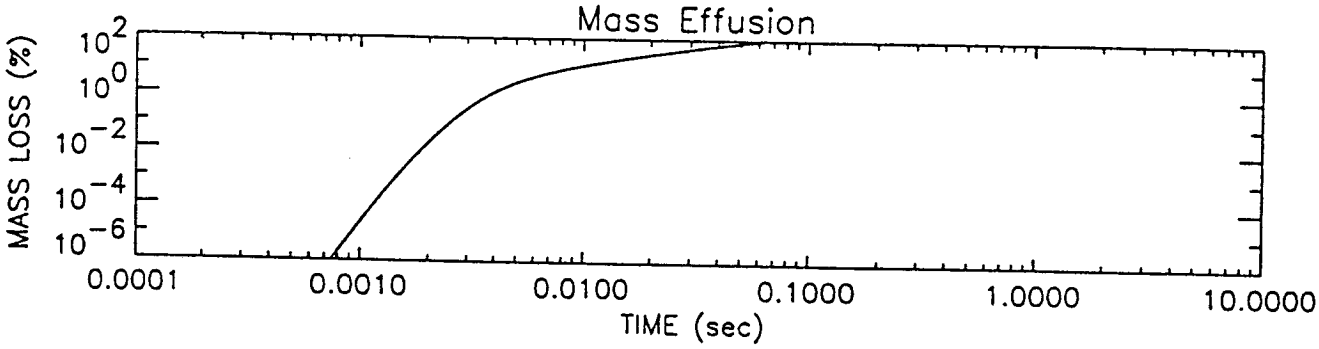


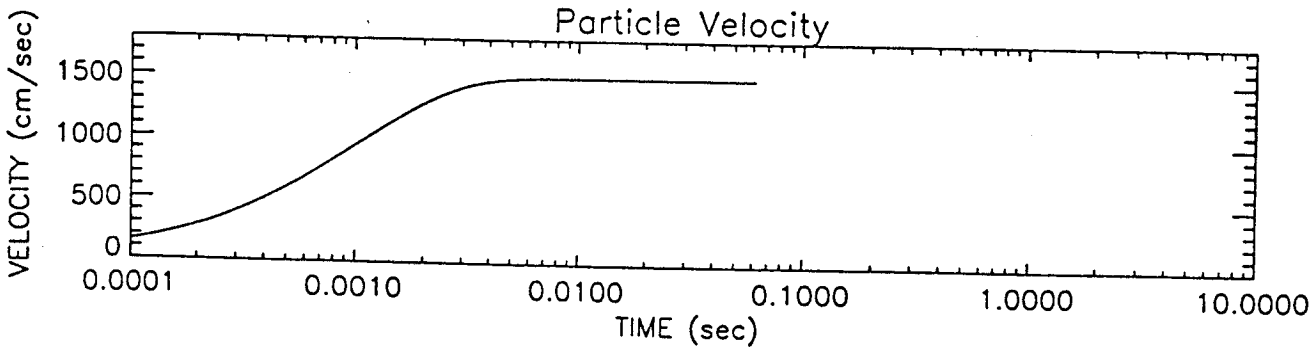

Stream Temp=3000. Particle Diameter= 100. Time for run= 2.00 Emissivity= 0.2

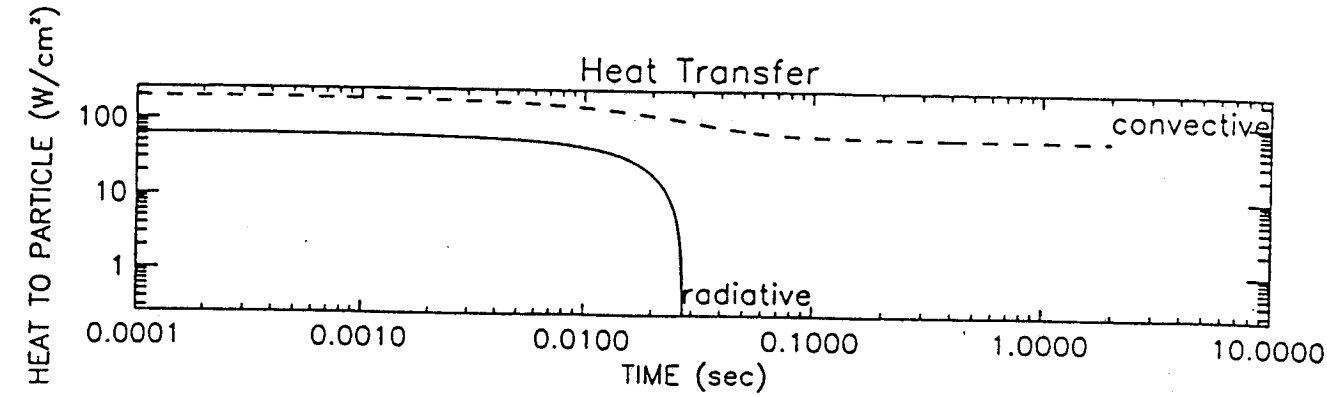


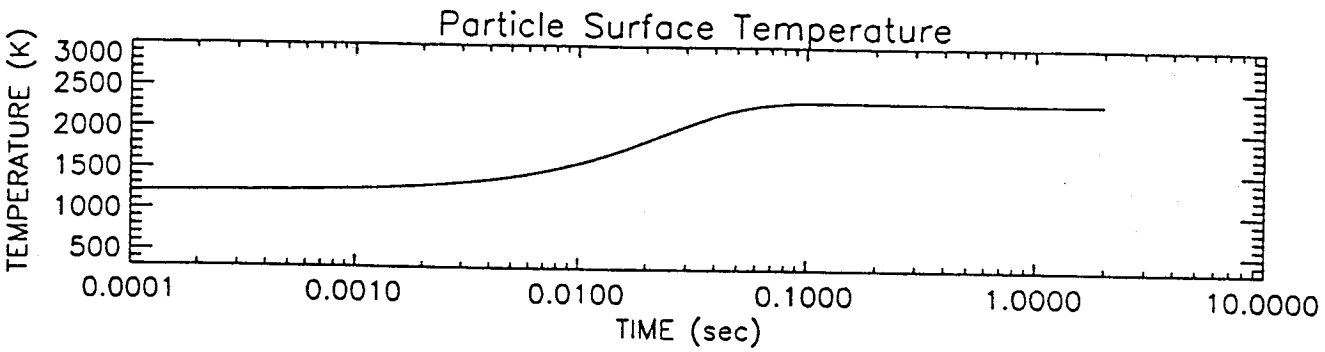


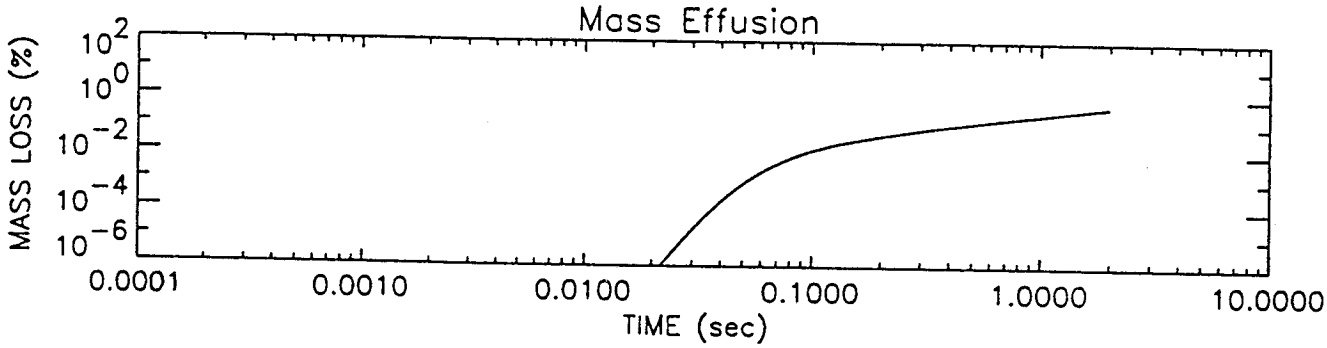


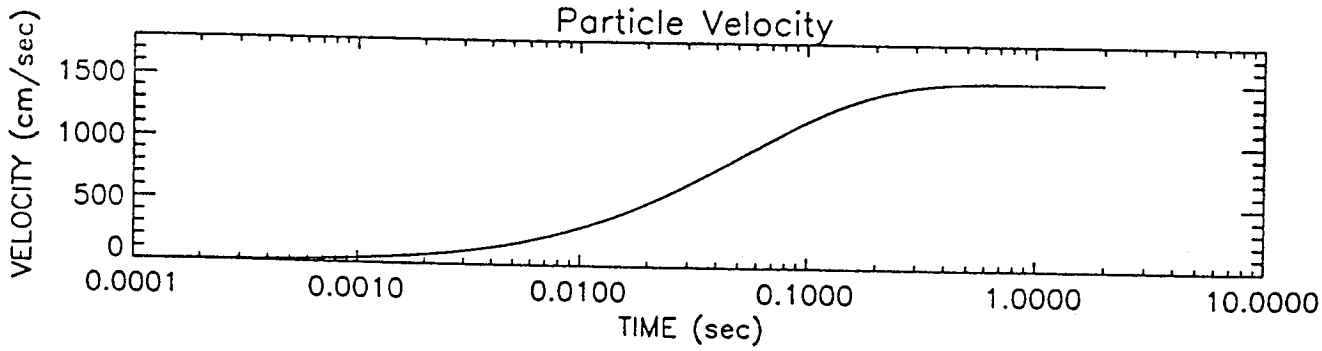

Stream Temp=3000. Particle Diameter=1000. Time for run= 2.00 Emissivity= 0.2

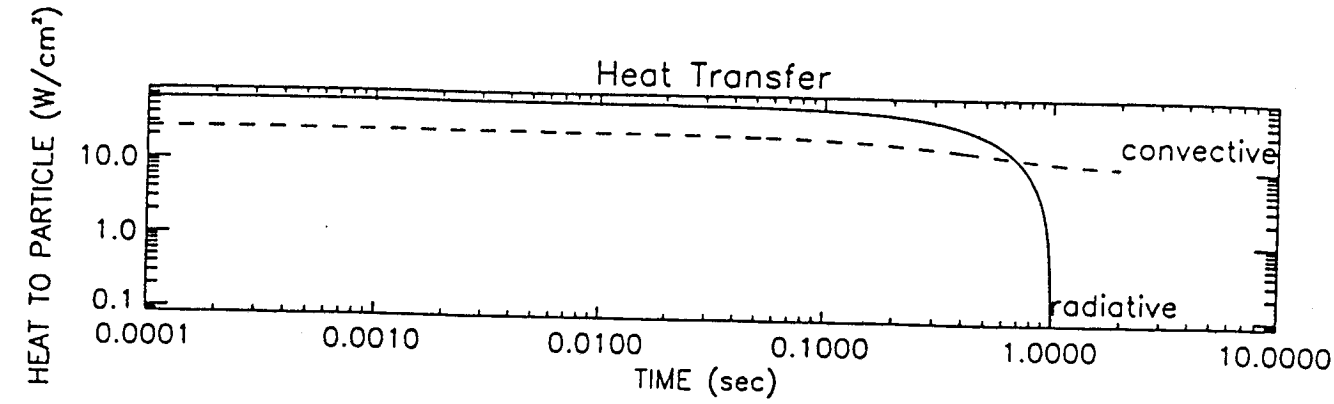


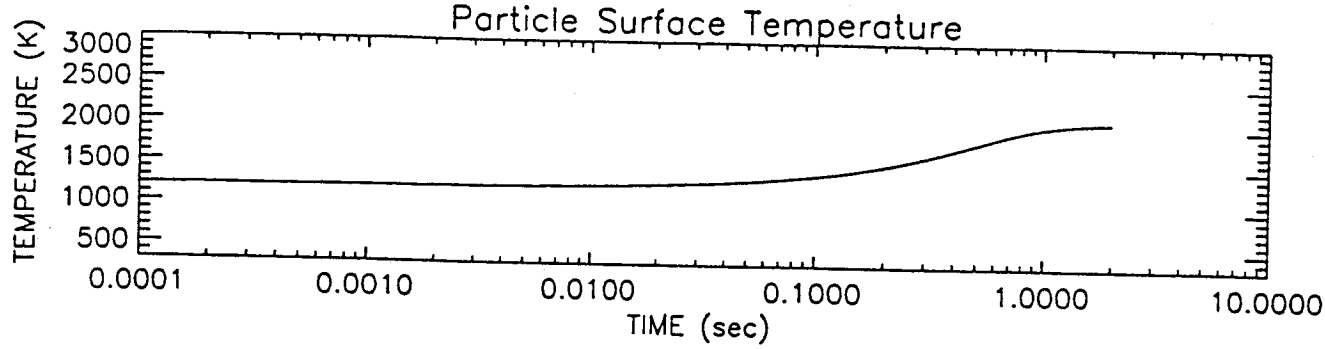


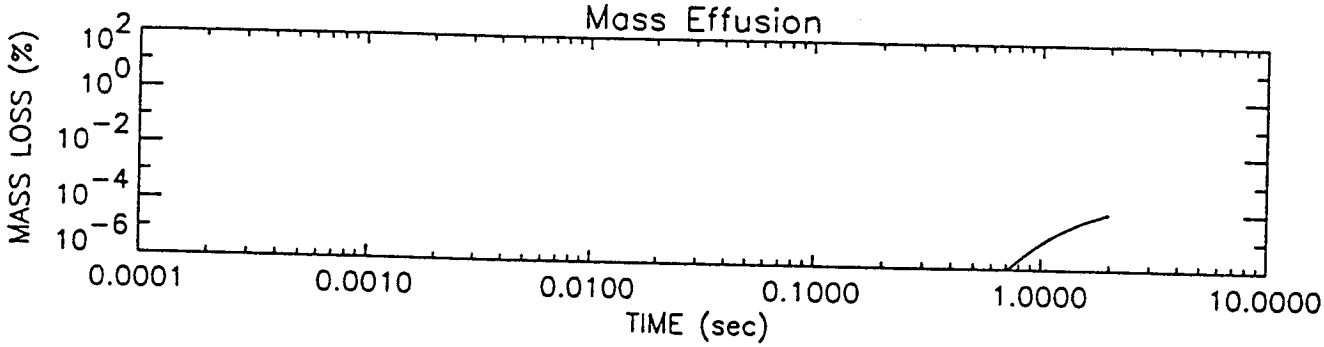


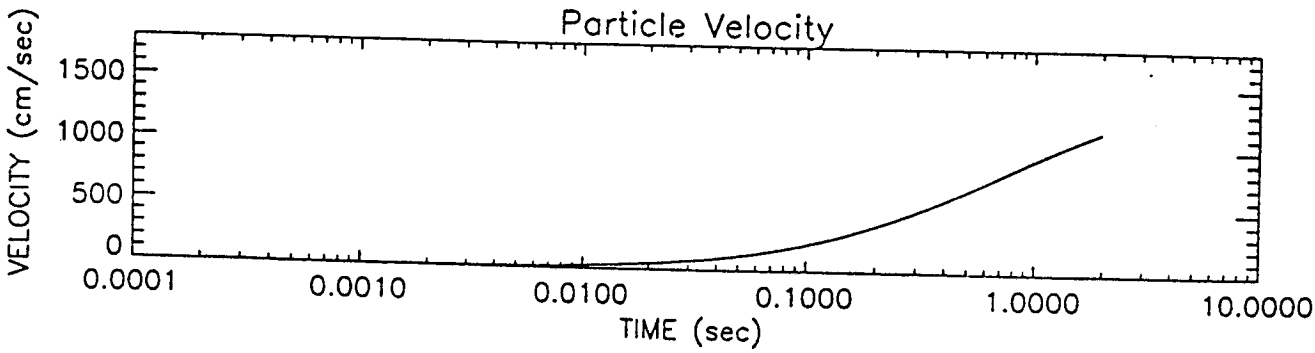

Stream Temp=1700. Particle Diameter= 10. Time for run= 2.00 Emissivity= 0.8

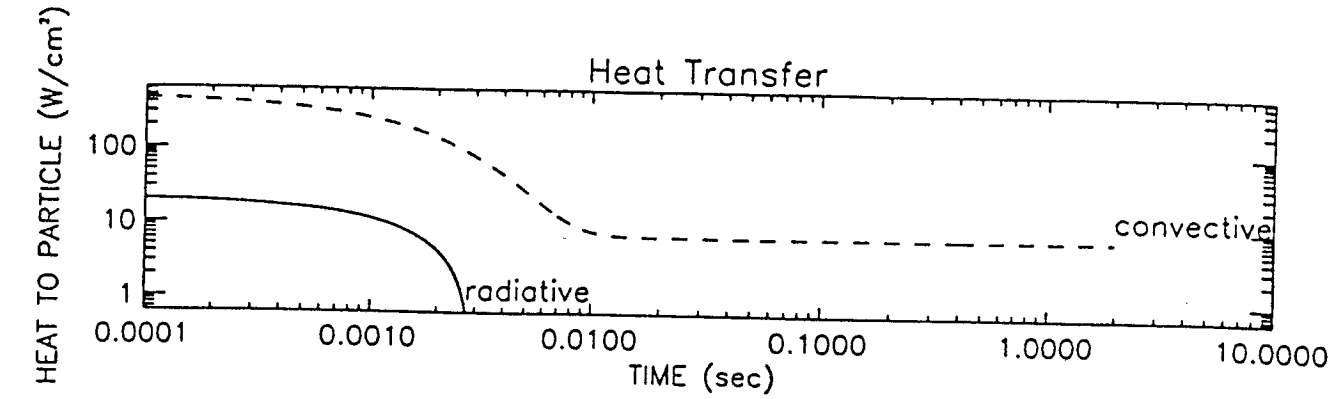


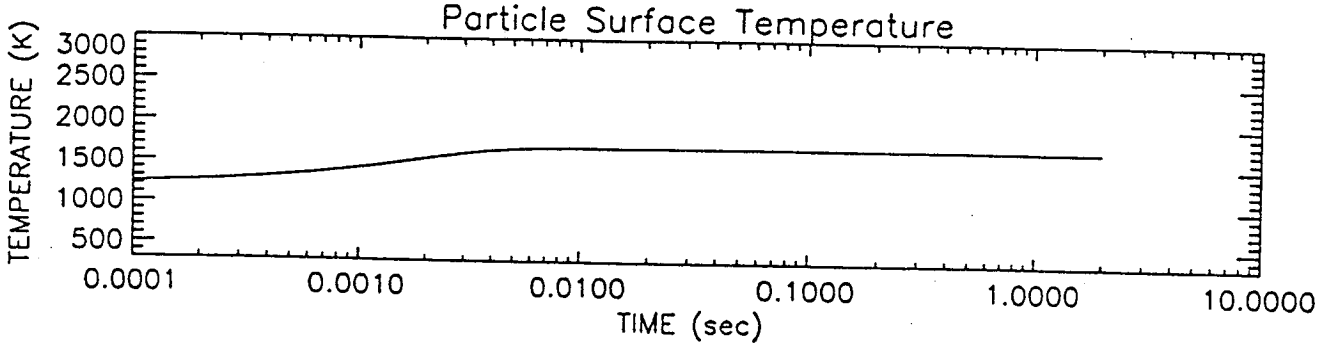


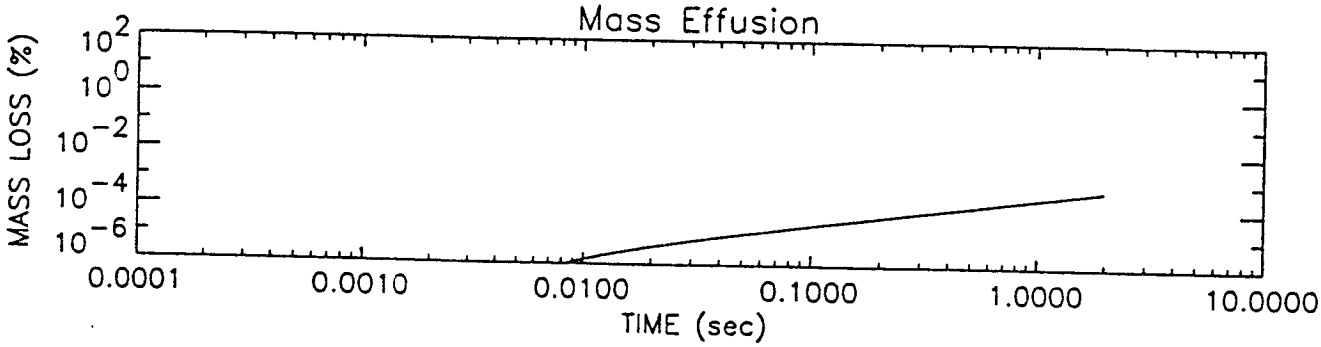


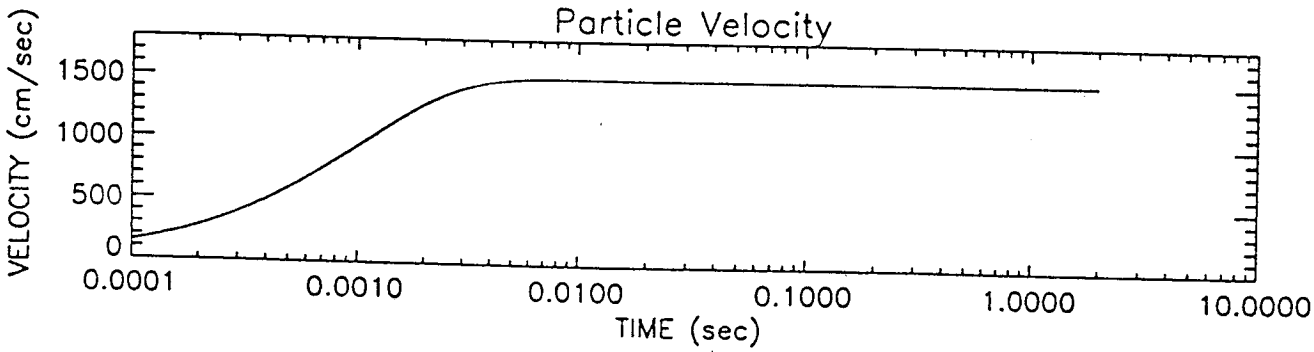

Stream Temp=1700. Particle Diameter= 100. Time for run= 2.00 Emissivity= 0.8

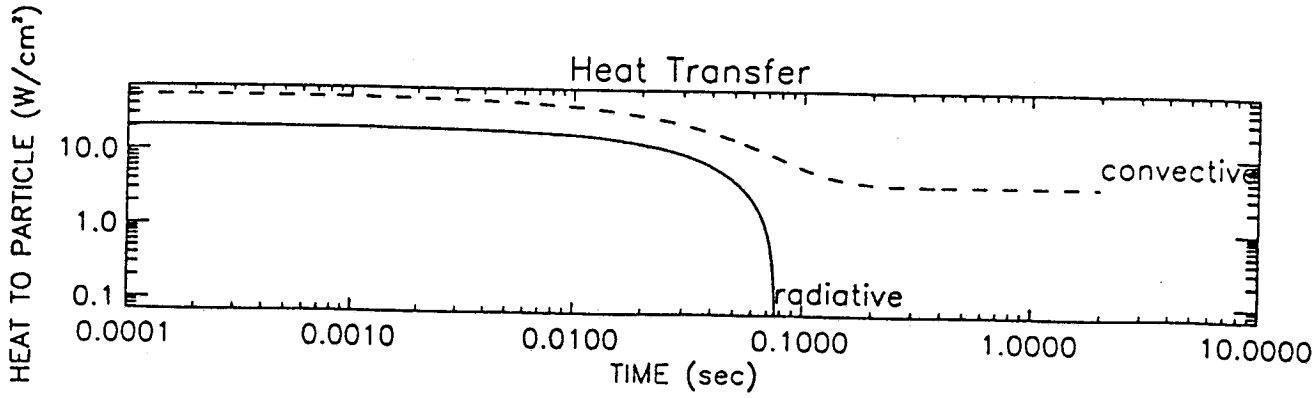


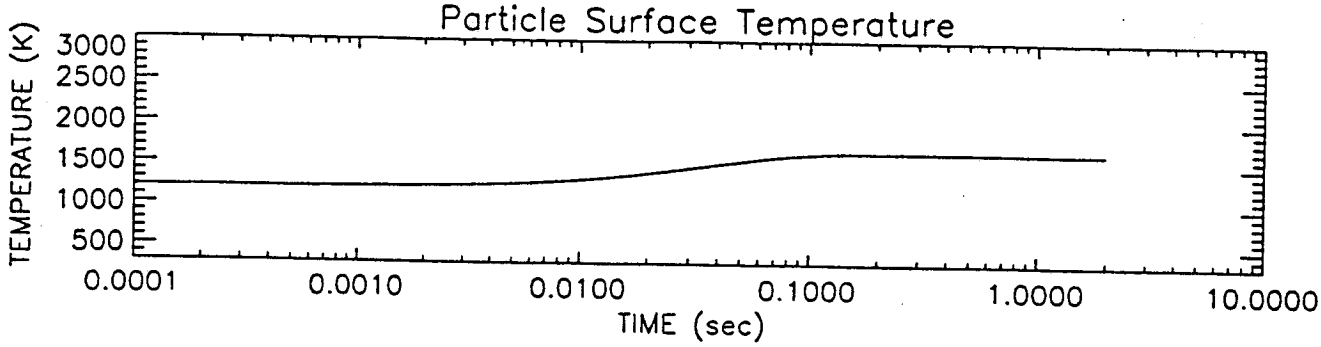


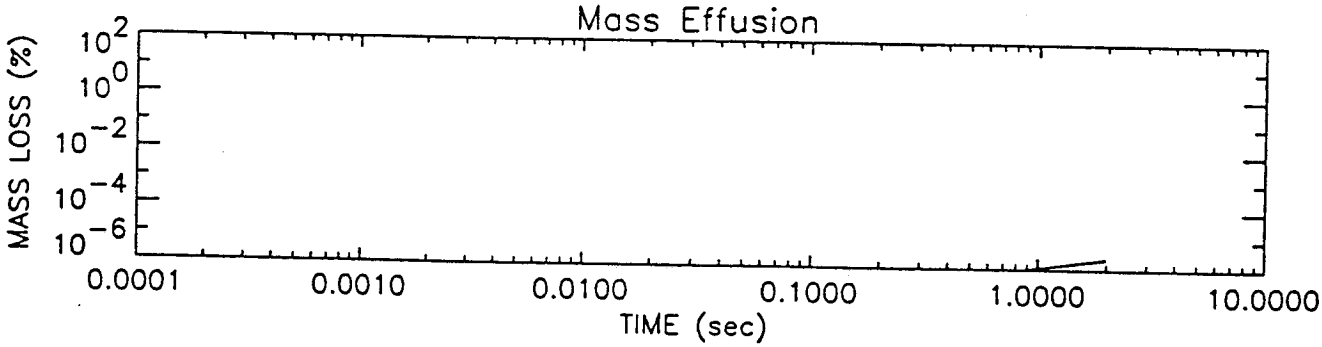


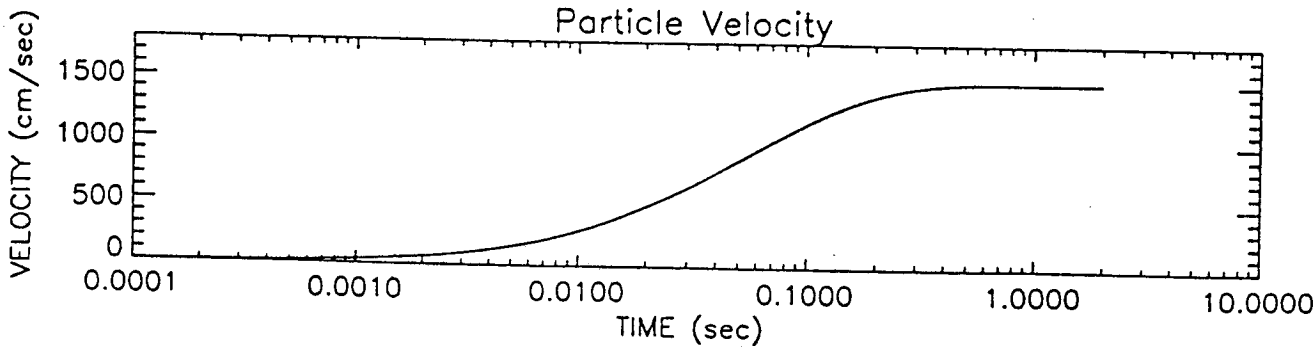

Stream Temp=1700. Particle Diameter=1000. Time for run= 2.00 Emissivity= 0.8

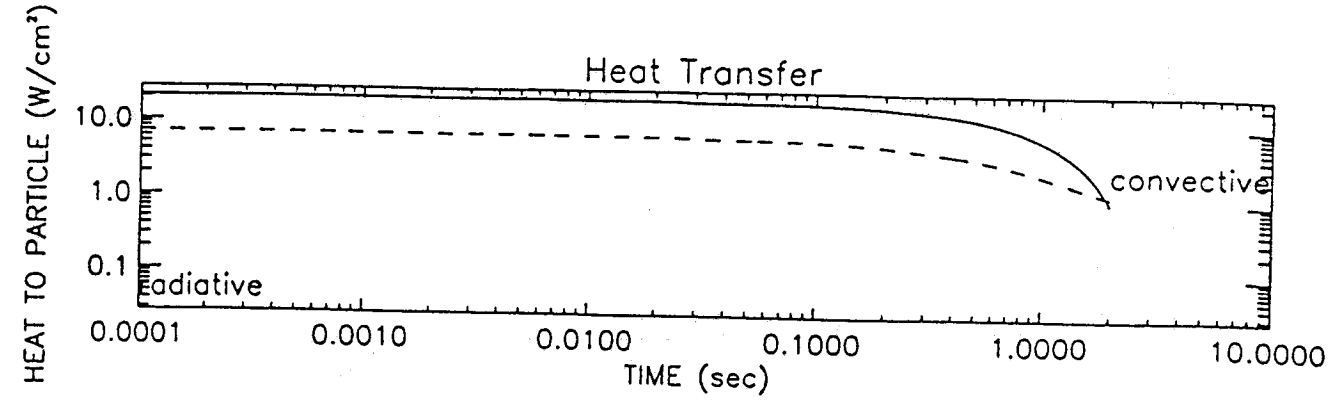


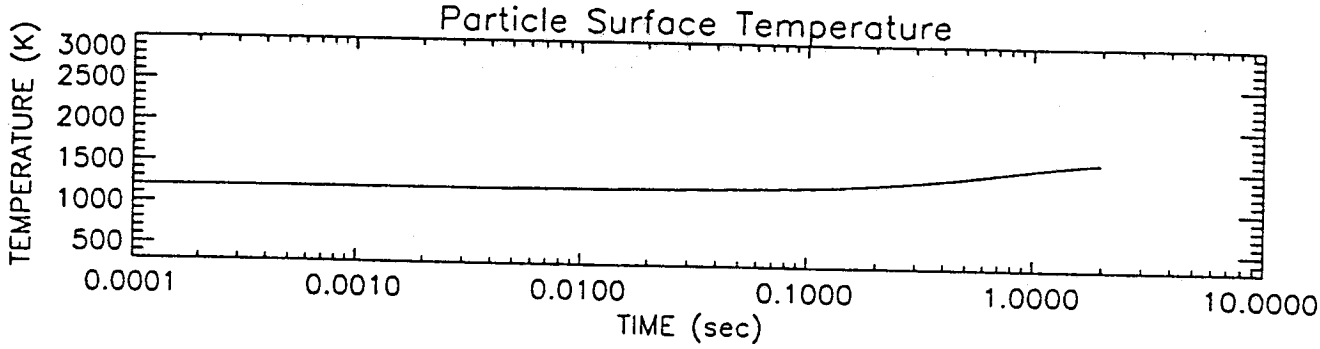


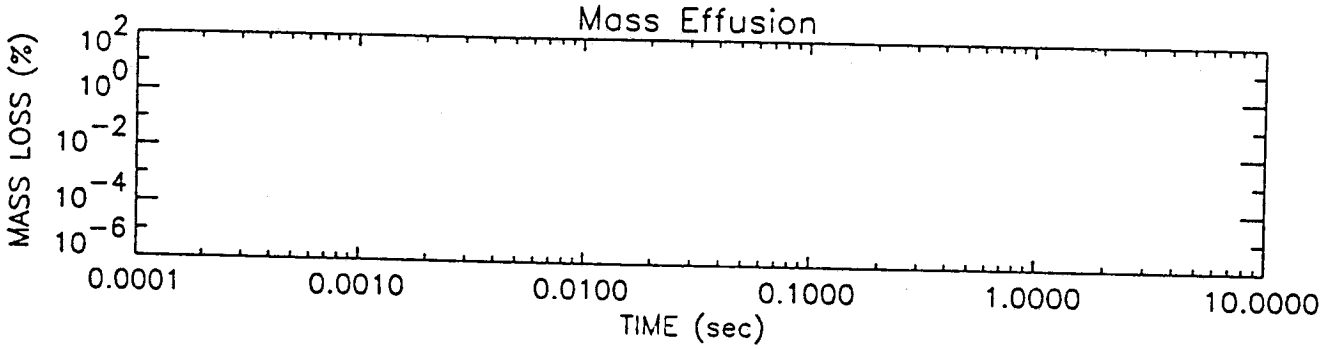


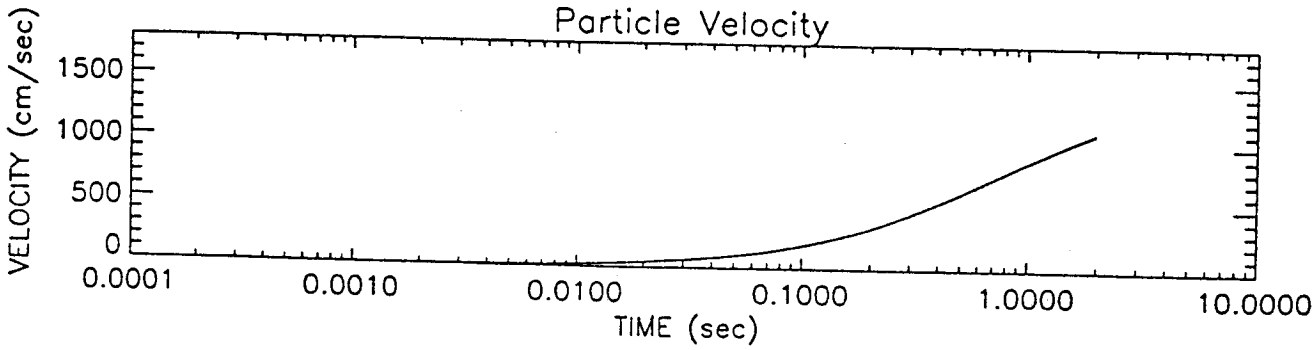

Stream Temp=2000. Particle Diameter=1000. Time for run= 2.00 Emissivity= 0.8

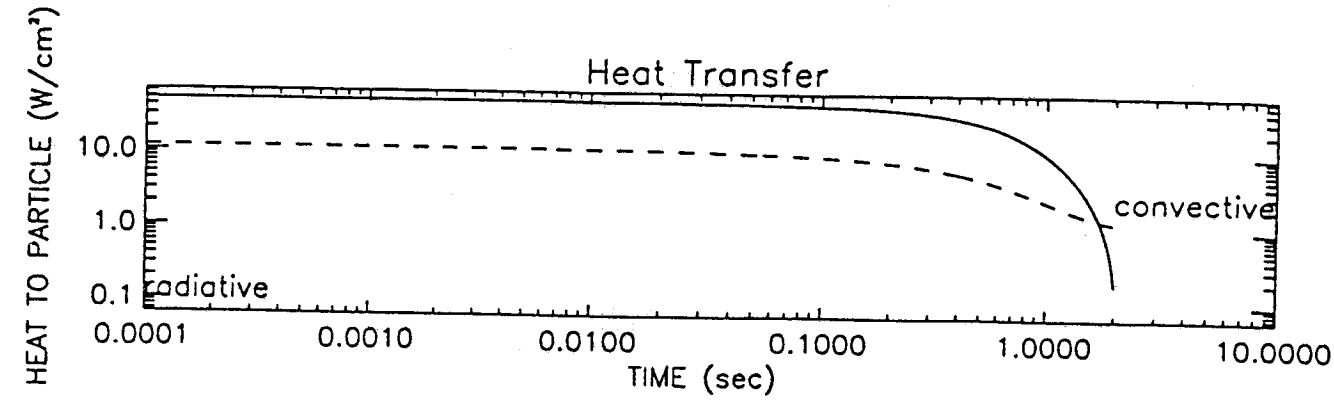


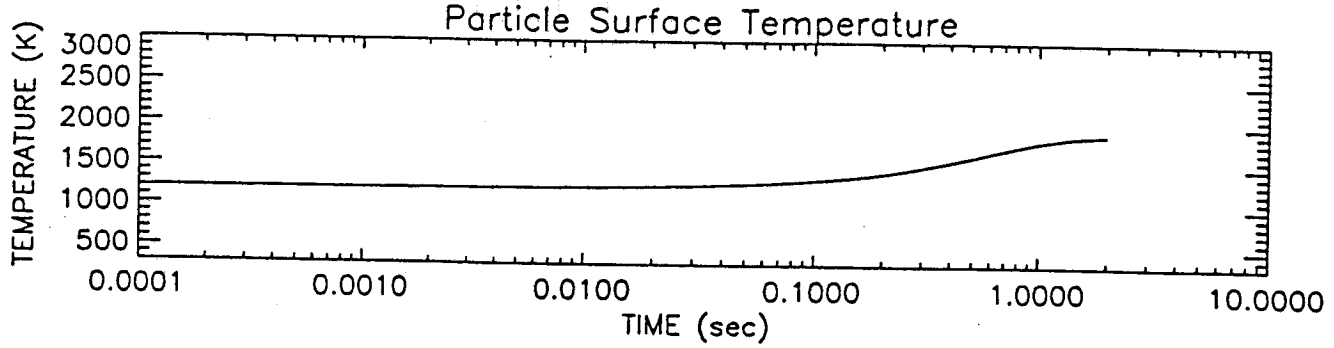


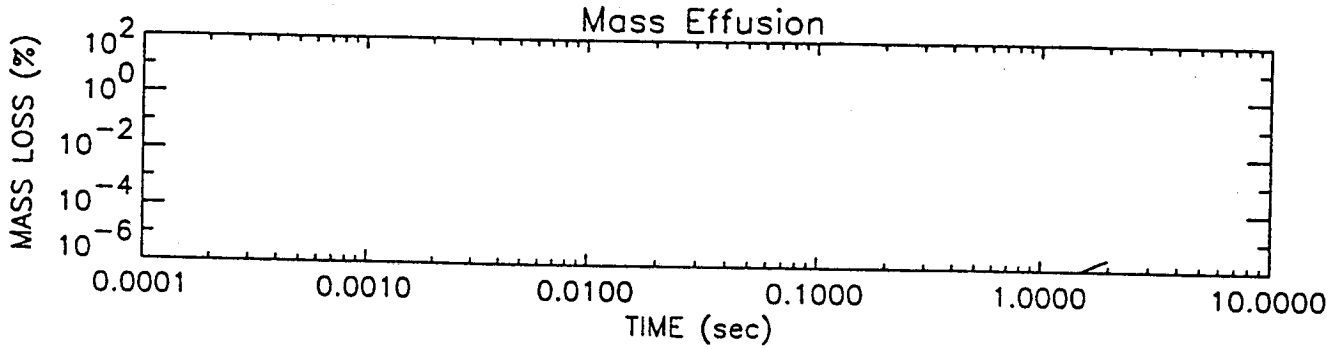


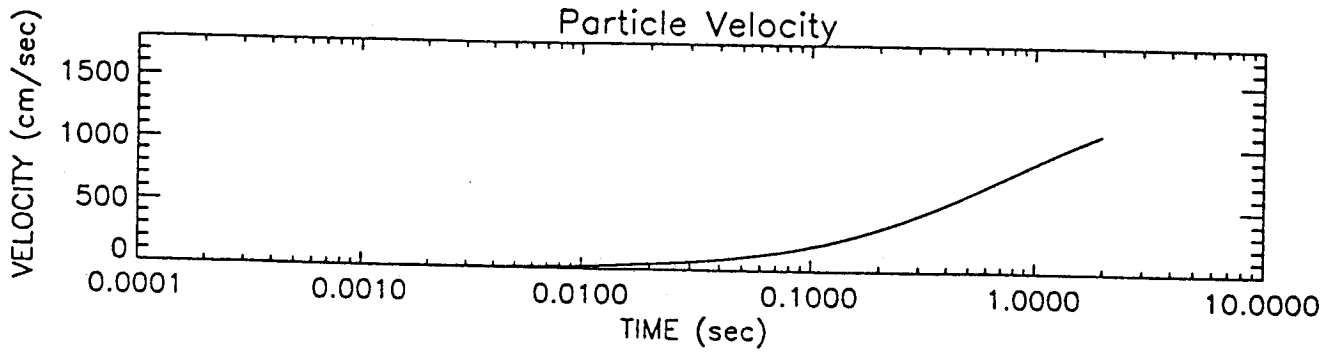

Stream Temp=2200. Particle Diameter= 10. Time for run= 2.00 Emissivity= 0.8

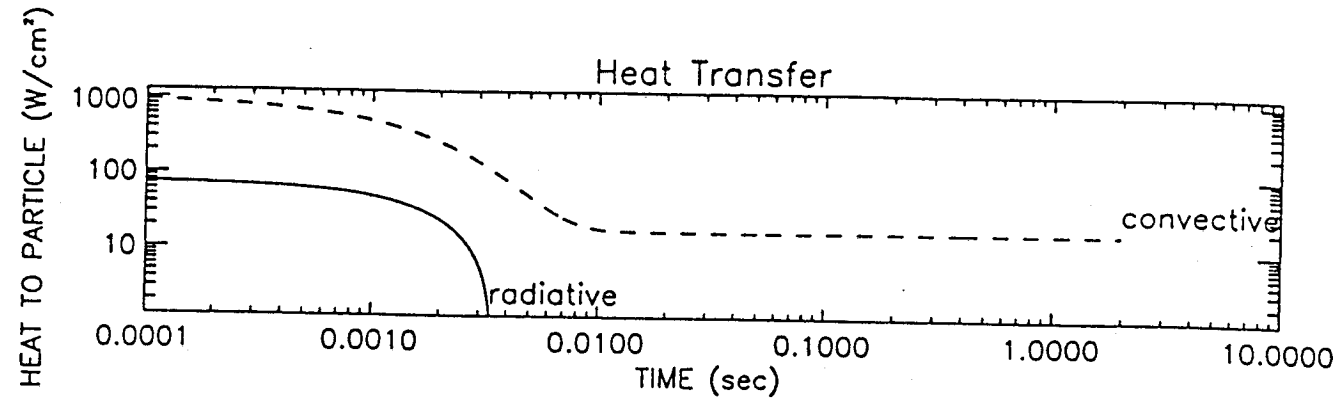


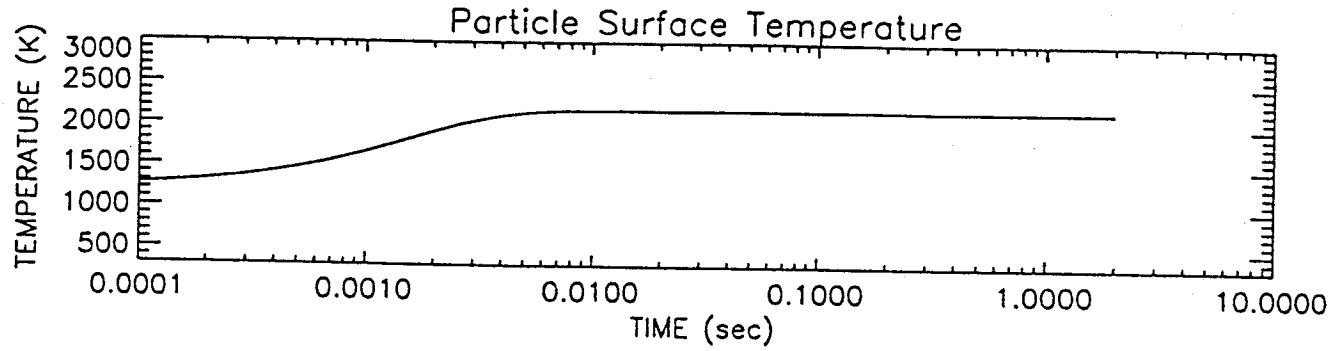


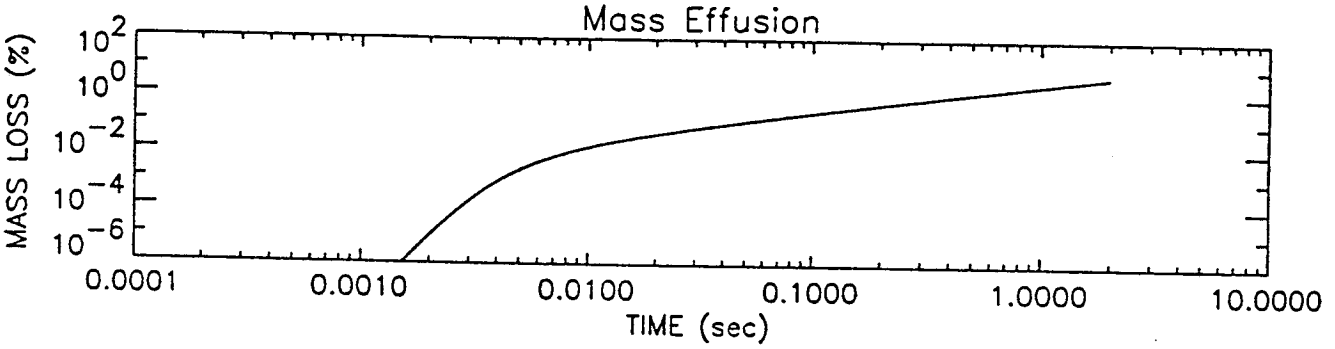


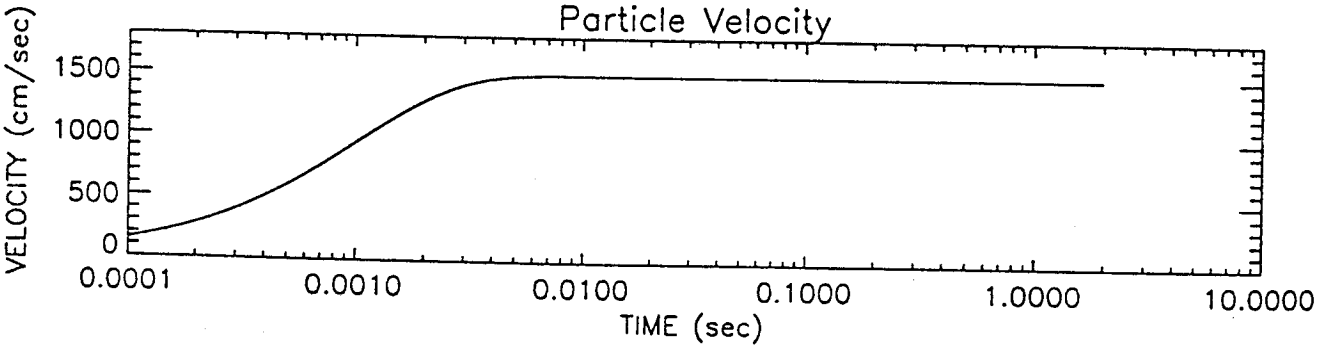

Stream Temp=2200. Particle Diameter= 100. Time for run= 2.00 Emissivity= 0.8

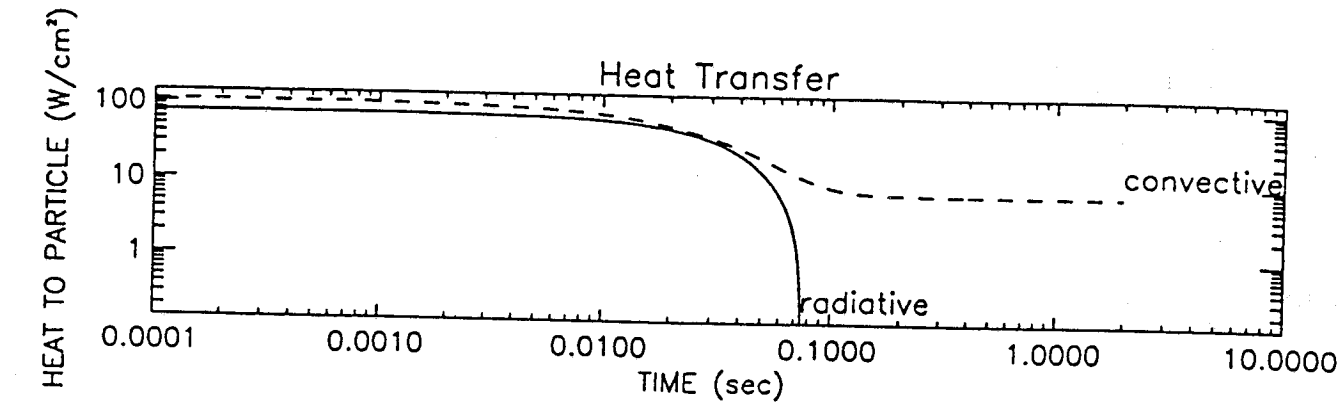


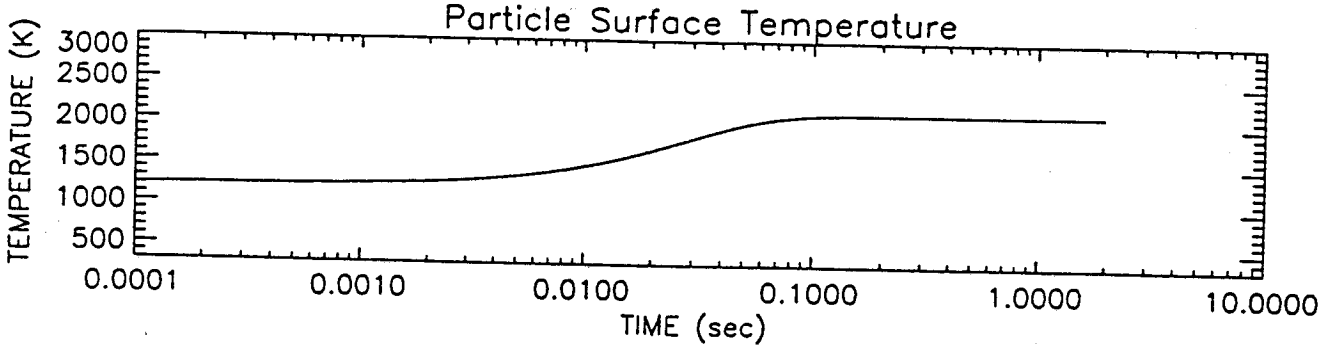


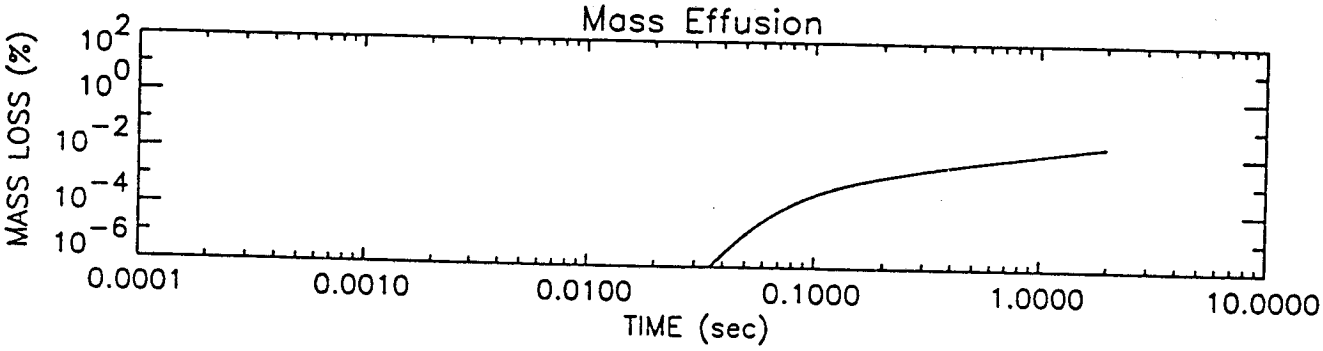


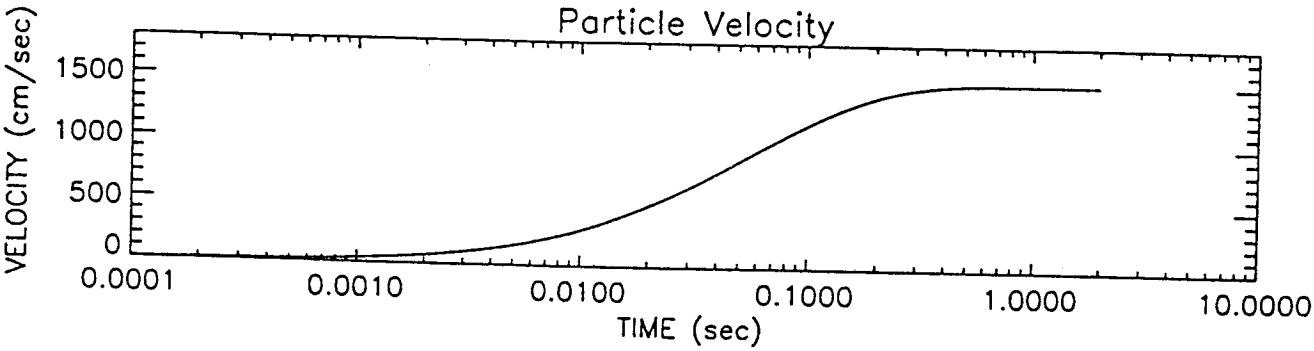

Stream Temp=2200. Particle Diameter=1000. Time for run= 2.00 Emissivity= 0.8

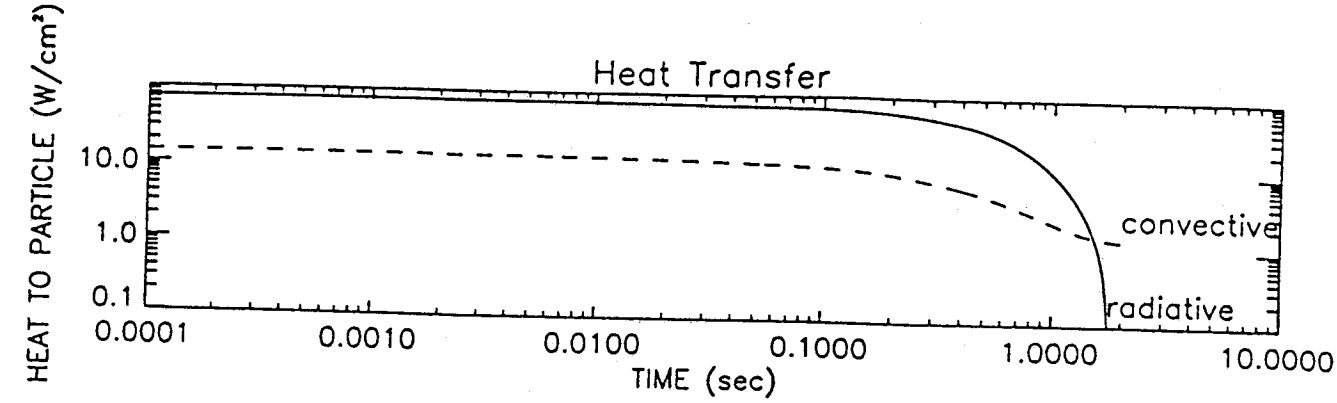


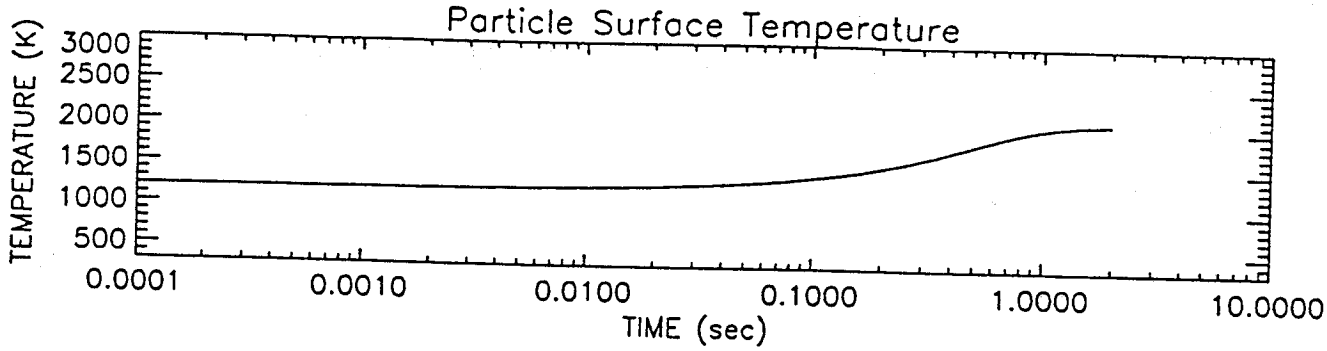


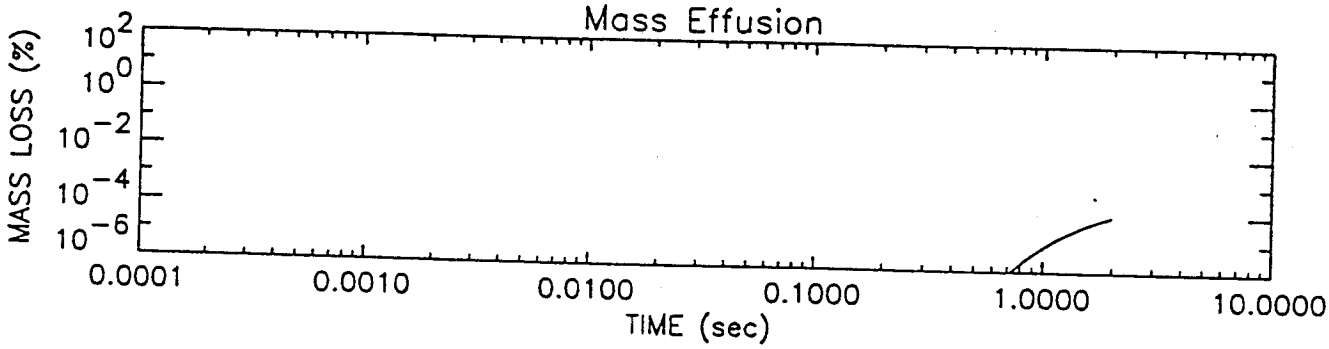


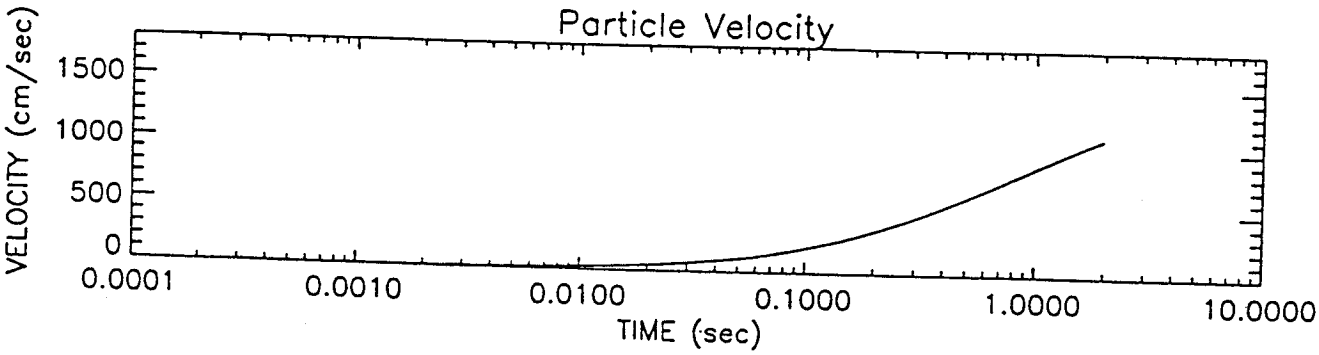

Stream Temp=2500. Particle Diameter= 10. Time for run= 2.00 Emissivity= 0.8

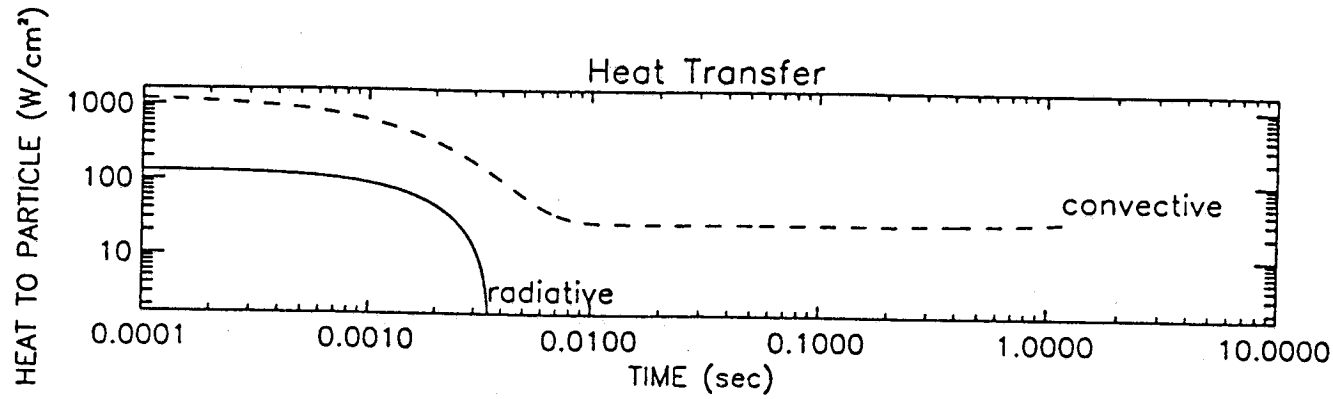


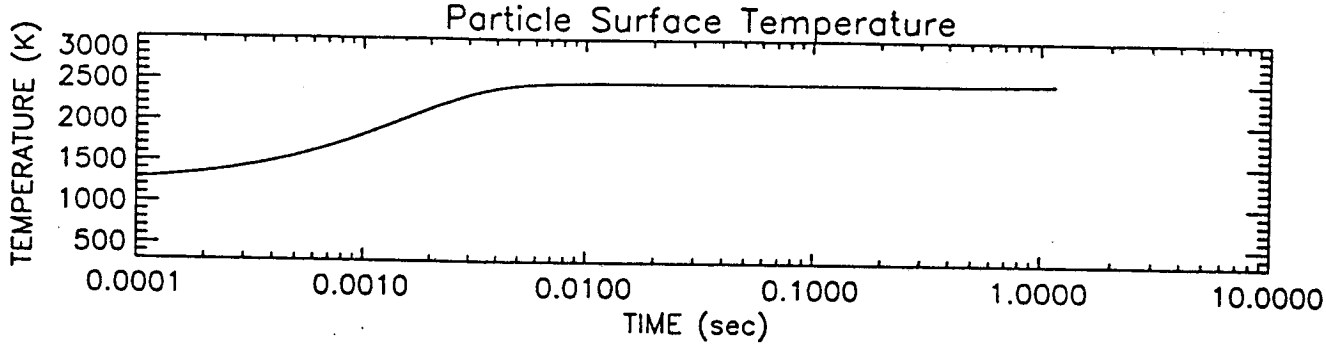


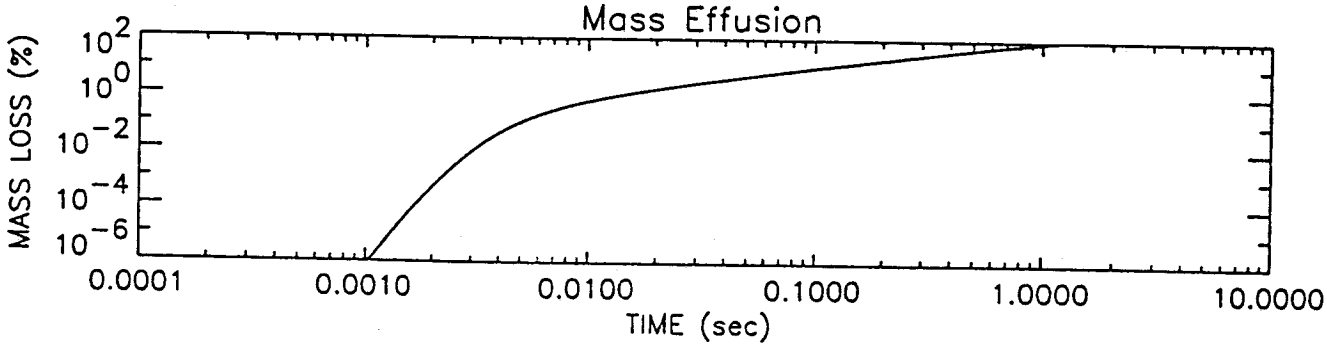


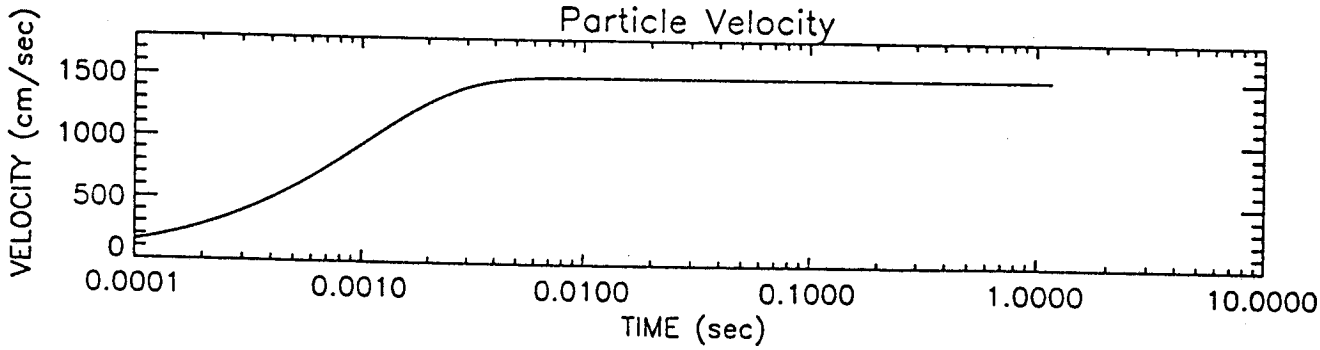

Stream Temp=2500. Particle Diameter= 100. Time for run= 2.00 Emissivity= 0.8

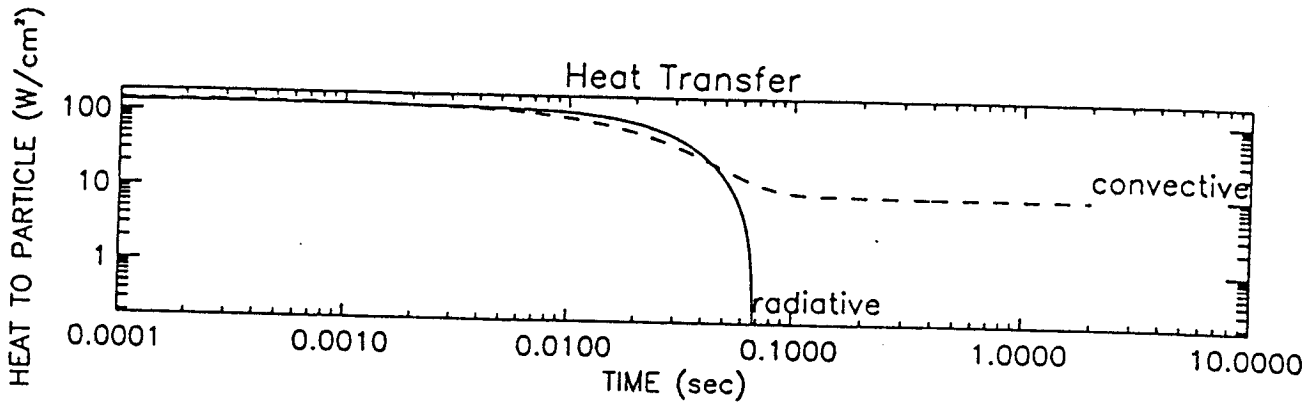


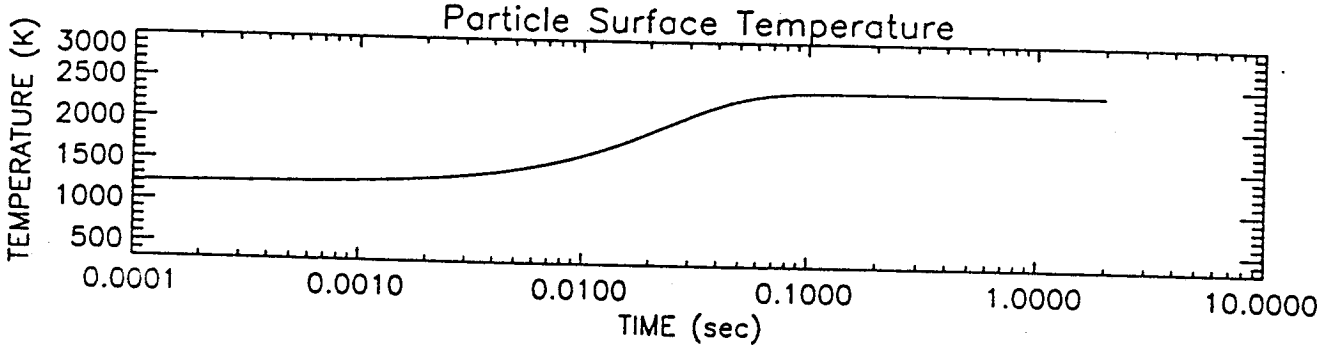


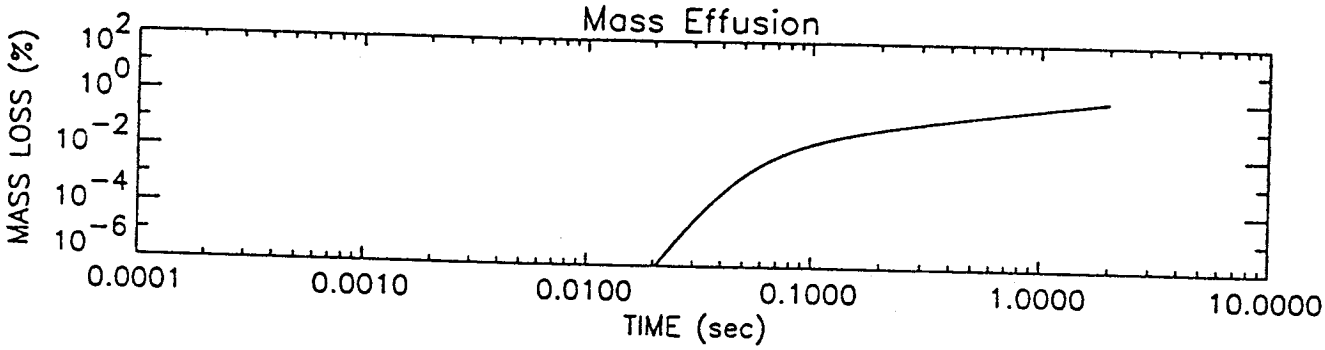


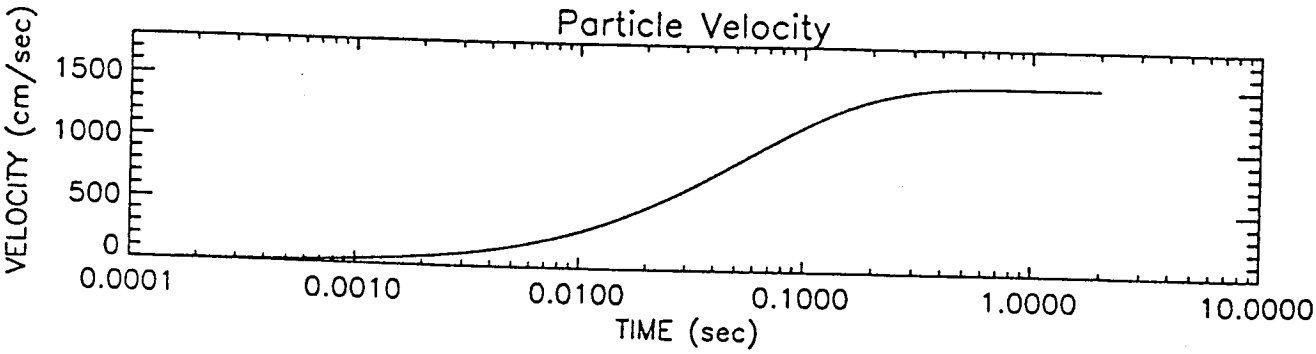

Stream Temp=2500. Particle Diameter=1000. Time for run= 2.00 Emissivity= 0.8

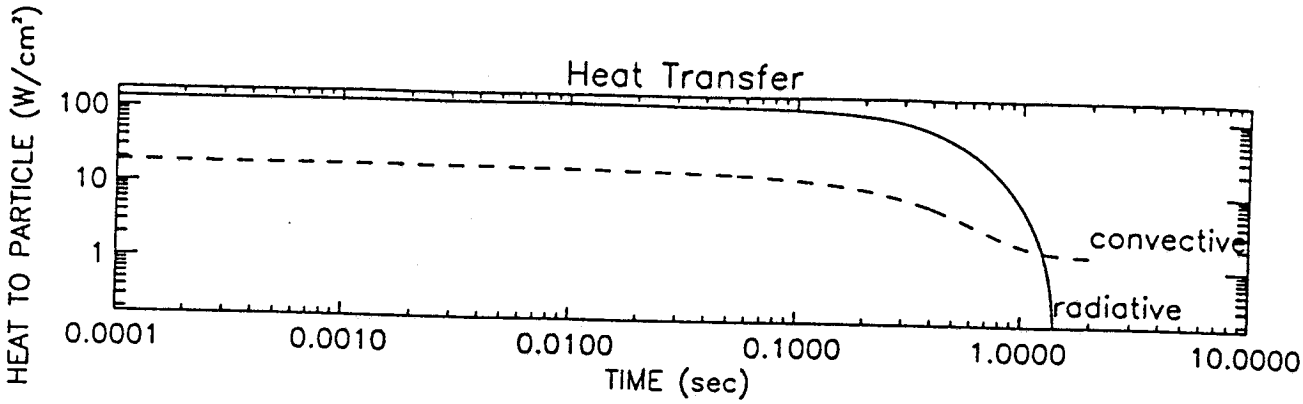


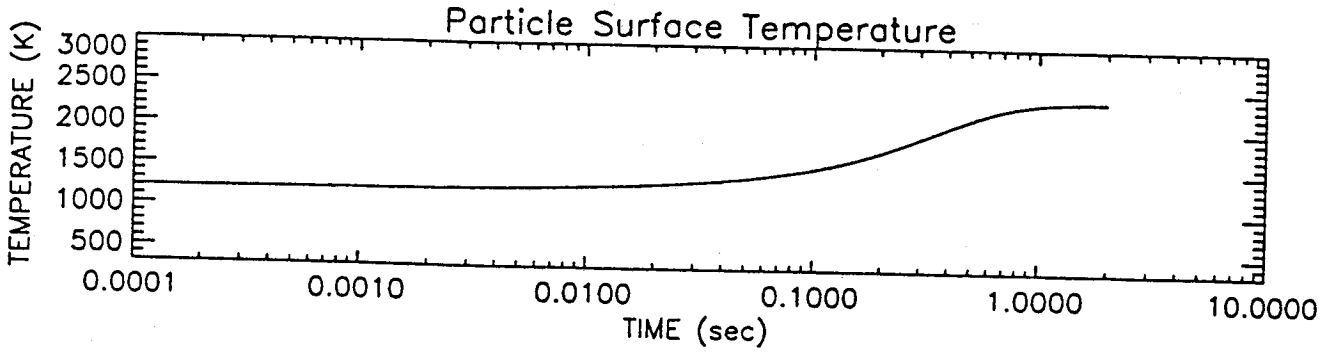


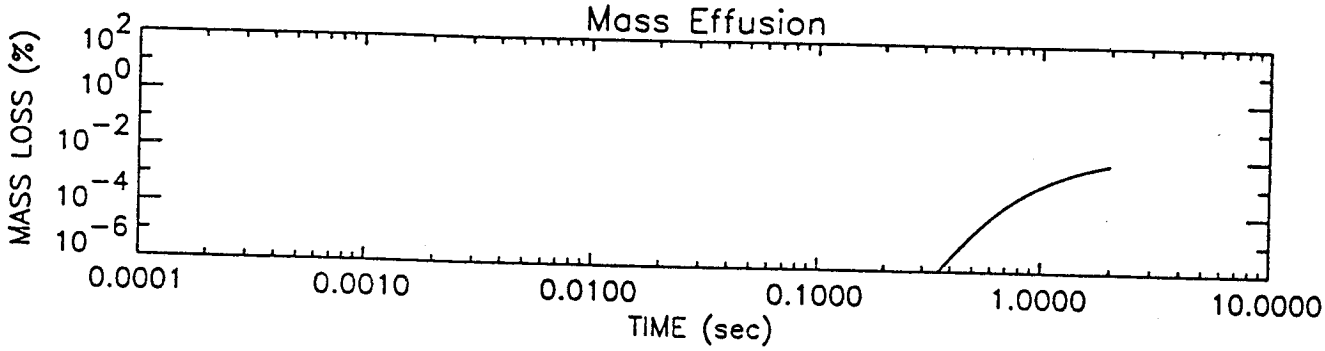


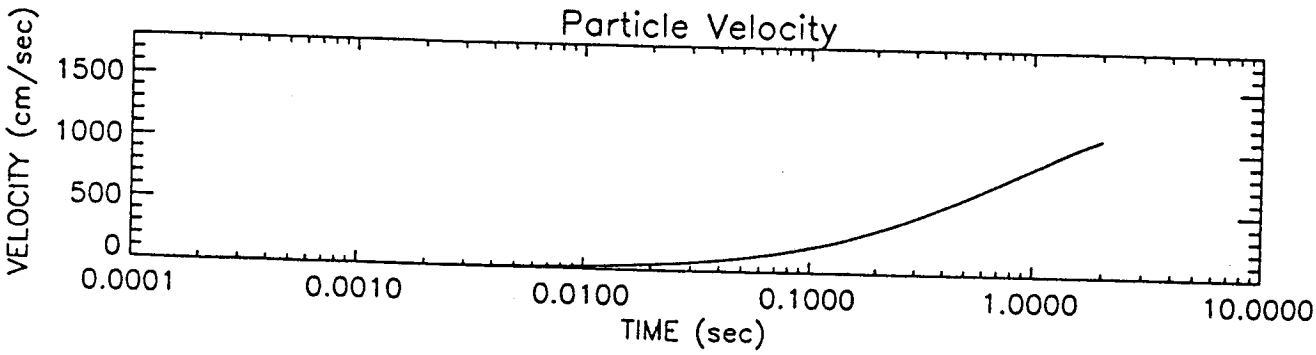

Stream Temp=3000. Particle Diameter= 10. Time for run= 2.00 Emissivity= 0.8

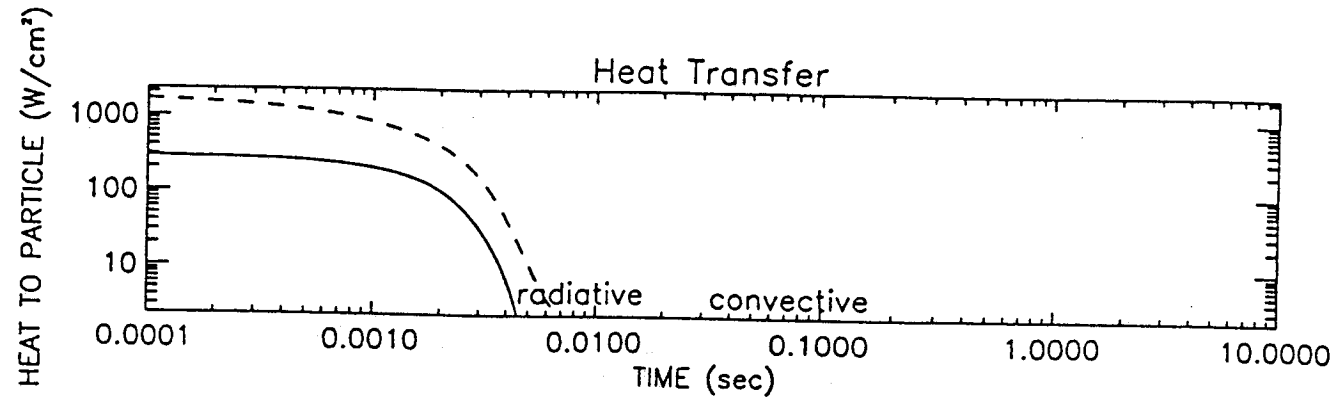


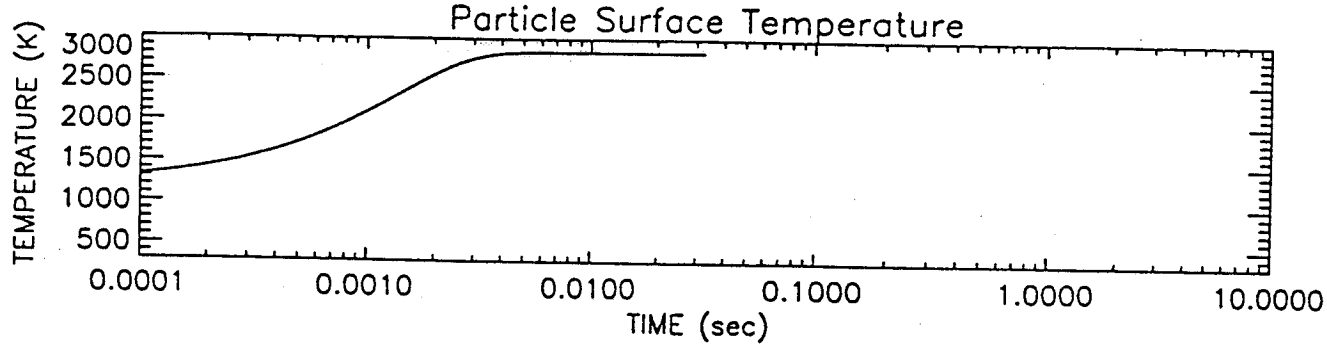


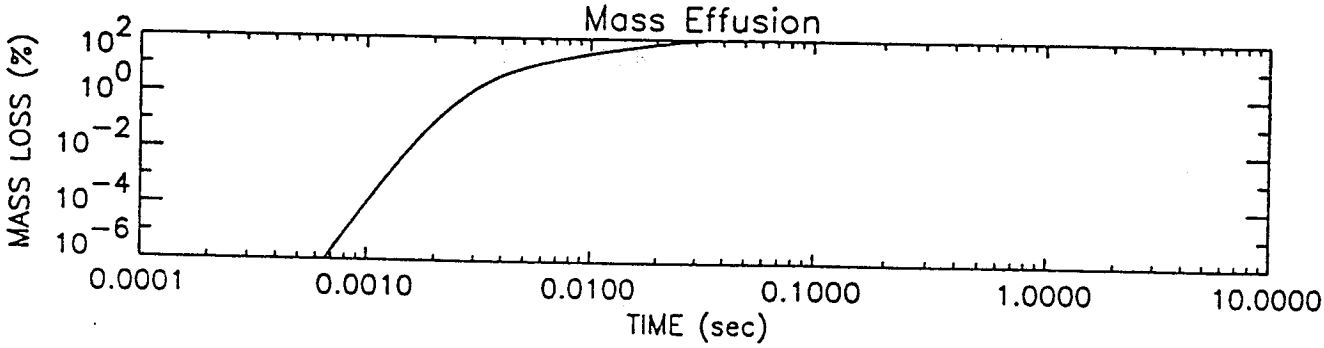


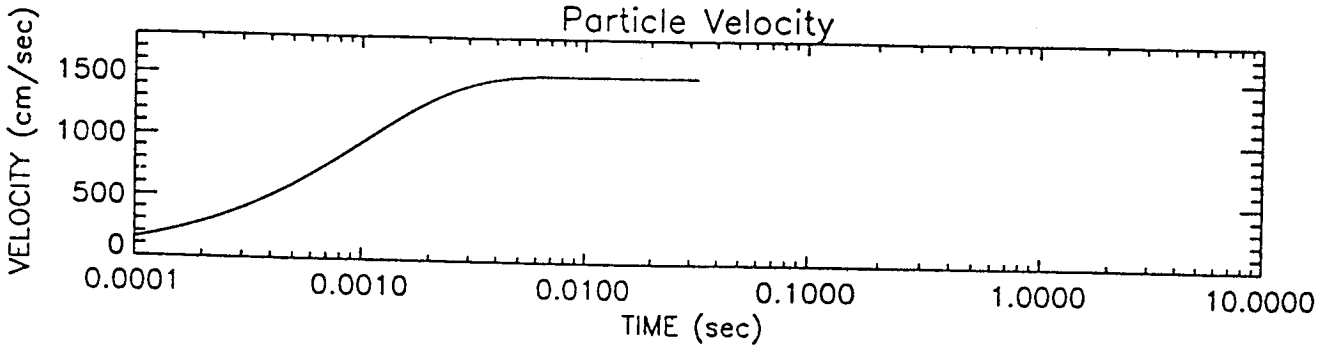

Stream Temp=3000. Particle Diameter= 100. Time for run= 2.00 Emissivity= 0.8

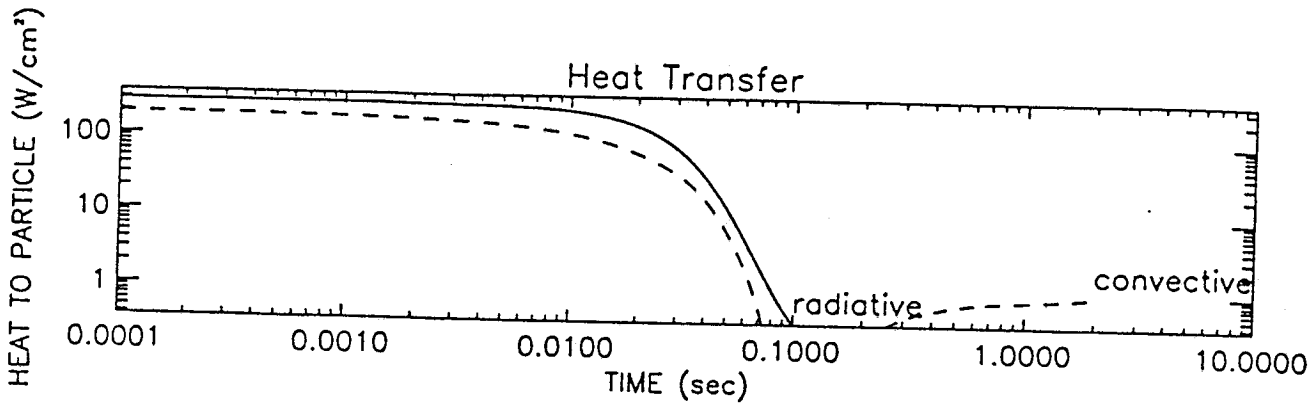


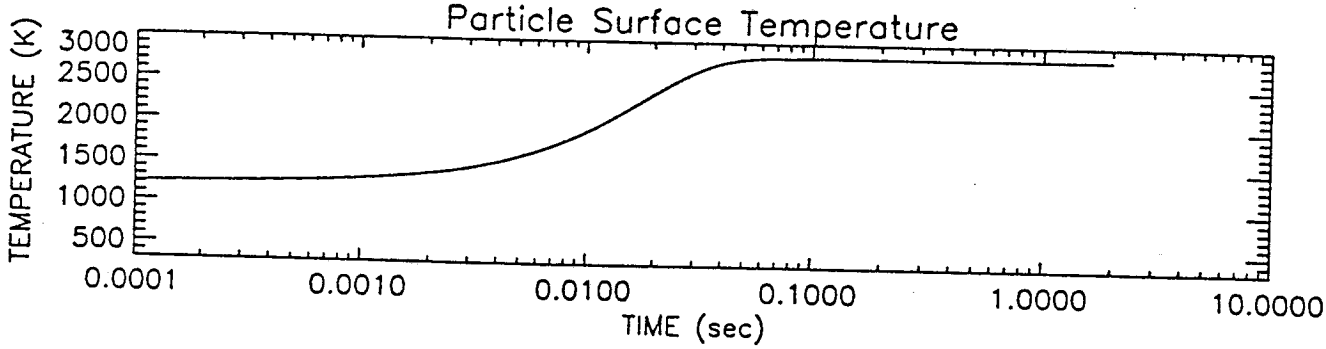


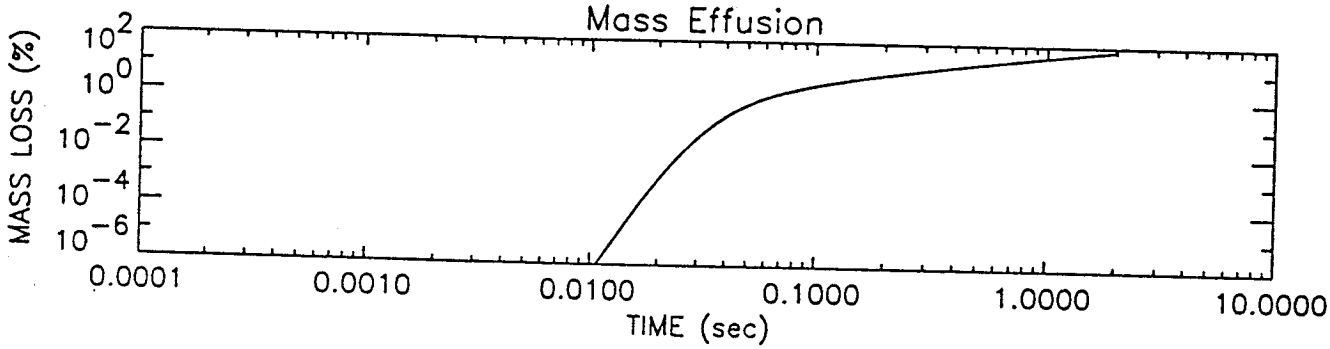


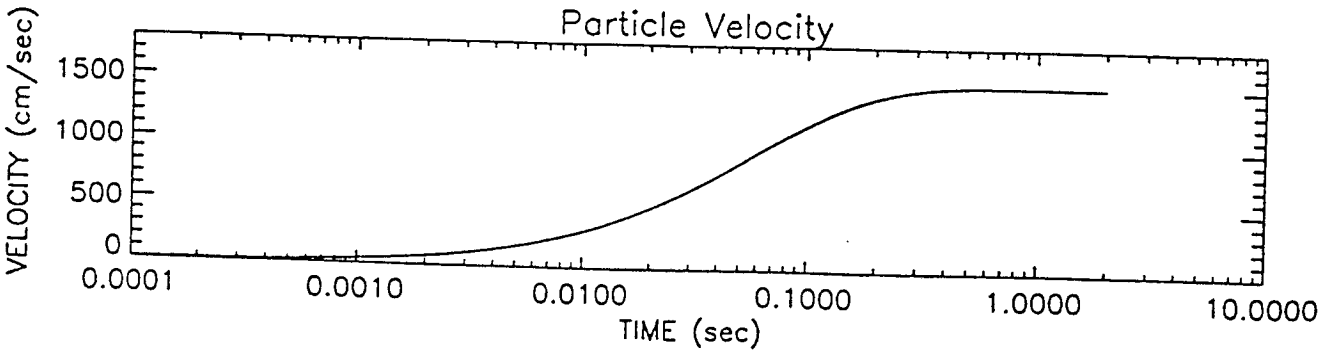

Stream Temp=3000. Particle Diameter=1000. Time for run= 2.00 Emissivity= 0.8

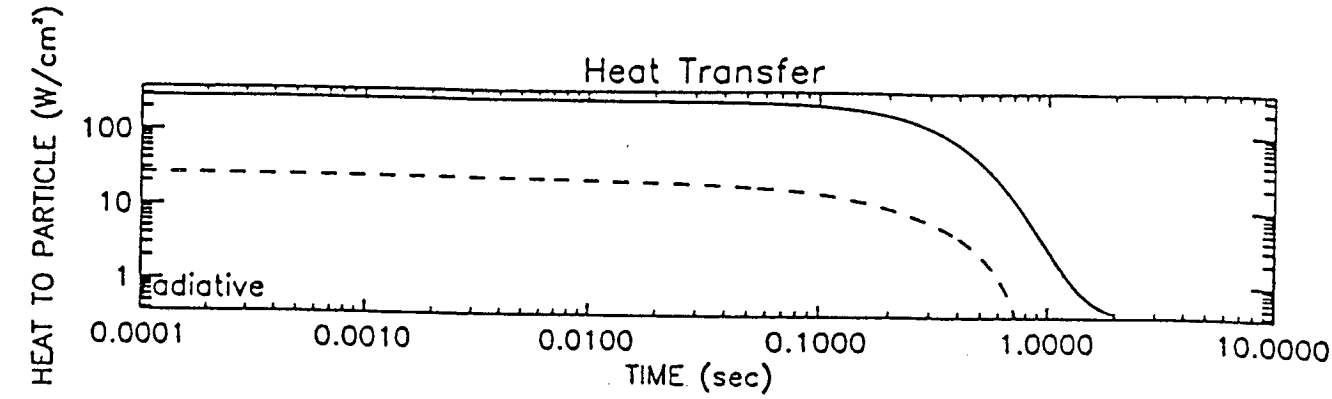


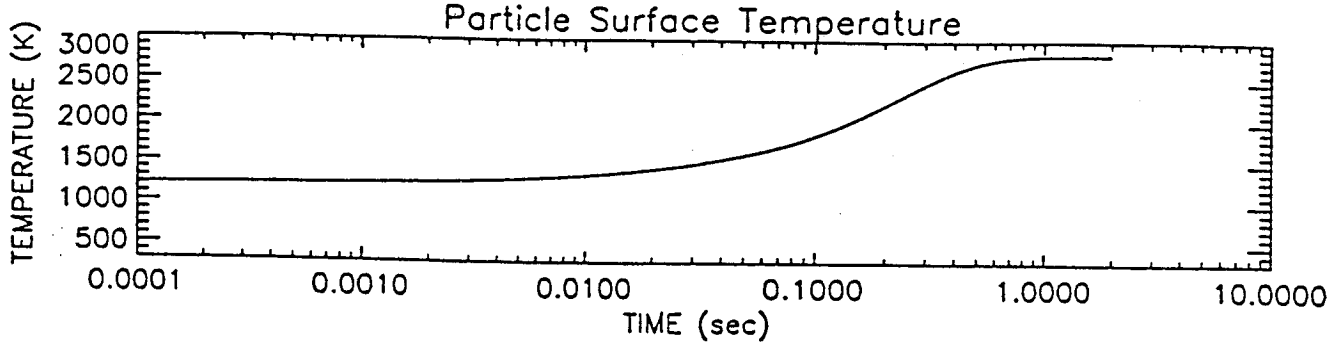


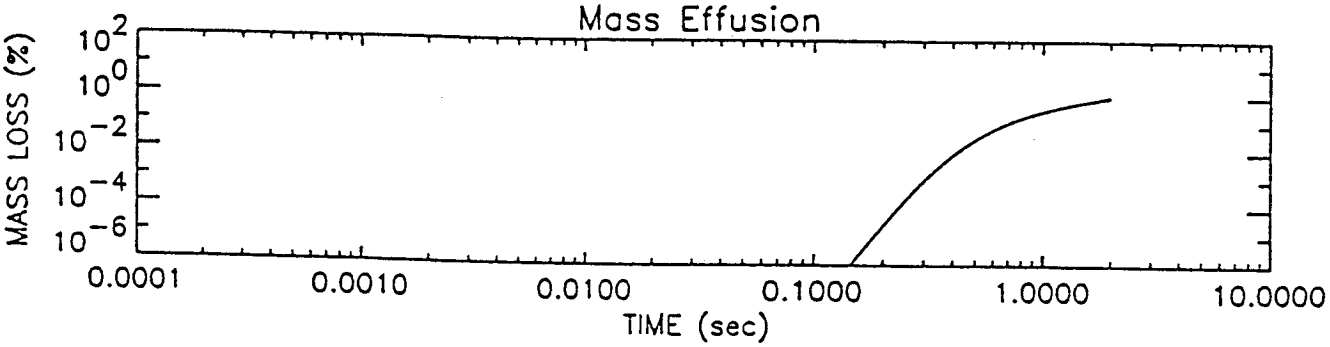


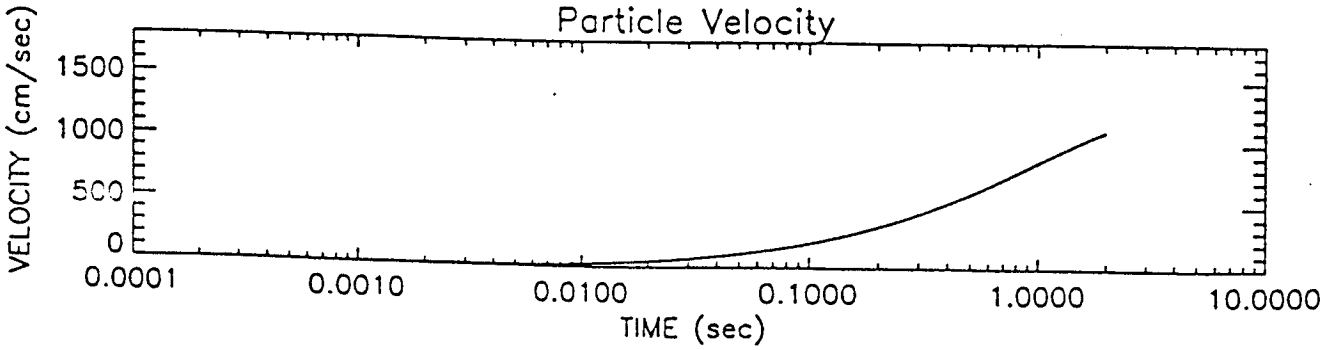

# Distribution

| Organization | No. of Copies |
|---|---|
| **John Taylor Enterprises** | |
| John Taylor | 1 |
| **Research Triangle Institute** | |
| Wallace Boggs | 1 |
| **Air Force 45 SPW/SEY** | |
| Ken Kaisler | 1 |
| **Department of Defense** | |
| Lou Ullian | 1 |
| **NASA Langley Research Center** | |
| G. Burton Northam | 1 |
| **NASA Johnson Space Center, Houston** | |
| Jim Milhoan/ES36 | 1 |
| **NASA Johnson Space Center White Sands Test Facility** | |
| Laboratories Office | 3 |
| **AlliedSignal Technical Services Corp. Team Johnson Space Center White Sands Test Facility** | |
| Laboratories Department | 1 |
| Science and Engineering Section | 3 |
| Publications Group | 2 |
| Technical Library | 3 |